Self-Heating Electrically Conductive Concrete Demonstration Project

Final Report
October 2021

IOWA STATE UNIVERSITY

Institute for Transportation

Technical Report Documentation Page

1. Report No. IHRB Project TR-724	2. Government Accession No.	3. Recipient's Catalog No.	
4. Title and Subtitle Self-Heating Electrically Conductive Concrete Demonstration Project		**5. Report Date** October 2021	
		6. Performing Organization Code	
7. Author(s) Amir Malakooti (orcid.org/0000-0001-8177-3571), Sajed Sadati (orcid.org/0000-0002-5512-5615), Halil Ceylan (orcid.org/0000-0003-1133-0366), Sunghwan Kim (orcid.org/0000-0002-1239-2350), Kristen Sara Cetin (orcid.org/0000-0003-2662-8480), Peter C. Taylor (orcid.org/0000-0002-4030-1727), Mani Mina (orcid.org/0000-0002-1500-9492), Bora Cetin (orcid.org/0000-0003-0415-7139), and Wei Shen Theh (orcid.org/0000-0002-4755-0961)		**8. Performing Organization Report No.** InTrans Project 17-610	
9. Performing Organization Name and Address Institute for Transportation Program for Sustainable Pavement Engineering and Research Iowa State University 2711 South Loop Drive, Suite 4700 Ames, IA 50010-8664		**10. Work Unit No. (TRAIS)**	
		11. Contract or Grant No.	
12. Sponsoring Organization Name and Address Iowa Highway Research Board Iowa Department of Transportation 800 Lincoln Way Ames, IA 50010		**13. Type of Report and Period Covered** Final Report	
		14. Sponsoring Agency Code IHRB Project TR-724	
15. Supplementary Notes Visit https://intrans.iastate.edu for color pdfs of this and other research reports.			

16. Abstract

Many transportation agencies allocate significant time and resources each year to remove ice and snow from their paved surfaces to achieve a safe, accessible, and operational transportation network. An electrically conductive concrete (ECON) heated pavement system (HPS) has been shown to be a promising alternative to conventional snow removal operations using snowplows and deicing chemicals, which is time-consuming, labor-intensive, and environmentally unfriendly.

An ECON HPS utilizes the inherent electrical resistance of concrete to maintain the pavement surface at above-freezing temperatures and thus prevent snow and ice accumulation on the surface. Such a sustainable concrete pavement system improves its infrastructure resiliency by allowing it to be safe, open, and accessible during even harsh winter storms.

The purpose of this study was to demonstrate the full-scale implementation of 10 ECON HPS slabs at the Iowa Department of Transportation headquarters' south parking lot in Ames, Iowa. This study consisted of system design and control, field implementation, and sensor instrumentation procedures for the construction of the ECON HPS, which took place during October 2018. A programmable logic controller (PLC) was designed, programmed, and utilized to remotely control, operate, and monitor the system, and the heating performance of the remotely operated ECON slabs was evaluated during the 2018 to 2021 winter seasons using the instrumented sensors under the snow and ice. The performance evaluation showed promising results in achieving snow- and ice-free pavement surfaces through several winter weather events.

17. Key Words		18. Distribution Statement	
concrete pavement system—electrically conductive concrete—heated pavement system—pavement construction—resiliency—resistive heating—winter maintenance		No restrictions.	
19. Security Classification (of this report) Unclassified.	**20. Security Classification (of this page)** Unclassified.	**21. No. of Pages** 103	**22. Price** NA

Form DOT F 1700.7 (8-72)   **Reproduction of completed page authorized**

SELF-HEATING ELECTRICALLY CONDUCTIVE CONCRETE DEMONSTRATION PROJECT

Final Report
October 2021

Principal Investigator
Halil Ceylan, Director
Program for Sustainable Pavement Engineering & Research (PROSPER)
Institute for Transportation, Iowa State University

Co-Principal Investigators
Sunghwan Kim, Associate Director
Program for Sustainable Pavement Engineering & Research (PROSPER)
Institute for Transportation, Iowa State University

Peter C. Taylor, Director
National Concrete Pavement Technology Center, Iowa State University

Mani Mina, Associate Professor
Industrial Design and Electrical and Computer Engineering, Iowa State University

Research Assistants
Amir Malakooti, Sajed Sadati, and Wei Shen Theh

Authors
Amir Malakooti, Sajed Sadati, Halil Ceylan, Sunghwan Kim,
Peter C. Taylor, Mani Mina, and Wei Shen Theh

A report from
Institute for Transportation
Iowa State University
2711 South Loop Drive, Suite 4700
Ames, IA 50010-8664
Phone: 515-294-8103 / Fax: 515-294-0467
www.intrans.iastate.edu

TABLE OF CONTENTS

LIST OF FIGURES

LIST OF TABLES

ACKNOWLEDGMENTS

EXECUTIVE SUMMARY

Many transportation agencies allocate significant time and resources each year to remove ice and snow from their paved surfaces to achieve a safe, accessible, and operational transportation network. An electrically conductive concrete (ECON) heated pavement system (HPS) has been shown to be a promising alternative to conventional snow removal operations using snowplows and deicing chemicals, which are time-consuming, labor-intensive, and environmentally unfriendly. An ECON HPS utilizes the inherent electrical resistance of concrete to maintain the pavement surface above freezing and thus prevent snow and ice accumulation on the surface. Such a sustainable concrete pavement system improves infrastructure resiliency by allowing it to be safe, open, and accessible even during harsh winter storms. The primary objective of this study was to demonstrate the full-scale implementation of 10 ECON HPS slabs at the Iowa Department of Transportation (DOT) headquarters' south parking lot in Ames, Iowa.

To identify the most electrically and thermally efficient type of electrode through experimental testing and theoretical analysis, several laboratory and preconstruction investigations were conducted regarding the influence of electrode size and geometry on the resistive heating performance of an ECON HPS. In addition, a theoretical formulation showing the relationship between thermal and electrical performance as well as the material properties in an ECON HPS was developed for the first time. Testing electrodes in water as a conductive medium was also found to be a quick, nondestructive, and cost-effective alternative method for monitoring the thermal performance of electrodes.

The field demonstration study consisted of developing the system design and identifying electrode and sensor instrumentation procedures for the construction of the ECON HPS, which took place during October 2018. The system design included the ECON mix design, electrode configuration design, sensor selection, and control system design using a programmable logic controller (PLC) to remotely control, operate, and monitor the system. Electrode and sensor instrumentation procedures included identifying suitability in terms of performance and finding appropriate sensors for monitoring system behavior to compare and contrast different electrode design configurations.

The heating performance of the remotely operated ECON slabs was evaluated during the 2018 through 2021 winter seasons using instrumented sensors located under the snow and ice. The performance evaluation showed promising results in producing snow- and ice-free pavement surfaces through several winter weather events.

Considering the variety of tested configurations, this study provides guidance on the design of ECON HPSs for various weather conditions, and its key findings and recommendations are as follows:

- As the largest ECON HPS implementation project, 10 ECON HPS test slabs with various electrode configurations were constructed in the south parking lot of the Iowa DOT headquarters. All the test slabs exhibited promising snow- and ice-free capabilities through a variety of winter weather events.

- The power density range for all the slabs was between 10.2 W/ft^2 (109.8 W/m^2) and 45.6 W/ft^2 (491.5 W/m^2), with an average of 24.6 W/ft^2 (265.1 W/m^2).

- Increasing the electrode diameter in circular solid bars resulted in an increase in the power density for all electrode spacings.

- Based on the theory, the experimental study, and the finite element (FE) model, the temperature increase rate of an electrode is influenced by its surface contact area (perimeter).

- A theoretical formulation was developed to describe the ECON HPS thermal behavior.

- An increase in electrode size resulted in an increase in energy conversion efficiency.

- Falling weight deflectometer tests showed that the average heated pavement deflections were about 10% lower than those of regular concrete pavement slabs, indicating that the heated slabs are stiffer with a higher modulus.

- The best operational practice for heated pavements is to turn the system on before the snow event starts and/or before snow accumulation is initiated, and the operational time and consequent operational cost will decrease if this is done.

1. INTRODUCTION

Transportation networks often experience a significant reduction in mobilization capacity due to delays, sometimes resulting in a complete shutdown of some parts of a network, due to snow and ice accumulation during winter seasons (De Langhe et al. 2013). Departments of transportation (DOTs) and airports annually spend millions of dollars to remove snow and ice from pavements and maintain the safety of the transportation infrastructure (O'Donnell 2008). For example, US freeways, including interstates, experience 5% to 40% average speed reduction and 12% to 27% mobilization capacity reduction during snow and ice precipitation (FHWA 2017). Implementing heated pavement technology, especially in supporting critical infrastructure (e.g., airports, highways), can reduce these costs by increasing transportation network resiliency during the winter season, particularly as climate change continues to make winter seasons harsher, resulting in more extreme conditions in some regions (Nahvi et al. 2018).

Conventional methods for removing ice and snow include the use of snow-removal equipment and anti-icing or deicing chemicals (Baskas 2011). In 2019, the US consumed 27 million tons (24.5 million metric tons) of rock salt for roadway deicing purposes (Bolen 2020). Such methods are time-consuming, labor-intensive, and negatively impact the environment (Arabzadeh et al. 2017a, Ceylan et al. 2014), because deicing chemicals contaminate soil, surface runoff, and groundwater, thereby impacting the ecological system as a whole. It has been estimated that 50% of the world's arable land could be salinized by 2050, directly affecting the global food supply (Jamil et al. 2011). Deicing with chemicals not only affects the ecosystem but also increases the rate of corrosion of already aging infrastructure (Guo et al. 2019).

In Iowa, snow and ice removal are expensive components in winter road maintenance for the state DOT as well as for counties and cities. The Iowa DOT, alone, is responsible for snow and ice removal on more than 9,000 miles (14,000 km) of Iowa highways, uses approximately 900 snowplow trucks, and uses approximately 200,000 tons (181,000 metric tons) of rock salt each year in snow and ice removal on Iowa roadways.

Several innovative techniques have been proposed for facilitating the removal of ice and snow from surfaces by other than these conventional methods. These include hydronic-heated pavement systems (HHPSs) (Habibzadeh-Bigdarvish et al. 2019, Thurston et al. 1995), phase-change materials (PCMs) used in integrated pavement systems (Farnam et al. 2016), and electrically conductive concrete (ECON) heated pavement systems (HPSs) (Abdualla et al. 2016, Arabzadeh et al. 2018, Gomis et al. 2015, Sadati et al. 2017). An HHPS circulates heated glycol, potentially toxic and harmful to the environment, especially if leakage occurs, within embedded pipes to heat the pavement (Ceylan et al. 2014). PCM-integrated pavement systems utilize the heat of fusion generated by phase transformation to increase the pavement temperature. This technology has been found to have an adverse effect on both the dynamic elastic modulus and the compressive strength of concrete, and it is not applicable in harsh climates (Farnam et al. 2016). The ECON HPS has gained increasing attention in recent years based on promising results from full-scale field implementations at the Des Moines International Airport (DSM) in 2016 and the Iowa DOT headquarters in 2018 (Arabzadeh et al. 2017b, Ceylan et al. 2014, Malakooti et al. 2020, Xi and Olsgard 2000).

ECON, using regular portland cement concrete (PCC) combined with a conductive additive material (e.g., carbon fiber, steel shaving), relies on resistive heating of the ECON when embedded electrodes are subjected to an applied electric potential difference (voltage) (Abdualla et al. 2016). To properly facilitate the flow of electricity, a minimum dosage of conductive additive based on the mix's percolation threshold must be present in the mix (Gong et al. 2016, Kim et al. 2016, Liang and Yang 2017, Ravindren et al. 2019, Ceylan et al. 2014); 1% by volume has been found to be an adequate amount of carbon fiber for ECON HPS purposes (Notani et al. 2019, Sassani et al. 2018a).

The advantages of ECON HPS technology include electrification and automation of winter maintenance operations, environmental-friendliness, extended pavement life through elimination of deicing chemicals, and providing a safer platform for use by aircraft, vehicles, and pedestrians (Abdualla et al. 2016). Another application of ECON HPS is self-sensing and dynamic infrastructure monitoring using the operating conductivity range of ECON (Forintos and Czigany 2019, Nguyen et al. 2020, Tian et al. 2019, Zhang et al. 2020). Figure 1 is a conceptual diagram of an ECON HPS in which a pair of electrodes connected to the electrical source establishes a voltage gradient throughout the ECON material.
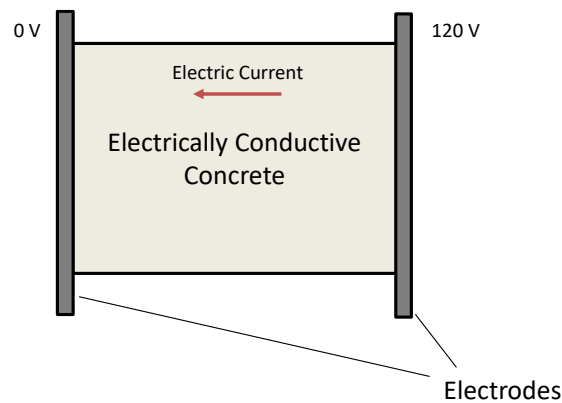
Figure 1. Simplified ECON HPS concept

Given that weather conditions impact the performance of an ECON HPS, each specific region needs a particular design for ensuring the best system performance (Sadati et al. 2018). The design parameters for an ECON HPS include the thicknesses of the regular and conductive concrete layers, joint spacing, electrode spacing, and electrode size and shape. Among these parameters, electrode spacing and electrode size and shape are those unique to the ECON HPS design and not required for conventional rigid pavement systems. Electrodes, which are essential parts of the ECON HPS design, should exhibit an acceptable level of electrical conductivity to convey electrical current from a power supply into the ECON to increase the surface temperature to a value above the freezing point (41°F [5°C]) and melt accumulated ice and snow on the ECON surface. Adequate bonding between the electrodes and the ECON is critical for achieving satisfactory resistive heating for this system (Chen and Gao 2012, Hou et al. 2007, Tian and Hu 2012).

The objective of this study was to construct, demonstrate, and monitor a full-scale implementation of the largest-to-date operational ECON HPS using different electrode configurations. Ten full-scale slabs were constructed at the south parking lot entrance of the Iowa DOT headquarters in Ames, Iowa, as part of a reconstruction project. These slabs contained various electrode configurations with different spacings, sizes, and shapes to evaluate their effect on the energy and thermal performance of the ECON HPS. Along with the 10 ECON HPS slabs, the test setup included standard concrete slabs as control sections to compare the structural performance of the ECON HPS to standard rigid pavements.

1.1. Report Content Overview

The remainder of this report is structured as follows:

- Chapter 2. Summary of First ECON HPS at a US Airport
- Chapter 3. Preconstruction Investigations
- Chapter 4. Description of System Design Elements
- Chapter 5. Iowa DOT Full-Scale ECON HPS Construction Demonstration
- Chapter 6. Iowa Dot ECON HPS Performance Evaluation
- Chapter 7. Summary, Conclusions, and Recommendations
- References
- Appendix A. Draft Standard Specification for ECON HPS Construction at The Iowa DOT South Parking Lot
- Appendix B. ECON HPS Approval Process Summary
- Appendix C. Draft User Manual for Iowa DOT ECON HPS

2. SUMMARY OF FIRST ECON HPS AT A US AIRPORT

This chapter describes the experimental setup of the ECON HPS test slabs at the DSM and the temperature and electric current values measured during selected previous snowfall events. Two slabs were constructed at the DSM site in November 2016 (Figure 2) for evaluating the design and construction processes of a carbon fiber-based ECON HPS and the testing system performance in terms of its heating capacity and energy use. (The material and equipment used for this project are reported in (Abdualla et al. 2018 and Sassani 2018b).

Figure 2. Construction of two ECON HPS test slabs at DSM

The constructed slabs were 149.6 in. (3.8 m) wide and 181.1 in. (4.6 m) in length, and the total concrete thickness was 7.5 in. (19 cm), comprised of 3.5 in. (8.9 cm) ECON for the top layer and 4 in. (10.1 cm) standard concrete for the bottom layer (Figure 3).

Sadati et al. 2020a, © 2020 Springer Ltd. All rights reserved., used with permission

Figure 3. Pavement layers for ECON HPS test slabs at DSM

Table 1 shows the slab dimensions, thicknesses, and construction time.

Table 1. DSM concrete pavement system information

Items	DSM
Slab dimensions	12.5 ft (3.8 m) × 15 ft (4.6 m)
Number of slabs	2
ECON thickness	3.5 in. (8.9 cm)
PCC thickness	4 in. (10.1 cm)
Electrode type	Angle
Electrode spacing	3 ft (91.4 cm)
Construction time	November 2016

Abdualla et al. (2018) provided a detailed description of construction techniques and system requirements for these ECON HPS slabs. The pavement design was based on Federal Aviation Administration (FAA) requirements for a general aviation apron area. The operation control and the data acquisition systems were installed in a nearby existing airplane hangar belonging to the DSM. The voltage applied to each pair of electrodes was 240 VAC; an existing electrical power supply system was used to operate the slabs. The Iowa DOT construction was five times larger than the DSM project, and this led to construction challenges that are presented and discussed in Chapter 5.

The ECON HPS at DSM was energized during observed snowfall events, and measured values of the electric current and temperature in different pavement system layers are shown in Figure 4 and Figure 5 for testing on December 24 and 27, 2017, respectively.

Figure 4. Current and temperature variations in pavement layers and ambient temperature on December 24, 2017

Figure 5. Current and temperature variations in pavement layers and ambient temperature on December 27, 2017

It should be noted that because of the existence of an electric current in the ECON layer that could interfere with the sensor readings, there are some missing values for one of the sensors located 3.5 in. (9 cm) below the pavement surface. However, considering the number of sensors and the 10-minute sampling interval, the other measured data were found to be sufficient for this study.

As shown in Figure 4 and Figure 5, as soon as the system was turned on, the electric current value increases, producing a continuous increase in pavement temperature, with temperatures in the deeper pavement layers initially higher than those in surface layers. Given that the surface of the pavement experiences the largest heat loss, the sensors closest to the surface are usually indicative of the lowest temperatures during the winter season before the system is turned on. The ECON layer thickness was 3.5 in. (9 cm), and given that the electrodes were placed at the bottom of this layer, the bottom of the ECON layer heated faster, and the temperature at a 3.5 in. (9 cm) depth was higher than the others when the system was energized. When the system was turned off (i.e., the current value dropped to zero), the pavement temperature began to decrease faster at the surface because of heat loss due to convection, except when solar radiation heated the surface.

Figure 6 shows the system's performance during a 1.5 in. (4 cm) snow event on January 24, 2017.

(a)   (b)

Figure 6. ECON HPS slab performance: (a) melting snow and (b) infrared thermography
($^{\circ}$F = [$^{\circ}$C $\times$ 1.8] + 32)

3. PRECONSTRUCTION INVESTIGATIONS

3.1. Effects of Electrodes on Performance

A laboratory investigation was conducted to see the effects of electrode configuration on the electrical and thermal performance of an HPS. Electrodes, which are essential parts of the ECON HPS design, should exhibit an acceptable level of electrical conductivity to convey electrical current from a power supply into the ECON to increase the surface temperature to above the freezing point (41°F [5°C]) and melt accumulated ice and snow on the ECON surface.

Adequate bonding between the electrodes and the ECON is critical for achieving satisfactory resistive heating for this system (Chen and Gao 2012, Hou et al. 2007, Tian and Hu 2012). Different types of electrodes for resistive heating, including copper mesh, steel mesh, and perforated galvanized steel bars, have been studied by other researchers (Gopalakrishnan et al. 2015, Wu et al. 2014). In perforated galvanized steel angles, perforations larger than the nominal maximum aggregate size have been suggested because such perforations would help provide satisfactory interlock between the electrode and ECON (Abdualla et al. 2017). Use of angle-shaped electrodes, however, increases crack-formation potential in the concrete pavement due to stress concentration at the angled edge, potentially resulting in durability issues during the pavement lifetime (Abdualla 2018). Corrosion of steel bars has been found to negatively impact temperature increase in an HPS because of weakened electrode-ECON contact (Heymsfield et al. 2013). While conductive adhesive on electrodes has also been used to ensure sufficient bonding between the ECON and electrodes, this method was found to have limited cost-effectiveness (Xie and Beaudoin 1995).

3.1.1. Theoretical Background

An ECON HPS relies on resistive heating, also known as Joule heating, by heat generation due to resistivity of a material when exposed to an electric current. In the resistive heating mechanism, electrical energy (E) is converted into thermal energy (Q) (Rao et al. 2019, Malakooti et al. 2021). Steady-state conditions and negligible losses in electrical and thermal performance is assumed here. Given this study is a comparative study under identical environmental conditions, the assumption of negligible losses is a fair assumption. Electrical energy can be calculated by multiplying power (P) by operational time (Δt), as shown in equation 1 (Rao et al. 2018).

$$E = P \cdot \Delta t = \frac{V^2}{R} \cdot \Delta t \tag{1}$$

where V is the applied voltage, and R is the electrical resistance of the material. R can be calculated using resistivity (ρ), a material property normalized by specimen dimensions (Arabzadeh et al. 2019), as shown in equation 2.

$$R = \frac{\rho \cdot L}{A} \tag{2}$$

where L and A are the length and the conductive cross-sectional area in the direction of current flow, respectively. Combining equations 1 and 2, electrical energy can be written as shown in equation 3.

$$E = \frac{V^2 \cdot A}{\rho \cdot L} \cdot \Delta t \qquad (3)$$

The thermal energy generated in a material can be calculated from the mass (m), the specific heat capacity (C), and the temperature increase in the material (ΔT) using equation 4 (Sadati et al. 2018).

$$Q = m \cdot C \cdot \Delta T \qquad (4)$$

Equation 5 results from equating the electrical energy with the thermal energy ($E = Q$) in equations 3 and 4 and rearranging as follows:

$$\frac{\Delta T}{\Delta t} = \frac{V^2 \cdot A}{\rho \cdot L \cdot m \cdot C} \qquad (5)$$

This equation determines the relationship between the temperature increase rate ($\Delta T / \Delta t$) and the specimen dimensions, and the electrical and thermal properties of a material undergoing resistive heating. It shows that the applied voltage has an exponential correlation with the temperature increase rate, while the other properties have a linear correlation.

In addition, voltage and the conductive cross-sectional area have positive correlations, while resistivity, length, mass, and specific heat capacity have negative correlations. Therefore, in order to maximize the temperature increase rate in an ECON HPS, higher applied voltage (V), larger ECON layer thickness with consideration to constant slab dimensions (A), lower ECON resistivity (ρ), and shorter electrode spacing (L) will result in better thermal performance. The conductive cross-sectional area (A) in equation 5 can also be represented as the electrode surface area given the first stage in which electricity is applied to the material is through the surface area of the electrode where the current flows to the material. The temperature increase rate is measured for different electrode sizes and geometries (different surface areas), and thermal and electrical performance is discussed in the following sections.

3.1.2. Methodology

3.1.2.1. Electrode Types for Thermal Performance Evaluation

Stainless steel 316L, a chromium-nickel stainless steel containing molybdenum, was chosen as the electrode material (ASTM A240/A240M 2017). This material is extremely corrosion-resistant, especially to acid sulfates and alkaline chlorides (ASTM A240/A240M 2017), so it would be expected to prolong the performance and durability of the concrete pavement system.

The stainless-steel electrodes used in this study have an electrical resistivity of 29.4 µΩ-in (74.6 µΩ-cm.) at 68°F (20°C) and are capable of conducting an electrical current into the ECON layer (ASTM A66-15 2015). Three different electrode geometries (solid circular, hollow circular, and flat bar) in different sizes were tested. The details of the electrode geometries and their respective unit prices per unit length are shown in Table 2.

Table 2. Selected electrodes with the associated cost

Electrodes	Geometry	Average unit price, USD/ft (USD/m)
0.5 in. (12.7 mm) OD	Smooth solid circular	3.3 (10.7)
0.75 in. (19.0 mm) OD	Smooth solid circular	6.0 (19.6)
1 in. (25.4 mm) OD	Smooth solid circular	10.7 (35.2)
1.5 in. (38.1 mm) OD	Smooth solid circular	28 (91.8)
1 in. (25.4 mm) OD, 0.75 in. (19.0 mm) ID	Hollow circular	9.7 (31.8)
1 in. (25.4 mm) × 3/16 in. (4.7 mm)	Flat bar	3.0 (9.9)

OD = outside diameter; ID = inside diameter
Source: Malakooti et al. 2021

The unit price is based on an average of 10 different market quotes for the same quantities. The unit price of electrodes increases significantly with an increase in electrode diameter, and hollow bars are also 10% cheaper than solid bars of the same diameter. Photographs of the individual electrodes selected are shown in Figure 7.
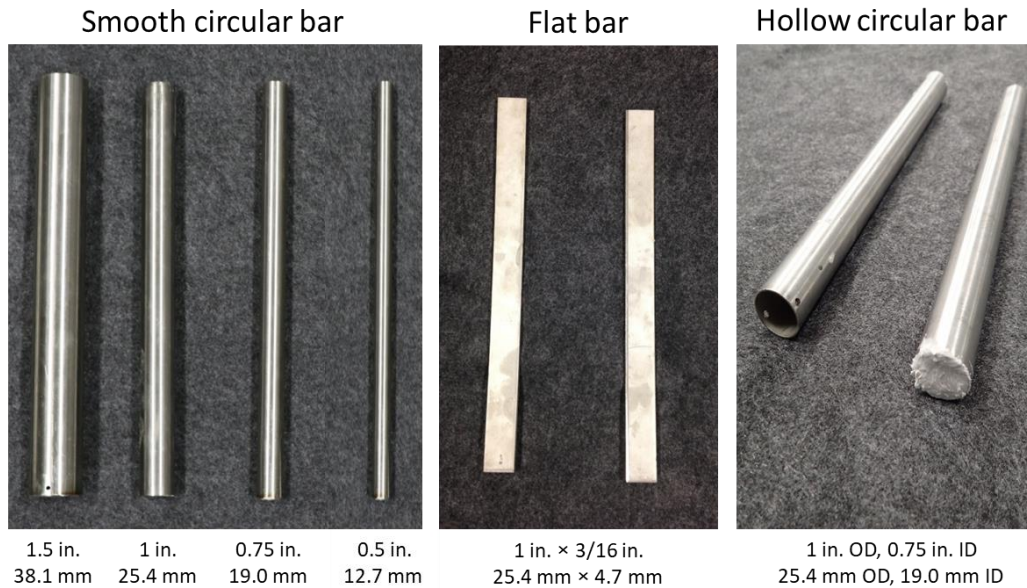
Smooth circular bar | Flat bar | Hollow circular bar

1.5 in. 38.1 mm | 1 in. 25.4 mm | 0.75 in. 19.0 mm | 0.5 in. 12.7 mm | 1 in. × 3/16 in. 25.4 mm × 4.7 mm | 1 in. OD, 0.75 in. ID 25.4 mm OD, 19.0 mm ID

Figure 7. Electrodes used in the study (in. = mm/25.4)

The following sections describe the test setup for thermal performance evaluation of electrodes in water, ECON prototype slab, and the developed finite element (FE) model.

3.1.2.2. Thermal Performance Test Procedure and FE Model of Electrodes in Water

The advantage of testing electrodes in water is that very good electrical contact can be achieved between the water and the electrodes; this is more difficult when testing electrodes embedded in ECON because of air pockets that can occur at the electrode-ECON interface. Testing electrodes in water represents an idealized situation in terms of electrical contact between an electrode and its surrounding matrix. Given water is also homogenous and hence provides virtually uniform heat distribution—while ECON is a heterogeneous material—testing in water, due to its nondestructive nature, represents a rapid, inexpensive, ideal, and cost-effective assessment method for validating hypotheses based on theory.

The water tank used in all tests was 9 in. (229 mm) long, 8 in. (203 mm) deep, and 4 in. (101 mm) wide, as shown in Figure 8a.
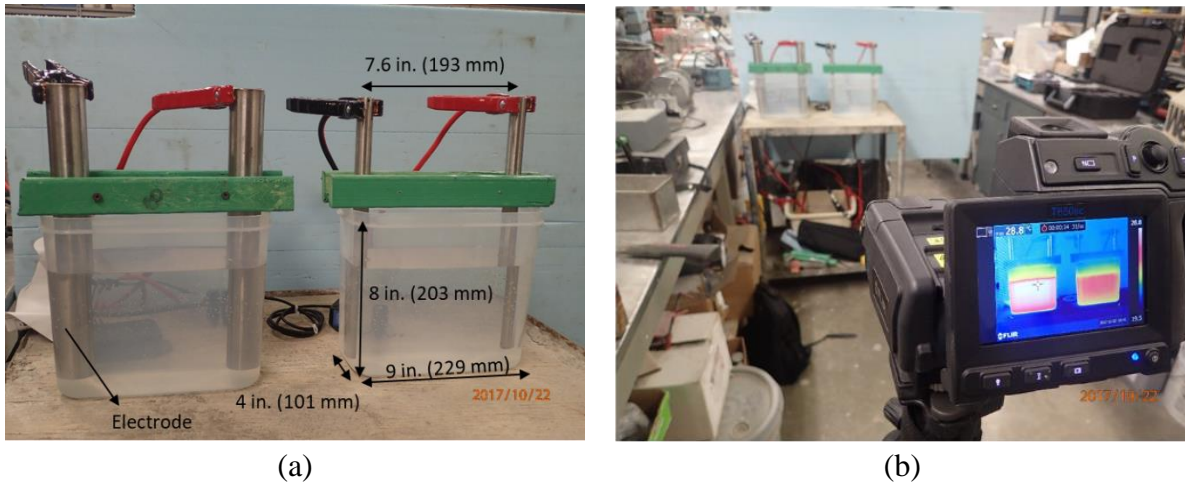
Figure 8. Electrode test in water: (a) tank dimensions and (b) setup

The water used in these tests was tap water with a measured average electrical resistivity of 571 Ω-in. (1,450 Ω-cm), and for each test, an identical amount of water (6.6 lb [3 kg]) was poured into the water tank. The electrodes were placed in the water at least eight hours prior to test initiation to allow both water and electrodes to reach thermal equilibrium at the ambient temperature (68°F [20°C]). A 120 volt alternating current (VAC) was then applied to the electrodes to pass an electric current into the water tank. The temperature and heat generation behavior were monitored using the FLIR T650sc infrared thermal camera shown in Figure 8b, and electrical current was measured using a Southwire TrueRMS clamp meter.

The electrodes were initially tested in water with a 2% (wt.) aqueous solution of sodium chloride, because the electrical conductivity of a sodium chloride solution is higher than that of pure and tap water due to its concentration of charge-carrying ions. However, given using sodium chloride led to sedimentation that resulted in heat concentration visible in the thermographic images at the tank bottom where the sodium chloride had settled (see Figure 9a), it was decided to eliminate the use of sodium chloride to achieve a more uniform temperature

11

increase within the water tank such that the performance of different electrodes in an ECON matrix could be more accurately simulated (see Figure 9b).
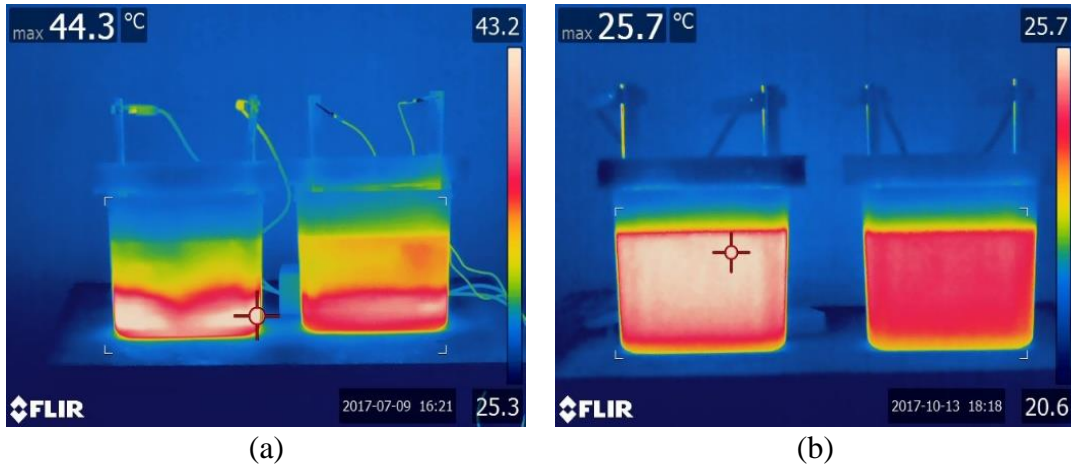
Figure 9. Electrode thermal performance in water: (a) with 2% sodium chloride and (b) without sodium chloride (°F = [°C × 1.8] + 32)

To compare the temperature increase measured in the tests performed in water with theoretical temperature increase values, an FE model of the electrodes in water was developed using ANSYS 2019 simulation software (Alimohammadi and Izadi Babokani 2019, ANSYS, Inc. 2018). The model was developed using eight-node SOLID5 elements capable of modeling resistive heating. The maximum mesh size of 0.4 in. (1 cm) was found by incrementally refining the mesh size until there were no significant changes in the model results. The final meshed model for a pair of 1 in. (25 mm) outside diameter (OD) circular electrodes is shown in Figure 10.
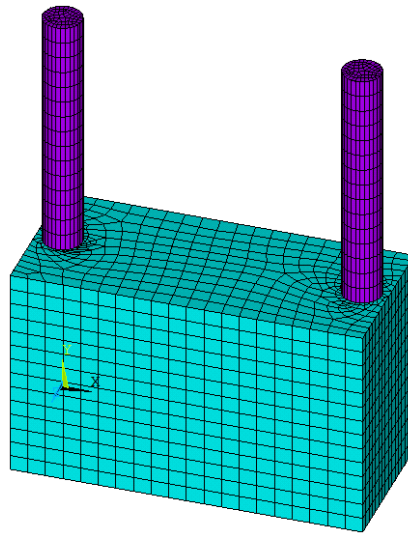
Figure 10. FE model mesh for a pair of 1 in. (25 mm) OD electrodes in water

Given the water container was a thin-walled plastic container, its impact on the temperature increase of the water and the heat transfer between the container wall and the surrounding air were assumed to be negligible. The material properties included in the model were density, heat capacity, electrical conductivity, and thermal conductivity; all except thermal conductivity were measured and used in the model. The thermal conductivity of water was used to calibrate the model. A trial value based on the literature was selected for the thermal conductivity of water, and the value was modified to make the model results match the measurements. This calibration was performed only for the model with the 1 in. (25 mm) OD circular pair of electrodes, and the value obtained for the thermal conductivity of water was used for all other models, i.e., all material properties were the same in all the models.

The material properties for the stainless-steel electrodes were obtained from existing data (Ho and Chu 1977). Figure 11 shows the temperature increase profile and model validation for the 1 in. (25 mm) OD electrodes in the FE model and the experimental data.
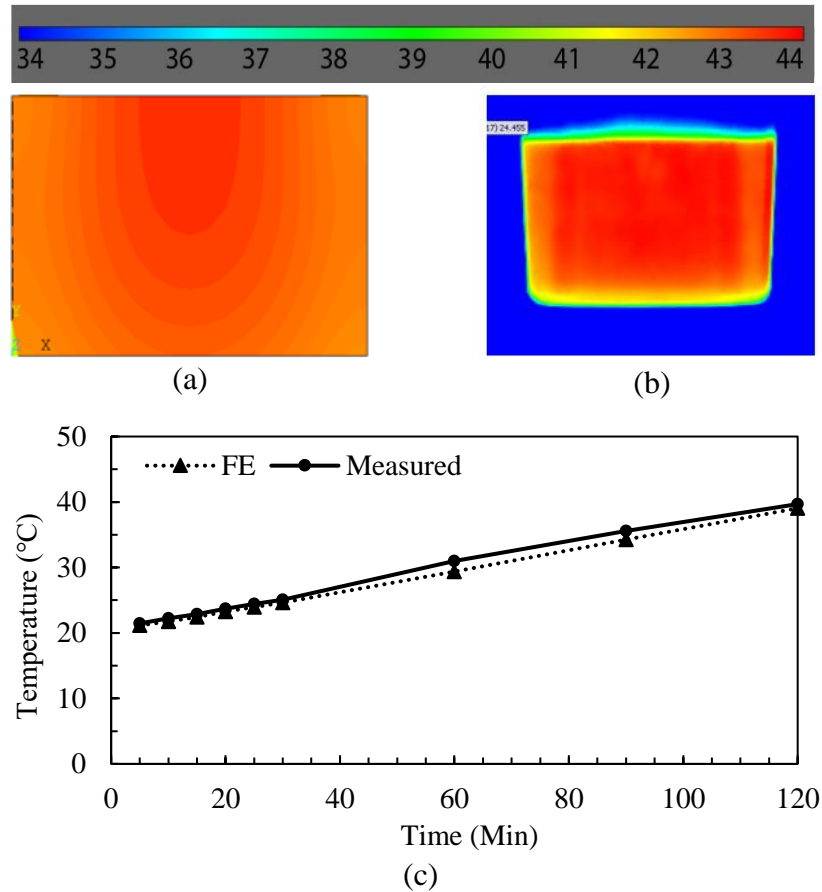
Figure 11. Heat generation profile for 1 in. (25 mm) OD electrodes: (a) FE model, (b) experimental results, and (c) model validation (°F = [°C × 1.8] + 32)

The profile shows a similar temperature increase for both the calibrated FE model and the experimental results. The FE model for the ECON slabs is not included in the scope of this

study, given it was covered in the literature for which the findings also back this current study (Sadati et al. 2019).

3.1.2.3. Thermal Performance Test Procedure of Electrodes in ECON

Five prototype slabs with different electrode geometries and sizes were designed and constructed, all with dimensions of 24 in. (610 mm) × 24 in. (610 mm) with a fixed center-to-center electrode spacing of 18 in. (460 mm). Figure 12 shows the plan and cross-sectional views of the constructed ECON prototype slabs.
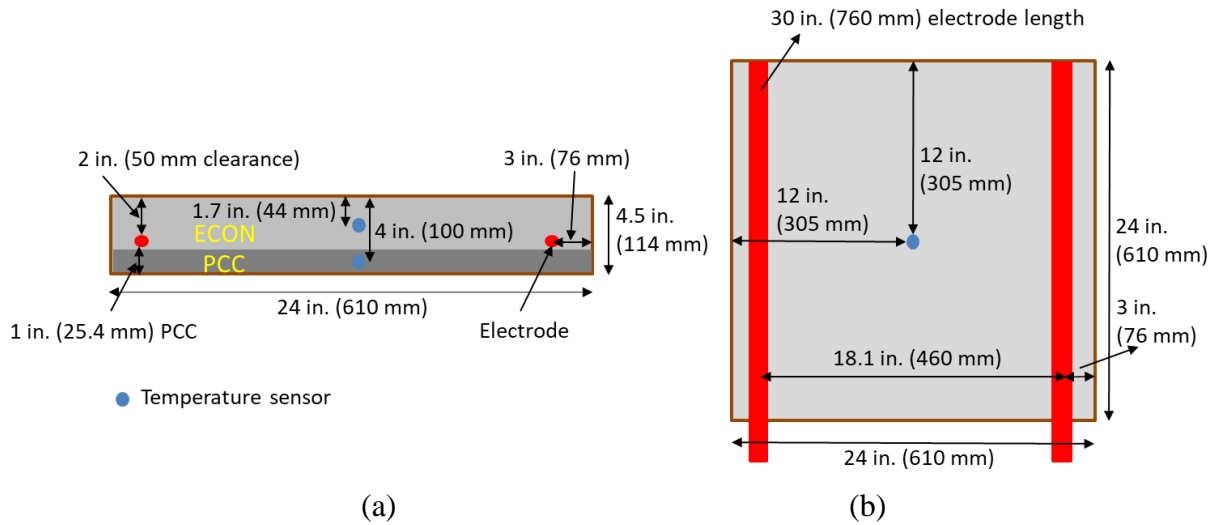
Figure 12. ECON prototype slab dimensions: (a) plan and (b) cross-sectional views

Identical features and parameters in all slabs included electrode spacing (1.5 ft [460 mm]), electrode cover (2 in. [50 mm]), applied testing voltage (60 VAC), and ECON mix design. The electrical resistivity of air-dried normal PCC is typically between 2.57×10^5 Ω-in. (6.54×10^5 Ω-cm) and 4.5×10^5 Ω-in. (11.4×10^5 Ω-cm) (Malakooti 2017, Mosavi et al. 2020, Whittington et al. 1981), while the average electrical resistivity of the ECON slabs in this study was 23.6 Ω-in. (60 Ω-cm) due to the presence of carbon fiber in the mix at 1% by volume.

The two-lift approach used in constructing the ECON prototype slabs (similar to the full-scale field implementation design) consisted of casting a 3.5 in. (89 mm) ECON layer on top of a 1 in. (25 mm) PCC layer. The first underlying reason for this design was to minimize costs, given using only one layer of ECON required less carbon fiber than using two layers of ECON combined with normal PCC of the same thickness. The second reason was to mainly generate heat closer to the surface where snow and ice accumulate. Two-lift paving is similar to retrofitting existing full-scale pavement systems, where the heated pavement would include overlaying ECON on an existing pavement. Figure 13a shows the main steps of constructing the ECON prototype slabs.
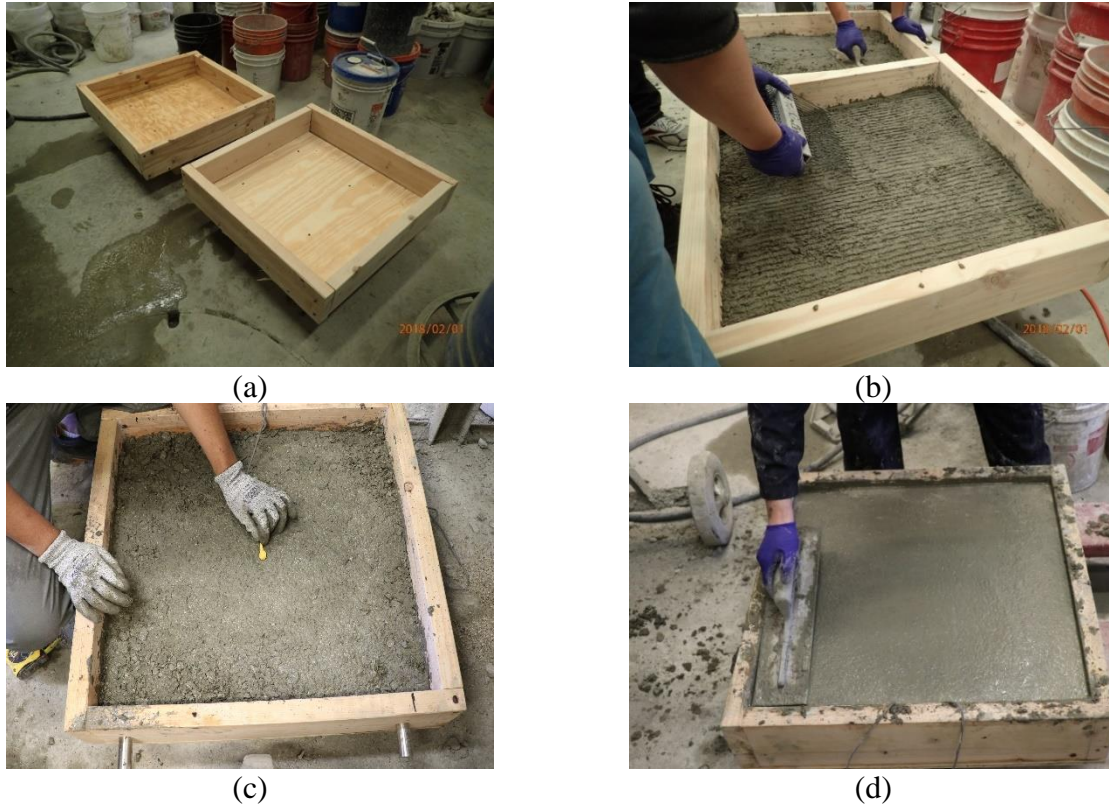
14

(a)

(b)

(c)

(d)

Figure 13. Construction of ECON prototype slabs: (a) fabricate mold, (b) cast normal PCC and roughen surface, (c) place temperature probe, and (d) cast and finish the ECON layer

First, a 1 in. (25 mm) PCC was cast with a temperature sensor placed at its center (4 in. [100 mm] below the slab surface). The PCC surface was then finished and tined, as shown in Figure 13b, to achieve a better bond between the standard concrete and the ECON layer. In the second step, a 3.5 in. (89 mm) thick ECON layer was placed on top of the hardened PCC layer, with sensors placed in the middle of the ECON layer 1.7 in. (44 mm) below the slab surface (Figure 13c). Consolidation was performed using a probe vibrator. The finished surface is depicted in Figure 13d.

While the 1 in. (25 mm) normal PCC layer for all tested slabs was constructed and cast at one time, the ECON layers were cast on separate days using the same process. The reason for this approach was to improve the uniformity of carbon fiber dispersion in the ECON mix by mixing in small batches. For larger batches, the mixing power of the drum mixer would have been insufficient to achieve better fiber dispersal within the concrete mixture. All slabs were wet-cured after casting for eight days using wet rags and were tested at the same age (eight days). The ECON mixing proportions used for casting the slabs are given in Table 3.

Table 3. ECON mix proportions

Components		Type	Content, kg/m³ (lb/yd³)
Basic	Coarse aggregate (3/4 in. [19 mm])	Limestone	1021 (606)
	Intermediate aggregate (3/8 in. [9.5 mm])	Limestone	510 (303)
	Fine aggregate	River sand	1163 (690)
	Fly ash	Class C	165 (98)
	Cement	Holcim Type I/II	654 (388)
	Water	Tap water	297 (176)
Admixtures	Derex Corrosion Inhibitor (DCI)	W. R. Grace & Co. DCI	44 (26)
	Air-entraining agent (designed for 6% air)	MasterAir AE 90	1 oz/cwt (29.6 ml/cwt)
	High-range water reducer (HRWR)	MasterGlenium 7500	0.5% wt. cem.
	Viscosity-modifying admixture	VMA	80 oz/yd³ (3100 ml/m³)
	Carbon fiber, 0.25 in. [6 mm]	Synthetic carbon fiber	0.97 (% vol.)

cwt = hundredweight of cementitious materials
Source: Malakooti et al. 2021

This mix design is based on previous studies (Sassani et al. 2017, 2018b), with the one difference being the inclusion of a viscosity-modifying admixture (VMA) to increase the mix viscosity for improvement of ECON finishing while decreasing the possibility of segregation.

3.1.3. Results

The following section presents the results from the water, ECON prototype slab, and FE modeling.

3.1.3.1. Water Test Thermal Performance and FE Model Results

Examples of thermal images taken during the electrode test in water are shown in Figure 14a.
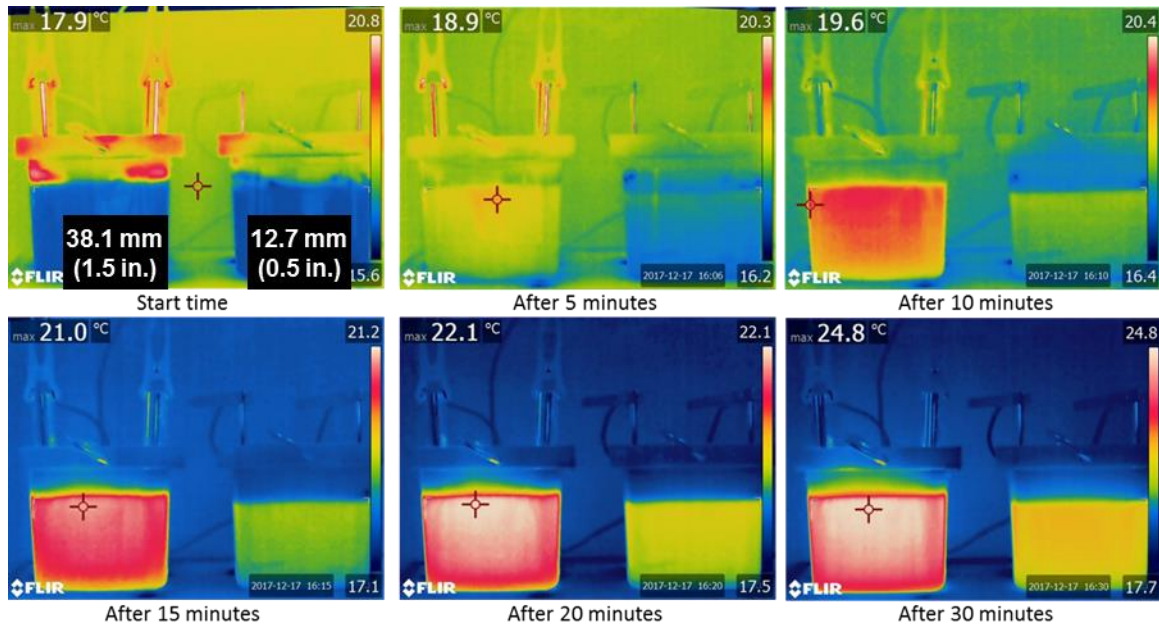
(a)
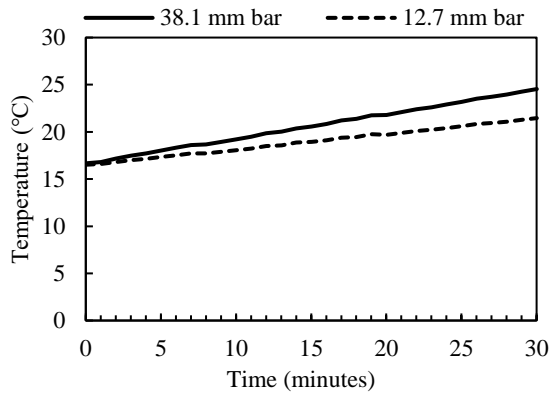
(b)   (c)
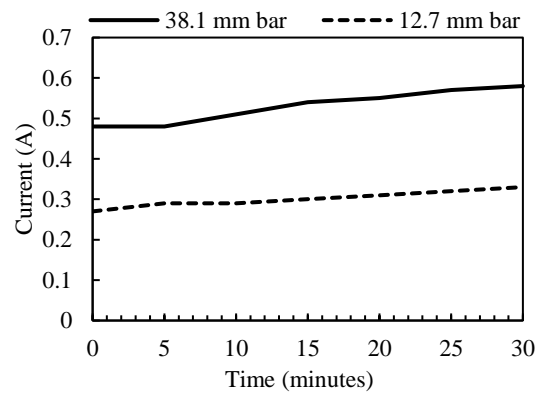
Figure 14. Electrode test in water: (a) thermography imaging, (b) temperature versus time plot, and (c) current versus time plot (in. = mm/25.4, °F = [°C × 1.8] + 32)

These images, captured at five-minute intervals, represent the performance of a 1.5 in. (38.1 mm) OD electrode (left) and a 0.5 in. (12.7 mm) OD electrode (right). The average surface temperatures of both water tanks were measured and are plotted in Figure 14b. The current readings during this test, taken every five minutes, is also shown in Figure 14c. Based on these figures, the temperature increase rate of the 1.5 in. (38.1 mm) OD electrode was higher than the 0.5 in. (12.7 mm) OD because of the larger surface contact area of this electrode with the water.

The temperature increase rate shows how quickly each electrode can generate heat and eventually, when used in an ECON HPS, melt ice and snow. It is essential to know how quickly the surface temperature of an ECON HPS rises above the freezing point (41°F [5°C]) to start the melting process. The temperature increase curve was found to be linear even when tested for

17

hourly durations, but it eventually reached a plateau because of the limitation of water ion availability. The current was also found to increase linearly, with larger electrodes exhibiting higher current values than smaller electrodes. Current is an important parameter in designing an ECON HPS system, given it directly impacts the power demand requirements for slab heating that also impacts operational costs. Temperature increase for all electrodes, similar to the one shown in Figure 14b, was found to be linear with respect to the amount of time in the water. Thus, the rates of temperature increase, i.e., the slopes of the plots of temperature versus time, were calculated and compared to determine both the most and least favorable electrodes in terms of the rate of temperature increase. Figure 15 shows the temperature increase rate for each electrode type obtained from the experimental tests and the FE models.
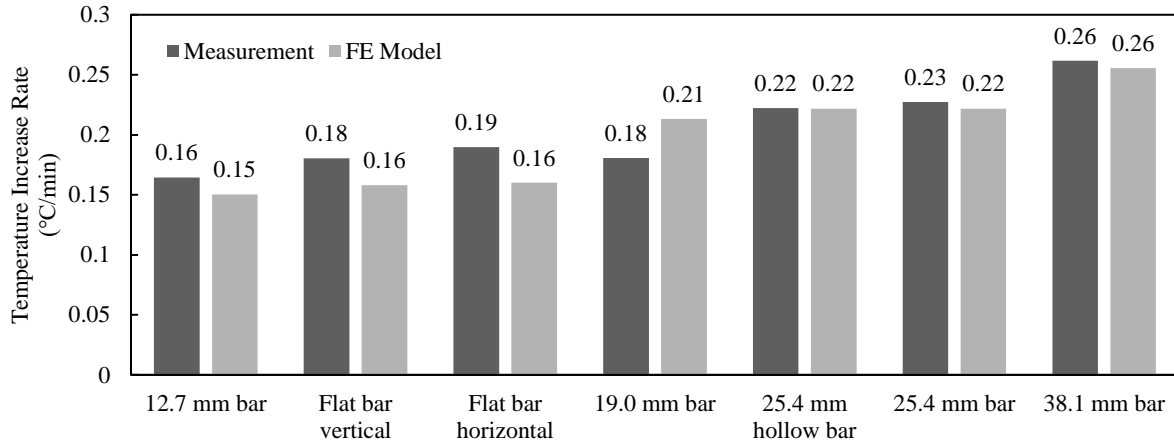
Figure 15. Temperature increase rate for electrodes in water (°F = [°C × 1.8] + 32)

The 1.5 in. (38.1 mm) OD smooth stainless-steel bar achieved the highest temperature increase, about 0.47°F (0.26°C) per minute, while the 0.5 in. (12.7 mm) OD electrode had the lowest rate among the electrodes tested. It should be noted that the greater heat generated by larger electrode sizes can be attributed to the larger contact area with the water that allows a greater amount of electric current to pass through. Note that in the case of the hollow bars, given the ends were blocked to ensure that contact between electrode and water occurred only on the outer surface of the electrodes, similar heat performance was observed between a 1 in. (25.4 mm) OD hollow electrode with blocked ends and a 1 in. (25.4 mm) OD solid electrode (same surface area).

These findings can help in the future design of more efficient HPSs using ECON, given hollow bars are less expensive and easier to transport. The results of the thermal performance tests also showed that changing the orientation of the same flat bar in the water tank (vertically and horizontally) produced no significant change in the rate of temperature increase. As shown in Figure 15, the temperature increase obtained by the FE model follows a similar trend to that of the experimental tests and the theory considered.

3.1.3.2. ECON Prototype Slab Thermal Performance Results

ECON prototype slab tests with an embedded 1 in. (25.4 mm) × 0.2 in. (5 mm) flat bar and an embedded 1 in. (25.4 mm) OD smooth solid circular bar are shown in Figure 16.
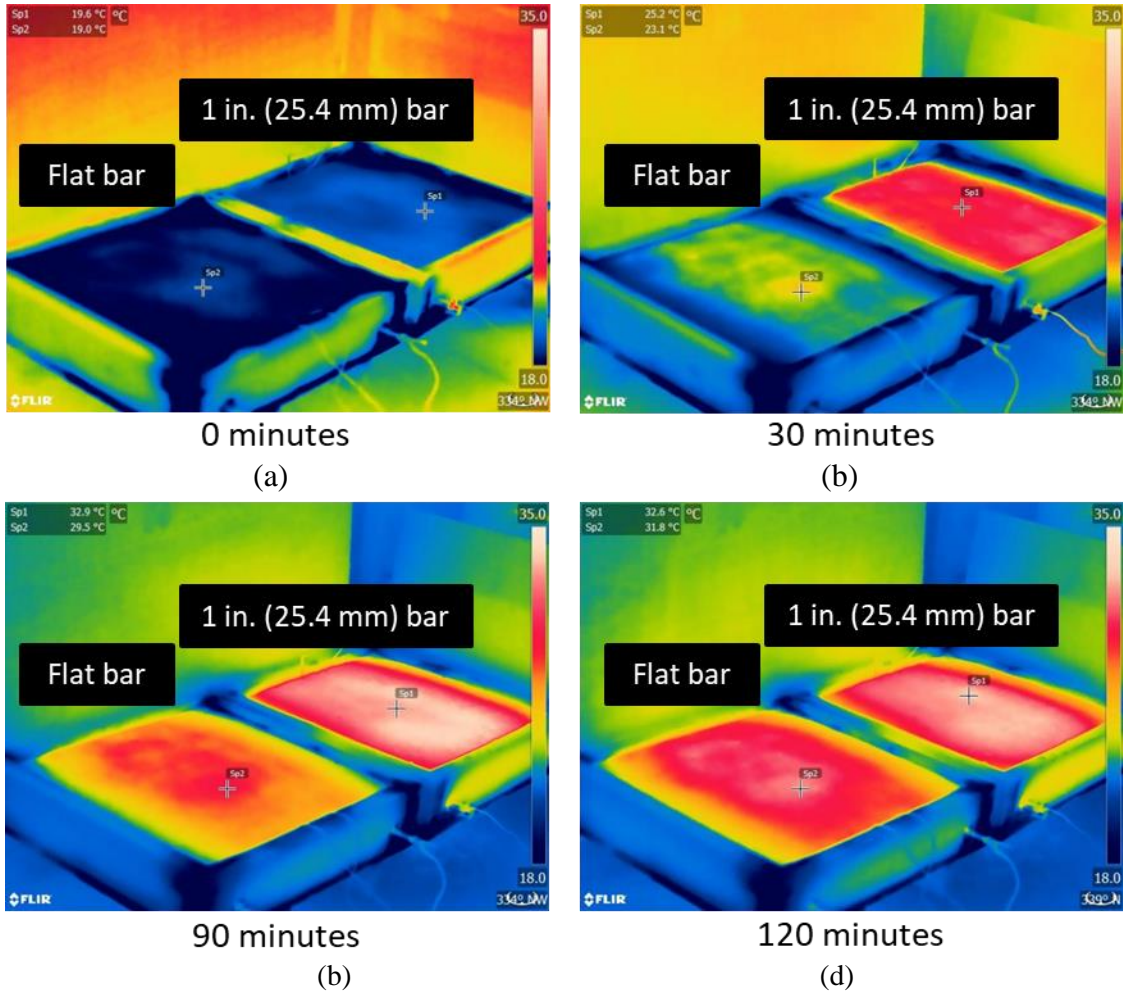
Figure 16. Thermographic imaging for sample ECON prototype slabs: at (a) initial condition, (b) 30 minutes, (c) 90 minutes, and (d) 120 minutes (°F = [°C × 1.8] + 32)

The left ECON slab represents the flat bar prototype slab, and the right slab represents a prototype slab with a 1 in. (25.4 mm) OD smooth electrode. Figure 16a shows the initial condition of the two slabs. Over time, the slab with the 1 in. (25.4 mm) OD smooth electrode exhibited a more rapid temperature increase than the slab with the flat bar (Figure 16b, Figure 16c, and Figure 16d). Figure 17a depicts the average surface temperature over time for the ECON prototype slabs.
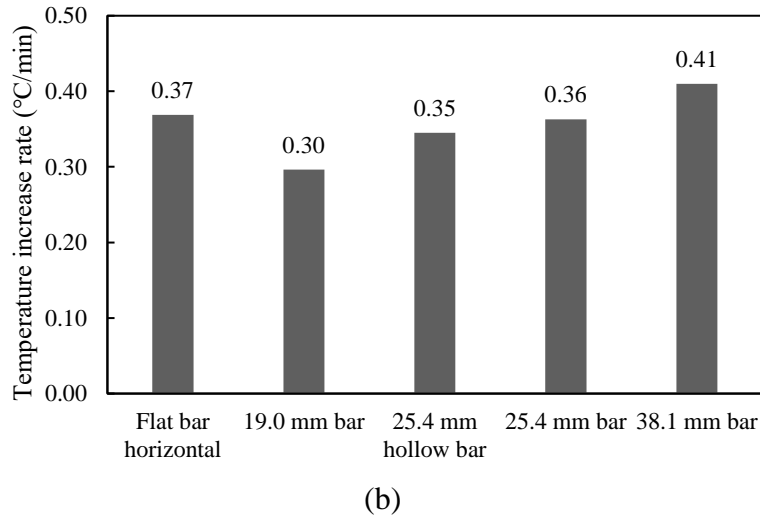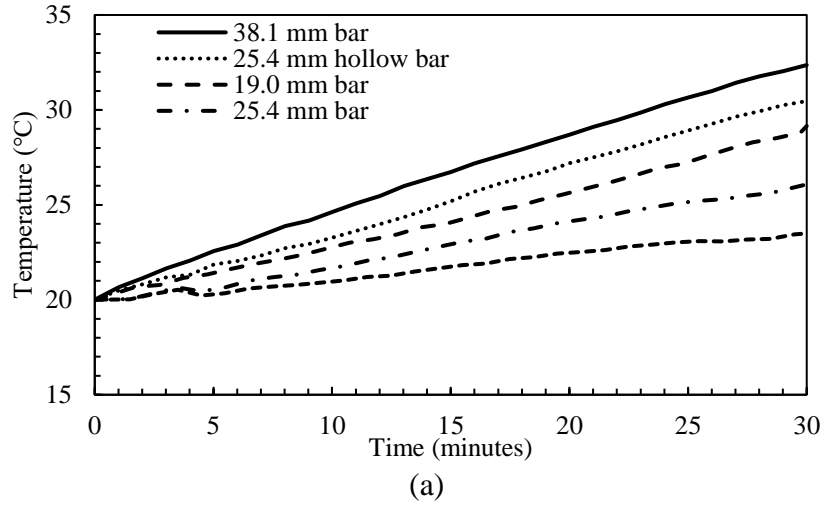
(a)

(b)

Figure 17. ECON prototype slab results: (a) average surface temperature versus time and (b) corrected temperature increase per minute for electrodes (in. = mm/25.4, °F = [°C × 1.8] + 32)

The slope of the temperature versus time curve is plotted in Figure 17b. The greater the slope, the greater the temperature increase rate associated with a specific electrode. The results show that a 1.5 in. (38.1 mm) OD smooth electrode provided the highest temperature increase rate among all the electrodes tested, in agreement with the electrode tests in the water, the FE model, and the theory.

The current remained nearly constant during all test periods. Table 4 shows the average measured current and the resistivity for each individual ECON prototype slab.

Table 4. Current and resistivity of ECON prototype slabs

ECON Prototype	Embedded electrode	Current, A	Resistivity, Ω-in. (Ω-cm)
1	Flat bar (1 in. [25.4 mm] × 3/16 in. [4.7 mm])	4.50	46.7 (118.5)
2	0.75 in. (19.0 mm) OD smooth solid circular bar	13.36	15.7 (39.9)
3	1 in. (25.4 mm) OD smooth solid circular bar	8.29	25.3 (64.3)
4	1 in. (25.4 mm) OD hollow circular bar	13.10	16.0(40.7)
5	1.5 in. (38.1 mm) OD smooth solid circular bar	13.76	15.3 (38.8)

Source: Malakooti et al. 2021

Despite similarities between the water tank and ECON experiments with respect to identifying the best-performing electrode, there were some discrepancies in terms of ranking of the electrodes' thermal performance. The performance ranking results from the slab tests for the flat bar and the 1 in. (25.4 mm) OD solid bar differed from those from the water test. This can be ascribed to the higher resistivity of the concrete in these slabs (see Table 4) compared to the other slabs due to the nonhomogeneous nature of the ECON layer. These two slabs, therefore, exhibited poorer performance given their higher resistivity will resist current and result in a lower rate of temperature increase (equation 5). Consequently, an adjustment to the temperature increase rate was necessary to eliminate the effect of resistivity in electrode heating performance for these two slabs. Given the temperature increase rate has a linear inverse correlation with resistivity (Sadati et al. 2018), the temperature increase rate for the two slabs with higher resistivities was adjusted by their respective resistivity values, as shown in Figure 17b.

The temperature increase rate for both the water and the ECON prototype slab tests is plotted against the perimeter of each electrode (Figure 18), clearly showing the correlation between the perimeter (electrode surface contact area) and the temperature increase rate.
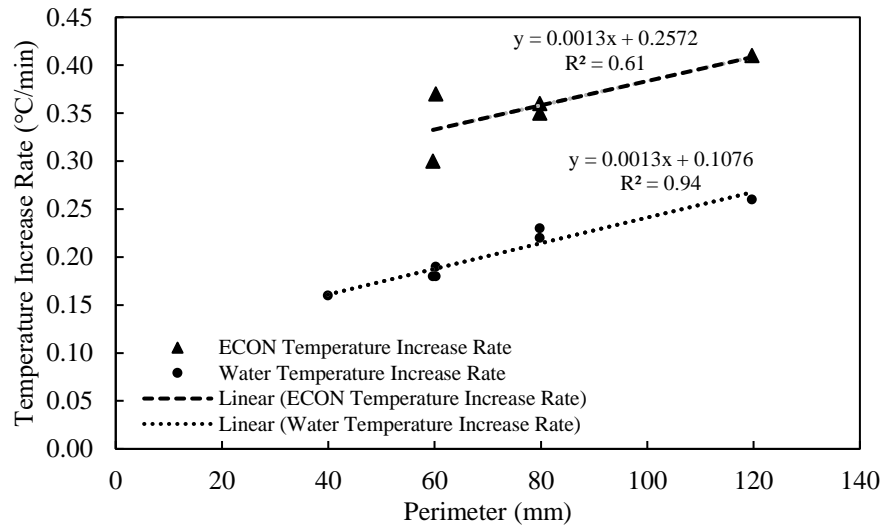
Figure 18. Temperature increase rate vs. perimeter for water and ECON tests (in. = mm/25.4, °F = [°C × 1.8] + 32)

The slope of the perimeter versus the temperature increase rate curve was found to be identical for the water and the ECON prototype slab tests. This is an important finding that can help future researchers, supporting the notion that water can be used for testing thermal performance as an easier, less expensive, and nondestructive test method. The theory also showed that the electrode surface contact area has a positive linear correlation, a similar result to the experimental and FE model findings in both water and ECON prototype slabs.

3.1.4. Discussion of Practical Implications

3.1.4.1. Energy Conversion Efficiency

In resistive heating, not all the electrical energy is converted to thermal energy, and the energy conversion efficiency (EF) is the efficiency of converting electrical energy (E) into thermal energy (Q), and thereby, energy conversion efficiency can be calculated using equation 6.

$$EF\ (\%) = \frac{Q}{E} \times 100 \tag{6}$$

Given both the thermal and electrical performance of the ECON prototype slabs were monitored during this study, both can be calculated. The electrical energy is calculated using equation 1, and thermal energy is calculated based on the thermal performance curves (see previous Figure 17a) and equation 4. Energy consumption and energy conversion efficiency calculations for all the ECON prototype slabs are given in Table 5.

Table 5. Energy conversion efficiency calculation for ECON prototype slabs (kW/ft^2 = kW/m^2 ÷ 10.764)

Electrode type	Voltage (VAC)	Current (A)	Power (kW)	Power density (kW/m^2)	Test duration (h)	Total energy density (kWh/m^2)	Input electrical energy (kJ)	Energy converted to heat (kJ)	Energy conversion efficiency in ECON (%)
						Energy consumption			
Flat bar	60	4.50	0.27	0.96	0.50	0.48	486	269	55
0.75 in. (19.0 mm) OD bar	60	13.36	0.80	2.86	0.50	1.43	1,443	704	49
1 in. (25.4 mm) OD solid bar	60	8.29	0.50	1.78	0.50	0.89	895	467	52
1 in. (25.4 mm) OD hollow bar	60	13.10	0.79	2.81	0.50	1.40	1,415	805	57
1.5 in. (38.1 mm) OD bar	60	13.76	0.83	2.95	0.50	1.47	1,486	951	64

Source: Malakooti et al. 2021

Based on these calculations, among the electrodes tested, the 1.5 in. (38.1 mm) OD bar exhibited the highest energy conversion efficiency, and the 0.75 in. (19.0 mm) OD bar the lowest. These results show that conversion efficiency is increased by increasing electrode size (electrode surface contact area) in the ECON prototype slab. The average energy conversion efficiency calculated based on this study was found to be 55.4%.

3.1.4.2. Cost Analysis

The cost analysis in this section focuses only on the cost of electrodes, one component of an ECON HPS, while also considering thermal performance of different electrodes. The bar plots shown in Figure 19 of the temperature increase rate were taken from the water (see previous Figure 15) and ECON prototype tests (see previous Figure 17b) and normalized by the average initial cost of each electrode (see previous Table 2).
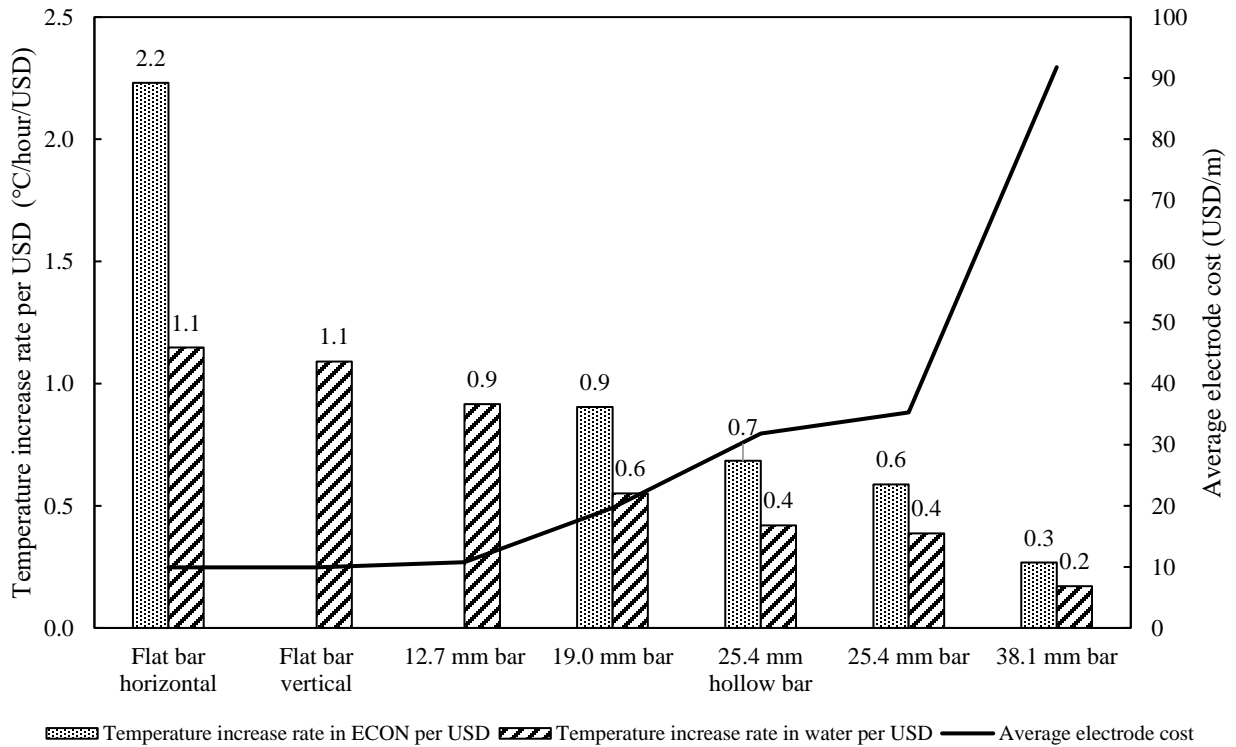
Figure 19. Temperature increase rate per average initial cost of electrode (ft = m×3.281, in. = mm/25.4, °F = [°C × 1.8] + 32)

This figure depicts the initial cost-effectiveness of each electrode, considering the temperature increase rate capacity, with a higher value corresponding to greater cost-effectiveness of that electrode. From this cost analysis, the flat bar was found to be the most cost-effective, and the 1.5 in. (38.1 mm) OD solid bar the least cost-effective electrode, with electrode cost-effectiveness decreasing with an increase in electrode size due to the higher cost of the larger-size electrodes relative to the temperature increase rate each can provide. This pattern was found

24

to be similar for both water and ECON prototype slab tests. The average electrode cost of each electrode is also plotted in the secondary vertical axis.

It is essential to note that the speed of ice and snow melting is important, and while larger diameter electrodes can provide more heat more quickly than smaller electrodes, they may not be as cost-effective, and larger electrodes also have slightly greater energy conversion efficiency. This issue would be more critical in locations such as airports or critical infrastructure requiring faster snow/ice clearing. This means that in choosing an electrode for ECON HPS design, the speed of temperature increase and cost-effectiveness of the electrode type should both be taken into consideration, so it is best when designing ECON HPSs for these types of infrastructure systems to continue using the most cost-effective electrode but at a higher voltage to achieve faster snow and ice melting.

3.2. Energy Requirements for Snow Melting in Ames, Iowa

Based on the methodology provided by the American Society of Heating, Refrigerating and Air-Conditioning Engineers (ASHRAE) handbook section on snow melting and freeze protection (ASHRAE 2009), the heat flux requirement for heated pavements at Ames, Iowa, were calculated. These calculations were based on the weather conditions. Weather conditions for Ames, Iowa, were downloaded from available data through the Iowa Environmental Mesonet website (IEM 2019). These weather data included air temperature, wind speed, snow precipitation rate, and dew point temperature. Figure 20 shows the resulting required heat flux for melting snow considering the snow events in Ames, Iowa, from 1996 to 2019.
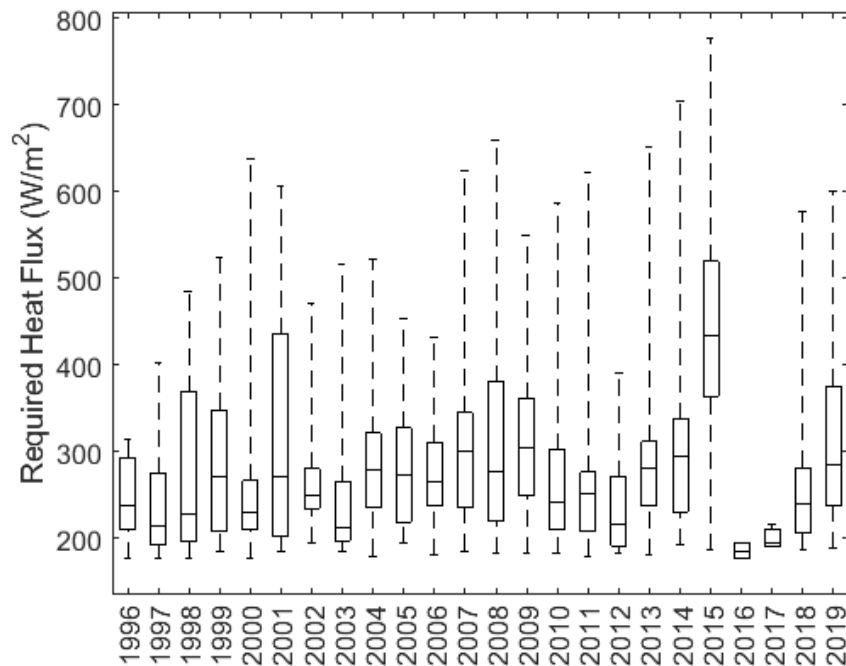
Figure 20. Required heat flux for snow events at Ames, Iowa, from 1996 to 2019 (W/ft^2 = W/m^2 ÷ 10.76)

The median of the required heat flux is less than 27.9 W/ft^2 (300 W/m^2) for all these years except 2015. Therefore, the Iowa State University (ISU) team targeted a heat flux of 27.9 W/ft^2 (300 W/m^2) to 37.2 W/ft^2 (400 W/m^2) for the ECON HPS developed for this project.

It should be noted that more than 70% of the snow events in Ames, Iowa, occurred in temperatures higher than 23°F [-5°C] (see Figure 21). The snow events occurring in colder temperatures would require a higher energy for snow melting.
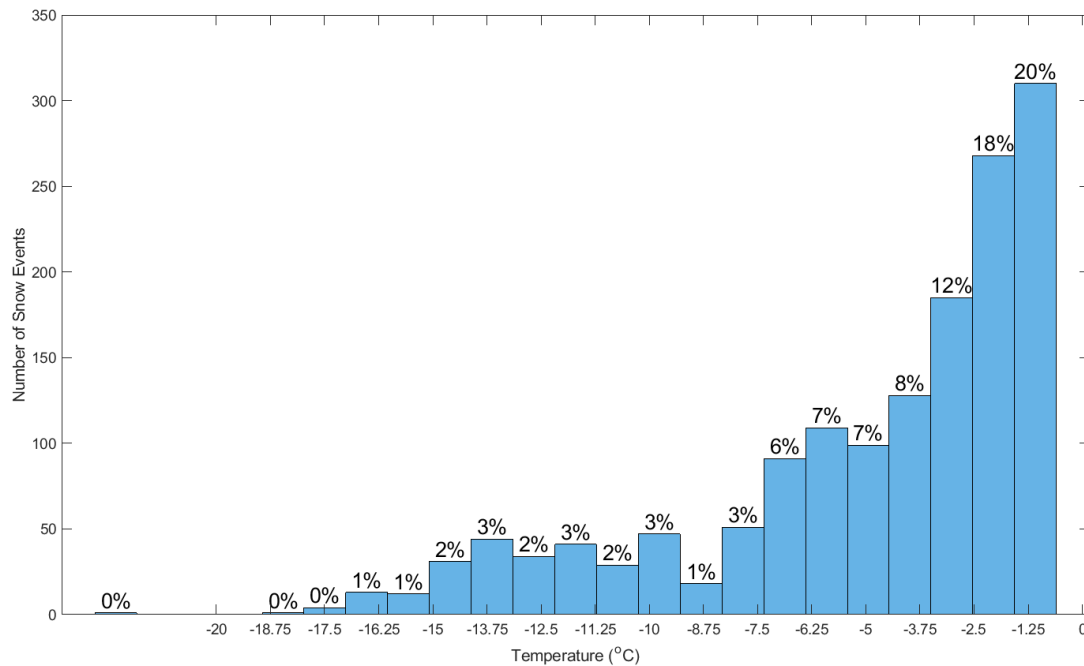
Figure 21. Snow event histogram in Ames, Iowa, in different temperatures (°F = [°C × 1.8] + 32)

4. DESCRIPTION OF SYSTEM DESIGN ELEMENTS

This chapter compares and contrasts system design elements between two ECON HPSs that were constructed, one at the general aviation area at the DSM and 10 ECON HPS slabs at the south parking lot entrance of the Iowa DOT headquarters in Ames, Iowa. The draft standard specification for the Iowa DOT project can be seen in Appendix A.

Table 6 shows the slabs dimensions, thicknesses, and construction time for both locations. The Iowa DOT construction was five times larger than the DSM project, and this led to construction difficulties that are explained in Chapter 5.

Table 6. DSM and Iowa DOT concrete pavement system information

Items	DSM	Iowa DOT
Slab dimensions	12.5 ft (3.8 m) × 15 ft (4.6 m)	12 ft (3.6 m) × 15 ft (4.6 m)
Number of slabs	2	10
ECON thickness	3.5 in. (8.9 cm)	7.6 cm (3 in.)
PCC thickness	4 in. (10.1 cm)	7 in. (17.8 cm)
Electrode type	Angle	Circular and flat bar
Electrode spacing	36 in. (91.4 cm)	20 in. (50.8 cm), 25.5 in. (64.8 cm), and 36 in. (91.4 cm)
Construction time	November 2016	October 2018

4.1. ECON Mix Design

The ECON mix design was similar to standard PCC mix design with carbon fiber added as a conductive agent. Table 7 gives a side-by-side comparison of the DSM and Iowa DOT ECON mix proportions.

Note that Table 7 information was gathered through experimental studies conducted during numerous laboratory investigations before it was chosen to be used in the field investigation (Abdualla et al. 2018; Malakooti et al. 2020; Sassani et al. 2017, 2018b).

The water/cementitious materials ratio for both mixes was set to 0.42, and aggregate gradation and proportion were similar for both mixes. The research team encountered loss of workability (flash set) during construction at the DSM because of both the long distance from the concrete plant to the construction site and incompatibility between some of the admixtures used. It was, therefore, decided to use 20% fly ash Class C replacement by weight for the Iowa DOT project and to eliminate methylcellulose and DCI admixtures from the ECON mix to solve the flash set problem, resulting in an ECON slump of 4 in. (10 cm). The carbon fiber content also increased from 1% to 1.25% because of the elimination of the fiber-dispersive agent (methylcellulose), reducing the risks of poor carbon fiber dispersion within the mix and insufficient carbon fiber at every location. This elimination also helped simplify the ECON mix design and make it easier to reproduce at any ready mixed concrete plant.

Table 7. ECON mix proportions for DSM and Iowa DOT projects

Components		Type	DSM lb/yd^3 (Kg/m^3)	Iowa DOT lb/yd^3 (Kg/m^3)
Basic	Coarse aggregate	0.75 in. (1.9 cm) concrete stone	1,001 (594)	986 (585)
	Intermediate aggregate	3/8 in. (0.95 cm) chips	499 (296)	507 (301)
	Fine aggregate	Concrete sand	1,134 (673)	1078 (640)
	Cement	Holcim type I/II	800 (475)	634 (376)
	Fly ash	Class C	--	163 (97)
	Water	Potable water	337 (200)	337 (200)
	Carbon fiber, 0.25 in. (0.64 cm)	Synthetic carbon fiber	1.00 (% vol.)	1.25 (% vol.)
Admixtures	Air entrainment	EUCON AEA-92	--	3 oz/cwt (89 ml/cwt)
	Water reducer	EUCON WR 91	--	7.5 oz/cwt (222 ml/cwt)
	Methylcellulose	Fiber dispersive agent	1.6 (0.95)	--
	DCI admixture	Corrosion inhibitor and conductivity agent	42.1 (25)	--

Sources: Abdualla et al. 2018; Malakooti et al. 2020; Sassani et al. 2017, 2018b

4.2. Voltage Selection

The applied voltage is directly correlated with snow/ice melting speed and the power consumption of the ECON HPS, i.e., the higher the voltage, the faster the snow melting and the higher the power consumed.

While the DSM project can only operate at 208 VAC, the Iowa DOT project can be operated using either 120 or 208 VAC. This flexibility of using two different voltages provides the ability to adjust the speed of melting to meet specific needs. For example, snow events started during busy weekdays can use 208 VAC, while snow precipitating during a weekend can be managed using 120 VAC.

4.3. Control System Design

The ECON HPS control system turns the system on and off using electrical switches. Arduino board microcontrollers were used in the DSM project, which are low-cost and easy-to-program control systems (Sadati et al. 2020b). Conversely, the disadvantage of the Arduino controller was that it required connection to a computer to control turning it on and off using its software, and it was also not capable of automatic system turn on/off based on pavement surface temperature to save energy. Therefore, a programmable logic controller (PLC) was chosen as the standard

control system for the Iowa DOT project, because it did not require an additional user laptop given it had onboard memory, central processing unit (CPU), and communication modules connected to the internet, allowing remote control. The expandable PLC system gave the user the flexibility in adding more modules and more slab control without additional cost.

A PLC also provides the capability for monitoring and controlling slab surface temperature using relays (switches) and different voltages (120 and 208 VAC) to affect the speed of snow and ice melting on the surface.

A recommendation for future control system design for ECON HPS projects would be to embed thermocouples within the ECON slabs and connect them to PLC analog temperature input modules, enabling the control system to continually monitor the temperature within the slabs (T_{slab}). When the ambient temperature drops, T_{slab} will decrease as well, and once this temperature has dropped below a predetermined temperature (T_{sys_on}), the control system will signal the relays to connect the ECON HPS to a 120 VAC power source, turning the system on and generating heat. If the temperature continues to drop below a specified threshold temperature (T_{thres}), the system will automatically switch to 208 VAC instead to generate more heat for efficiently melting the snow and ice on top of the slabs, thereby maintaining a surface temperature that discourages snow or ice buildup. After the ambient temperature has risen back above the freezing point, or T_{sys_on}, the system will turn off to save energy and eliminate overheating. In summary, the system will use higher voltage (208 VAC) if the weather condition is harsh and uses lower voltage (120 VAC) to maintain its temperature.

Figure 22 shows the flowchart of the procedures used by the control system.
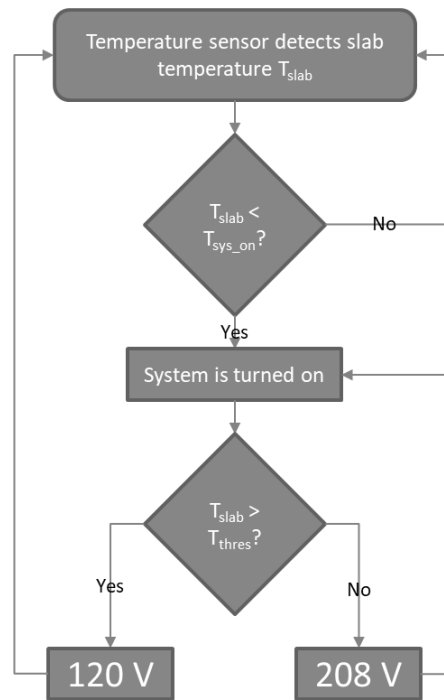
Figure 22. Control system flowchart to determine applied voltage

4.4. Electrode Configuration Design

4.4.1. Electrode Type

As previously shown in Table 6, the DSM project was constructed only with stainless-steel angle electrodes with fixed spacing, while the Iowa DOT project used various types of stainless-steel electrodes and spacings for 10 test slabs. Given the sharp edges of the angle electrodes produce stress concentration, creating a potential for cracking during the service life of the pavement, the research team decided to reinforce the DSM ECON structure with perpendicular fiberglass bars to eliminate this cracking potential (see Figure 23a). However, given that circular (i.e., smooth solid circular and hollow circular) and flat bar electrode shapes were chosen for the Iowa DOT project, their shape eliminated premature cracking and the need for fiberglass reinforcement during construction to save cost and time (see Figure 23b).

(a)

(b)

Figure 23. Electrode setup: (a) perpendicularly reinforced with fiberglass bar at DSM and (b) without fiberglass bar reinforcement at Iowa DOT

4.4.2. Numerical Analysis for Electrode Configuration Options

A numerical analysis was conducted by using an FE model to evaluate and identify electrode configuration options of each test slab (i.e., 10 test slabs in total) before the construction of the Iowa DOT project. The physical phenomenon underlying the heating process used in an ECON HPS is Joule heating (Sadati et al. 2018) based on a voltage gradient between the two ends of a conductive material. Assuming constant resistance (R), the higher the voltage gradient (V), the higher the power of heat generation (P), as reflected by equation 7.

$$P = \frac{V^2}{R} \tag{7}$$

Figure 24 depicts the constant voltage lines for the three different studied electrode shapes.
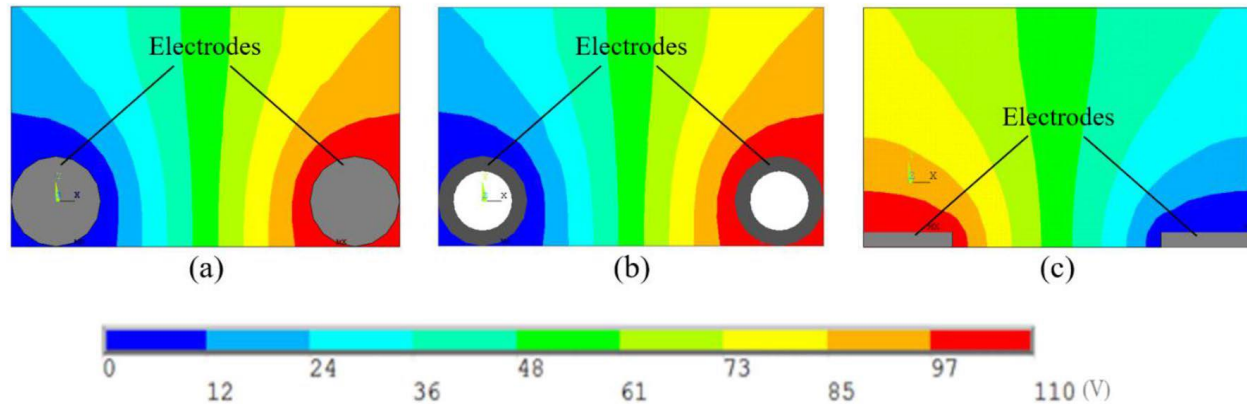
Figure 24. Voltage lines developed by different electrodes: (a) smooth solid circular bar, (b) hollow circular bar, and (c) flat bar

The distribution of these lines depends on the geometry of the concrete material and electrodes and the distance between the two electrodes. The closer the outer surfaces of the electrodes, the higher the voltage gradient in the material.

An FE model was developed in ANSYS (ANSYS, Inc. 2018) and validated with experimental data, as described in studies by Sadati et al. (2017, 2018), and the modeled loads and boundary conditions used are shown in Figure 25.
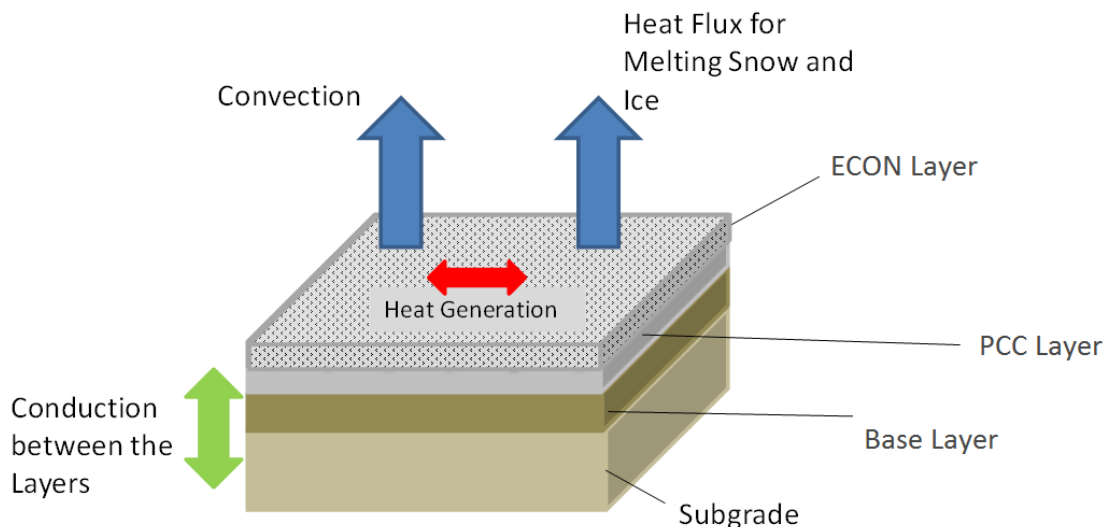
Figure 25. FE model developed to simulate all pavement layers and the interaction between the surface and the environment

ECON HPS heating is based on a Joule heating (or resistive heating) process, and the governing equations for this process are (Liu 2017) as follows:

$$E = -\nabla\phi, \tag{8a}$$

$$J = \frac{1}{\rho}E, \tag{8b}$$

$$\nabla.J = 0, \tag{8c}$$

where E is electric field (V/in.), ϕ is the electric potential (V), J is the electric current density (A/in.^{2}), and ρ is the electrical resistivity (Ω-in.). Transit thermal analysis for simulating the heating process that produces temperature variation by time is based on the following equations (Liu 2017):

$$q'' = -k\nabla T \tag{9a}$$

$$k\nabla^2 T + \dot{q} = \beta C_p \frac{\partial T}{\partial t} \tag{9b}$$

$$\dot{q} = \rho |J|^2, \tag{9c}$$

where q$''$is the heat flux (W/in.^{2}), k is the thermal conductivity (W/in.°F), T is the temperature (°F), $\dot{q}$ is the heat generation by Joule heating (W/in.^{3}), β is the mass density (lb/in.^{3}), C_p is the specific heat (J/lb°F), and t is time (s).

In the FE model, given that the temperature (T) varies in both space and time (ANSYS, Inc. 2018), the temperature at each node is considered to be dependent on time, and T can be calculated by multiplying element shape functions to the nodal temperature vectors of equation 10, given as follows:

$$T = \{N\}^T\{T_n\} \tag{10}$$

where $\{N\}$ is a space-dependent element shape function vector and $\{T_n\}$ is the time-dependent nodal temperature vector.

For a transient solution, given variation of T with time is sought for applied voltage assumed to be constant, the FE equation for this problem can be written as follows:

$$\begin{bmatrix} C & 0 \\ 0 & 0 \end{bmatrix}\begin{bmatrix} \dot{T} \\ \dot{\phi} \end{bmatrix} + \begin{bmatrix} K^t & 0 \\ 0 & K^e \end{bmatrix}\begin{bmatrix} T \\ \phi \end{bmatrix} = \begin{bmatrix} Q \\ I \end{bmatrix} \tag{11}$$

where I is the electric current, Q is the heat flux, C is the specific heat coefficient, K^t is the thermal conductivity, and K^e is the electrical conductivity. The time derivatives of T can be written as follows:

$$\dot{T} = \frac{\partial T}{\partial t}\{N\}^T\{T_n\} \tag{12}$$

Because of the symmetry of the model, to study the impact of electrode size and shape on thermal and energy performance, a two-dimensional (2D) FE model using shell elements was developed using the methodology described in (Sadati et al. 2018). Ten different configurations with various electrode spacings and electrode shapes were then modeled, and their performance were compared. FE elements for all pavement layers in the model, for a configuration including eight smooth solid circular electrodes with 8,150 elements, are shown in Figure 26.
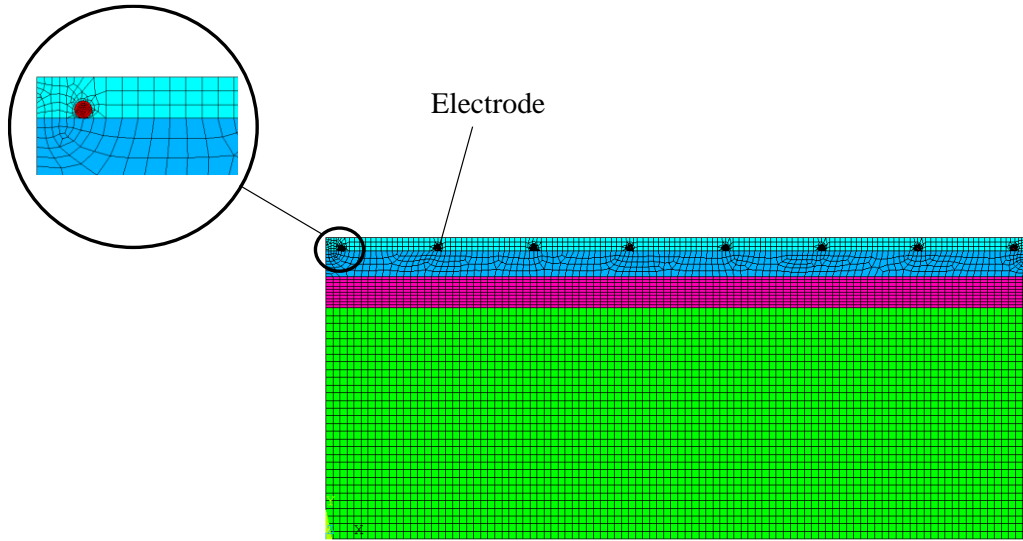
Figure 26. FE model of ECON HPS configuration with eight solid circular electrodes

The time step used for the transient analysis was five minutes. Both the number of elements and the time step were checked to assure the convergence of results.

A total time of 120 minutes was used in performing the FE simulation to evaluate and identify electrode configuration options for the 10 test sections at the Iowa DOT site. Contour plots of the temperature distribution for test sections 1, 8, and 10 are shown in Figure 27 as sample configurations with 10, 8, and 6 embedded electrodes, respectively.
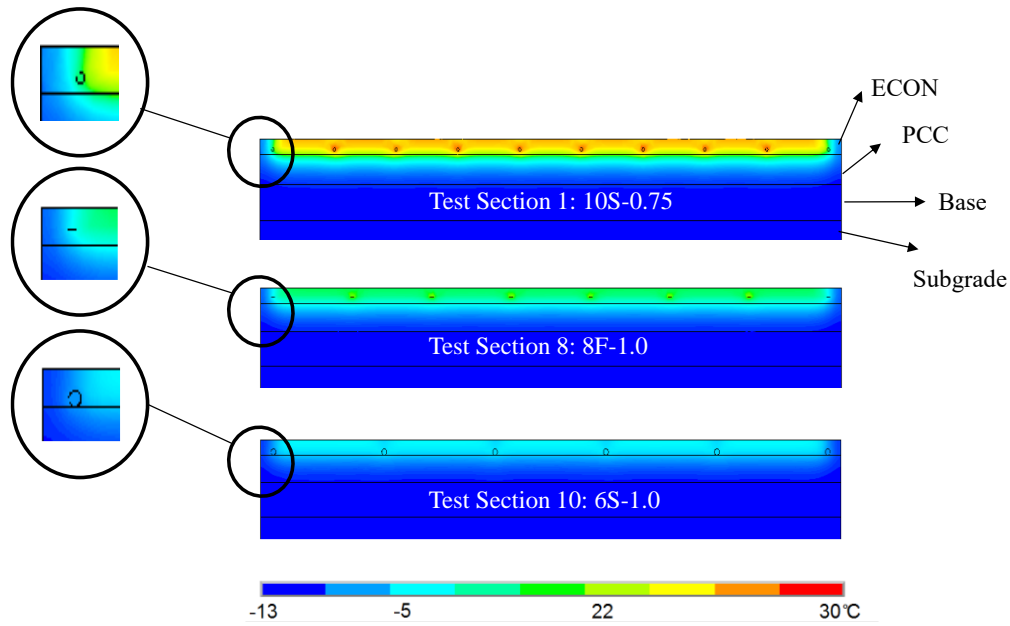
Figure 27. Temperature distribution of three design configurations: with 10 (Test Section 1), 8 (Test Section 8), and 6 (Test Section 10) electrodes

Note for Figure 27 that the electrodes used Test Section 1 are smooth solid circular bars. with a 0.75 in. (20 mm) diameter; the electrodes for Test Section 8 are flat bars with a 1 in. (25 mm) thickness; and the electrodes for Test Section 10 are smooth solid circular bars with a 1 in. (25 mm) in diameter.

Other configurations exhibited similar temperature patterns with different temperature values. The temperature distribution and power input obtained for each design configuration are given in Figure 28 and Figure 29, respectively.
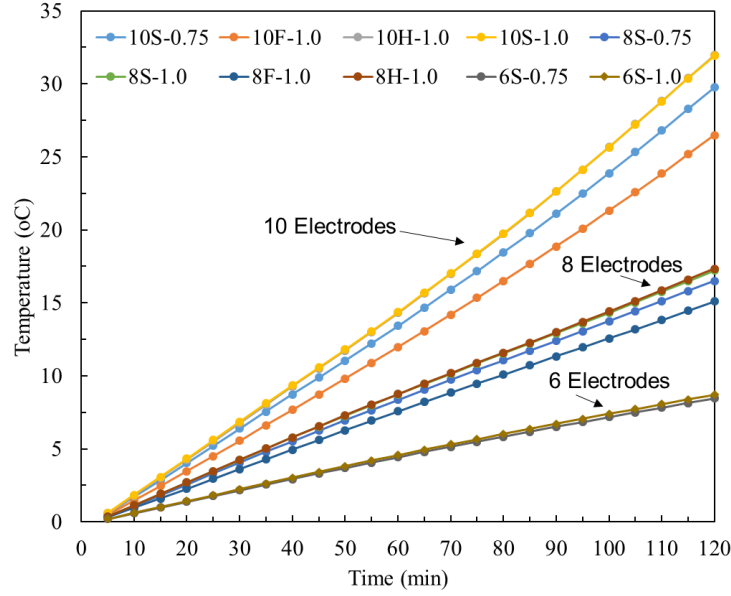
35

Figure 28. Estimated average surface temperature of each configuration (°F = [°C × 1.8] + 32)

Note that for Figure 28 the electrode design configuration option IDs are assigned to different configurations as "XY-D," where X stands for the number of electrodes in the section; Y stands for the shape of the electrodes (S for smooth solid circular, H for hollow circular, and F for flat); and D stands for the diameter (in.) in the cases of smooth solid circular and hollow circular bars and the thickness (in.) in the case of flat bars.
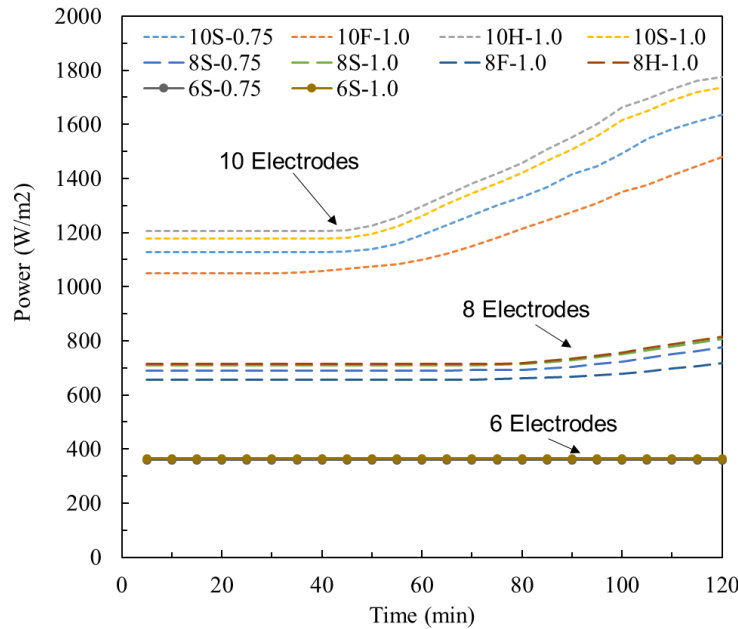
Figure 29. Estimated power density of each configuration (W/ft^2 = W/m^2 ÷ 10.76)

36

As shown in both these figures, both thermal and energy performance changed significantly with changes in electrode spacing. It was also observed that the inclusion of more electrodes increases the power input to the slabs and the resulting energy consumption. It should be noted that in order to adjust this energy consumption, the voltage applied to each pair of electrodes could also be adjusted; however, this was not within the scope of evaluation of this project.

4.5. Sensor Selection

Sensor instrumentation for monitoring or controlling the pavement surface temperature—not to prevent system overheating—is a part of the construction of any ECON HPS. The presence of carbon fiber makes ECON act as a semiconductor that can conduct a significant current between its electrodes (cathode and anode), and sensors can measure the current passing through the ECON. For example, given most sensors for measuring temperature (e.g., thermocouples) use two conductors that produce a temperature-dependent voltage to be measured and correlated with temperature, thermocouples or other sensors that use electrical readings must be protected by an insulation of both the measuring tip and the cable. The cable must also withstand the ECON operational temperature that can range from -30°F (-34°C) to 50°F (10°C) and be protected for temperature-related measurements.

The research team tested the Arduino temperature sensor at the DSM site and found that some of them ceased to measure the temperature while the ECON HPS was operating and resumed measurement when the system stopped operating. Consequently, the research team decided to use Campbell Scientific thermocouples (Type E) for the Iowa DOT; they are electrically insulated and can operate in the ECON operational temperatures at both the measuring tip and in the cable, allowing continuous temperature measurement even when the system was turned on. In summary, it was found best to first test different types of sensors in small ECON prototype slabs prior to use in field construction.

4.6. Cross Slope Design

The cross slope for allowing water to run off the road surface is a geometrically necessary feature of each pavement. If the cross slope is insufficient, the water will stay on top of the heated section and potentially freeze after the system is not operational, so this feature is essential for designing ECON HPS technology. It becomes even more important when some part of the area is heated, while other parts are not. In that scenario, the designer should design a heated pass for the water to a drainage outlet point so that water resulting from snow/ice melting does not refreeze.

During the performance evaluation of the two slabs at DSM, the research team encountered ice accumulation between the heated slab and the regular slab, so special attention was given at the Iowa DOT site to allow water to drain faster from the heated sections.

5. IOWA DOT FULL-SCALE ECON HPS CONSTRUCTION DEMONSTRATION

5.1. Planning Considerations

The test site was located at the south parking lot entrance of Iowa DOT in Ames, Iowa (Figure 30a).
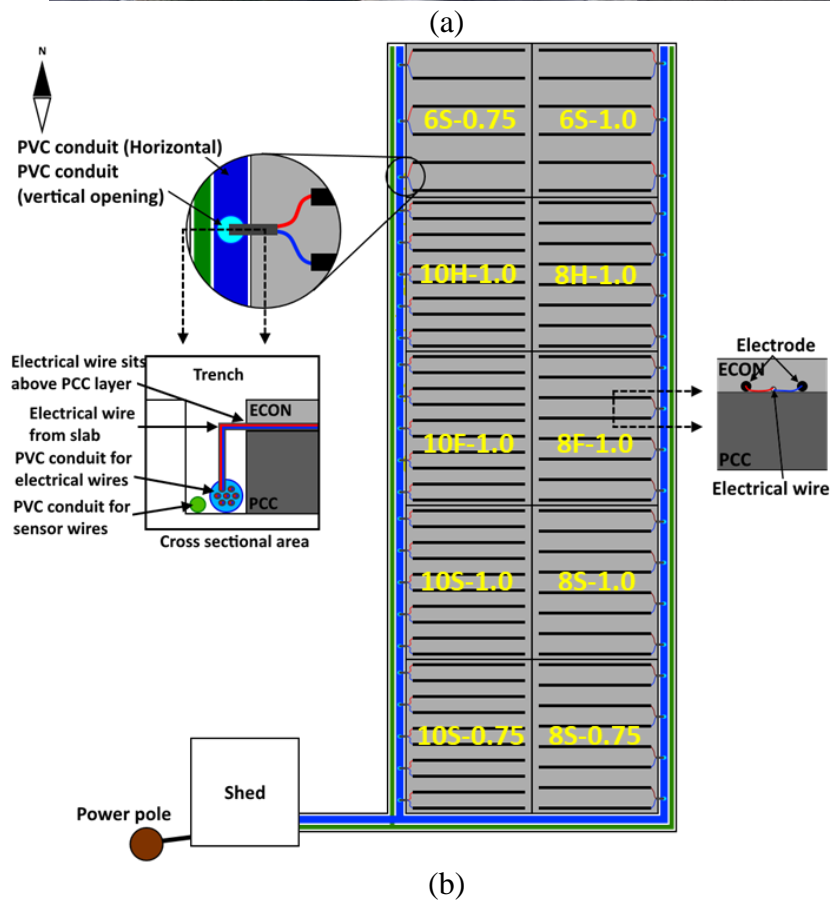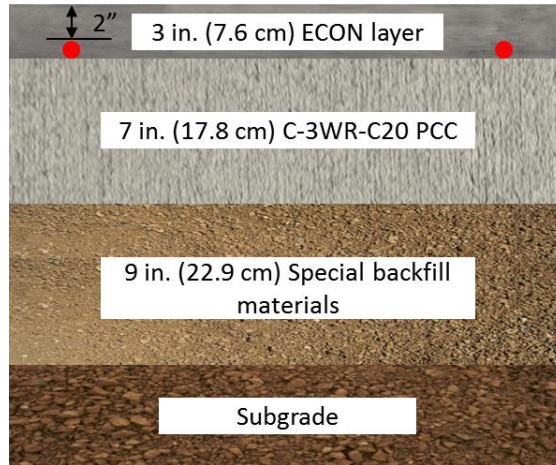
(a)

(b)

(c)

Figure 30. ECON HPS test site: (a) construction location, (b) plan view, and (c) cross-section view

As part of the reconstruction project, 10 slabs, each measuring 15 ft (4.6 m) long and 12 ft (3.6 m) wide, were dedicated to the ECON HPS implementation. The slabs near the south entrance were chosen as the heated pavement test site specifically because it was located in an area with a high and heavy volume of traffic.

5.2. Key Components of ECON HPS Technology

The key components of ECON HPS technology include an ECON layer (heating element), electrodes, temperature sensors, electrical wiring, polyvinyl chloride (PVC) conduit, a control system, and a power supply. This technology can be either constructed as an overlay on top of an existing pavement system if the pavement is in good condition or as a top layer of a two-lift paving for a new construction. Two-lift paving can be used to reduce construction material costs by reducing the ECON layer thickness, given it is necessary to heat only the surface of pavement where the snow and ice accumulation occurs.

Temperature sensors are installed to give the control system the ability to monitor the pavement surface temperature and set surface temperature to an above-freezing temperature (41°F [5°C]). This helps to reduce the possibility of overheating and to reduce energy consumption by not continuously operating the system when the surface temperatures are sufficiently warm. The energy consumption due to the thermal performance of the ECON HPS can be remotely monitored with wireless voltage and current sensors.

5.3. ECON HPS Design

The ECON HPS design consists of procedures to determine the required layer thicknesses for structural adequacy, electrode configuration based on the environmental conditions, and power

demand estimation. The layer thicknesses for the Iowa DOT ECON HPS project were designed based on a heavy traffic volume. Figure 30b shows the plan view of the construction site, which includes the 10 slabs, location of conduits, shed, and power supply.

All the electrical wiring from the electrodes to the power supply and the sensor wiring in each test section went through trenches to the shed. The control system and the data acquisition system were placed in the shed.

Figure 30c illustrates the cross-sectional view of different structural layers, which include a 9 in. (22.9 cm) special backfill base layer, 7 in. (17.8 cm) C-3WR-C20 regular PCC layer specified in the Iowa DOT Standard Specifications, which is explained in detail in Section 3.1 (Iowa DOT n.d.), and a 3 in. (7.6 cm) ECON layer. The electrodes were placed on top of the PCC layer, ensuring a 2 in. (5 cm) concrete cover on top of the electrodes.

The 10 constructed ECON slabs each have different electrode configurations. This was designed to monitor the performance of different electrode configurations in real pavement and environmental conditions. The electrode configuration for each test section is shown in Table 8.

Table 8. Electrode configuration in each slab

Test section	Section ID	No. of electrodes (spacing)	Size of electrodes, in. (cm)	Electrode type and shape
1	10S-0.75	10 (20.0 in./50.8 cm)	0.75 (1.9)	Smooth solid circular bar
2	10S-1.0	10 (20.0 in./50.8 cm)	1.00 (2.5)	Smooth solid circular bar
3	10F-1.0	10 (20.0 in./50.8 cm)	1.00 (2.5)	Flat bar
4	10H-1.0	10 (20.0 in./50.8 cm)	1.00 (2.5)	Hollow circular bar
5	6S-0.75	8 (25.5 in./64.8 cm)	0.75 (1.9)	Smooth solid circular bar
6	8S-0.75	8 (25.5 in./64.8 cm)	0.75 (1.9)	Smooth solid circular bar
7	8S-1.0	8 (25.5 in./64.8 cm)	1.00 (2.5)	Smooth solid circular bar
8	8F-1.0	8 (25.5 in./64.8 cm)	1.00 (2.5)	Flat bar
9	8H-1.0	6 (36.0 in./91.4 cm)	1.00 (2.5)	Hollow circular bar
10	6S-1.0	6 (36.0 in./91.4 cm)	1.00 (2.5)	Smooth solid circular bar

The electrodes chosen for field implementation were based on laboratory investigations and a numerical analysis conducted before the construction (Malakooti et al. 2019), and they are as follows:

- Smooth solid circular bars measuring 0.75 in. (1.9 cm) or 1.0 in. (2.5 cm)
- Hollow circular bars measuring 1.0 in. (2.5 cm) OD with 1/8 in. (0.3 cm) wall thickness
- Flat bars measuring 1.0 in. (2.5 cm) × 3/16 in. (0.4 cm)

Four slabs were designed with 10 electrodes (20.0 in. [50.8 cm] spacing), four slabs were designed with eight electrodes (25.5 in. [64.8 cm] spacing), and two slabs were designed with six electrodes (36.0 in. [91.4 cm] spacing).

Each test section was given a section ID, where the first number represents the number of electrodes in the test section (6, 8, or 10), followed by a letter representing the type of electrode (S for smooth circular solid bar, H for hollow circular bar, or F for flat bar), and it ends with a number indicating the size of the electrode in inches that has been used (0.75 or 1.0). As an example, a slab with an ID number of 10S-0.75 has 10 smooth solid circular bars with 0.75 in. (1.9 cm) outer diameter. The location of each constructed slab can be seen in the previously given Figure 30b.

5.4. Description of Materials

5.4.1. ECON and PCC Layer Mix Design

The ECON mix design was developed based on numerous trial batches in the laboratory (Malakooti et al. 2019) and the prior full-scale demonstration experience at DSM in 2016 (Sassani et al. 2018b).

First, the research team obtained samples from aggregate, cement, fly ash, and all the admixtures from the concrete plant. Second, numerous trial batches were made in the laboratory in order to attain a balanced ECON mix design to meet workability and mechanical property requirements in accordance with the Iowa DOT specifications as well as ensuring good electrical conductivity. Third, the concrete supplier was asked to batch 3 yd^3 (2.3 m^3) of the ECON mix design from the laboratory phase for laboratory testing. This step was taken as a precaution step before construction to ensure that the mixture from the batch plant was consistent with the construction specifications. It was found in the trial batch that the ECON was highly workable, but on the other hand, its electrical resistivity was high. Therefore, adjustments were made to the carbon fiber content and the admixture dosages to reduce the workability and resistivity. It was also found during the laboratory phase that (1) adding carbon fibers withholding moisture reduces the fiber loss during ECON production and (2) mixing fibers with aggregate before the presence of cementitious materials helped with achieving a better, more uniform fiber dispersion. Therefore, these suggestions were incorporated into the construction phase.

The finalized ECON mix design is shown in Table 9.

Table 9. ECON mix proportions for the Iowa DOT field implementation

Components		Type	Content lb/yd^3 (Kg/m^3)
Basic	Coarse aggregate	0.75 in. (1.9 cm) limestone	986.1 (585.0)
	Intermediate aggregate	0.375 in. (0.9 cm) chips	508.2 (301.5)
	Fine aggregate	Concrete river sand	1,079.2 (640.3)
	Cement	Holcim type I/II	632.7 (375.4)
	Fly ash	Class C	162.5 (96.4)
	Water	Potable water	336.9 (199.9)
	Carbon fiber	0.25 in. (0.63 cm) in length	1.25 (% vol.)
Admixtures	Air entrainment	EUCON AEA-92	3.0 oz/cwt (0.9 l/m^3)
	Water reducer	EUCON WR 91	7.5 oz/cwt (2.3 l/m^3)

The mixture contained 1.25% carbon fiber by volume and 20% fly ash replacement. The significant differences between this mixture and its predecessors (Sassani et al. 2017, 2018a, 2018b) were the addition of 20% fly ash to increase workability and durability and the elimination of methylcellulose fiber dispersion agent and corrosion inhibitor admixtures in order to decrease the possibility of unwanted chemical reactions between the admixtures. In addition, the carbon fiber content was increased from 1% to 1.25% by volume to account for any potential carbon fiber losses that may take place during batching and placing. The standard PCC layer (bottom layer) mix design was C-3WR-C20, and it is composed of 45% fine and 55% coarse aggregate with 20% Class C fly ash. It is worth mentioning that the typical electrical resistivity of a standard concrete is about 3.54×10^5 Ω-in. (9×10^5 Ω-cm) (Malakooti 2017, Malakooti et al. 2018, Melugiri-Shankaramurthy et al. 2019), while achieved electrical resistivity for ECON was 512 Ω-in. (1,300 Ω-cm) due to the addition of 1.25% carbon fiber into the mixture.

5.4.2. Electrodes

Electrodes in an ECON HPS have the role of applying the electricity to the ECON layer due to their high electrical conductivity properties. All the electrodes chosen were 316L grade stainless steel, which has promising resistance to corrosion. Therefore, the electrodes are better suited to withstand degradation and cracking, which will lead to system efficiency reduction and electrode debonding from ECON.

Circular and flat bar electrode geometries were chosen rather than angled electrodes, which have been used in predecessor projects (Abdualla et al. 2018) to minimize stress concentrations and thus reduce cracking potential. In addition, the chosen electrode geometries also eliminated using fiberglass bars perpendicular to the electrodes, which have been used in other projects to minimize the possible cracking (Abdualla et al. 2018).

All the electrodes were anchored to the PCC layer to secure them and minimize their movements during the pavement construction. The wires that were used to connect the electrodes to the

power supply were specially selected for 208 VAC, 600 A usage. The wires were also designed for use in a rough environment, such as a construction project, and had a special insulation layer.

5.4.3. Sensors and Data Acquisition System

Both wired and wireless sensors were utilized in the demonstration project. Table 10 and Table 11 summarize the types and numbers of sensors instrumented on 10 ECON slabs and 1 PCC slab (a control slab).

Table 10. Types and numbers of sensors instrumented on 10 ECON slabs

Sensor type	Sensor location	Sensors per single test section	Number of test sections	Sensors for total test sections
Thermocouples[1]	ECON, PCC, base, subgrade	6	10	60
Strain gauges[1]	ECON	8	3	24
Current sensors	Electrical power supply panel	1	10	10
Voltage sensors	Electrical power supply panel	1	10	10
Extra wireless temperature sensors[2]	Outside ECON HPS			2

[1] To be connected into data acquisition system for recording measurements; [2]several sensor trees using 15 wireless sensors that can be located far enough from the ECON slabs to be used as a reference

Table 11. Types and numbers of sensors instrumented on one PCC slab

Sensor type	Sensor location	Sensors per single test section	Number of test sections	Sensors for total test sections
Thermocouples[1]	PCC, base, subgrade	6	1	6
Strain Gauges[1]	PCC	8	1	8

[1] To be connected into data acquisition system for recording measurements

A total of 66 Campbell Scientific thermocouples (Type E), 32 GEOKON strain gauges, 10 wireless Monnit voltage sensors, and 10 wireless Monnit current sensors were installed. Thermocouples were embedded within each layer in the 10 ECON slabs and 1 PCC slab. Strain gauges were embedded within the ECON layer and PCC layer in the 10 ECON slabs and embedded within the PCC layers in the 1 PCC slab. Voltage and current wireless sensors were installed in the power distribution box within the shed to monitor the electrical consumption of each test section.

All the sensors were tested in the laboratory prior to the field installation. In order to gather all the data, two Campbell Scientific CR6 data loggers and five Campbell Scientific AM16/32B Multiplexers were installed in the shed. The Monnit voltage and current sensors transmit the readings to a gateway before being transferred to a cloud-based real-time monitoring system. All other sensors were connected to a laptop in the shed, which can be accessed remotely through a wireless hotspot provided in the shed. Therefore, system operation tasks, including turning the slabs on/off, data collection, and real-time monitoring can easily be conducted remotely.

5.4.4. Control System

The research team had selected a robust control system for this project. A PLC is an industrial standard control system. The PLC is a modular system comprising of a CPU, analog temperature input module, digital output module, and relays. In addition, the modular design will allow for expansion if the research team deems necessary in the future. One embedded thermocouple sensor in the center of each slab, 0.5 in. (1.3 cm) from the pavement surface, was linked to the PLC system. This enables the control system to monitor the pavement surface temperature. Once the pavement surface temperature drops below a predetermined temperature (41°F [5°C]), the control system activates the 120/208 VAC power source using the relays to generate heat within the ECON layer. The ECON system can melt ice and snow much quicker with 208 VAC compared to 120 VAC and can be used in times when the winter weather conditions are particularly harsh (e.g., snow/ice storms during a polar vortex), and the road serviceability needs to be maintained continuously under such harsh conditions.

5.5. Instrumentation and Installation Methods

The instrumentation plan for the ECON HPS consists of steps that were taken for installing electrodes, sensors, data acquisition system, and a power supply system. These steps have been developed based on extensive previous experiences during both field and laboratory experiments.

Figure 31 depicts the installation procedures for different components during the construction phase.

(a)
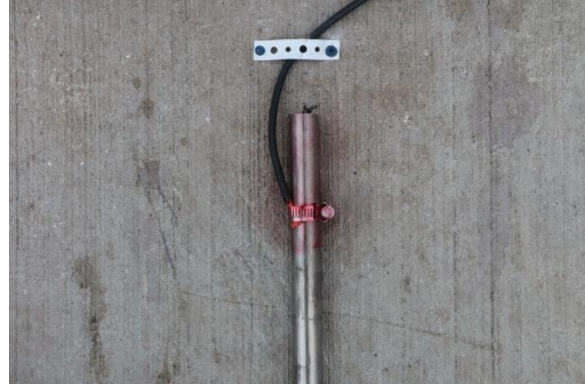
(b)
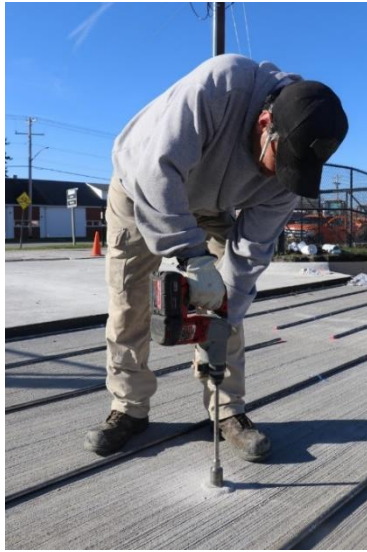
(c)
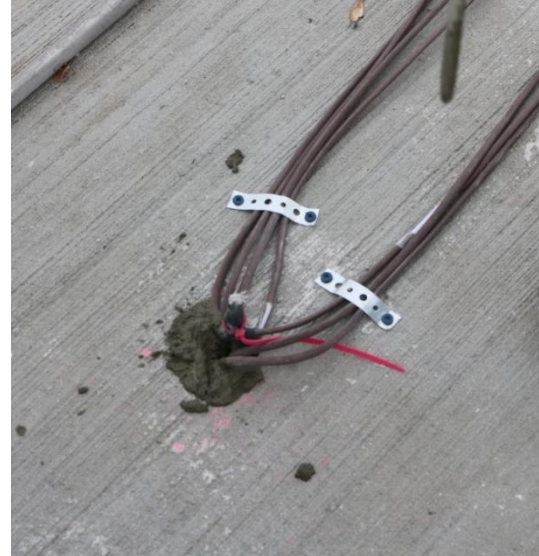
(d)

(e)
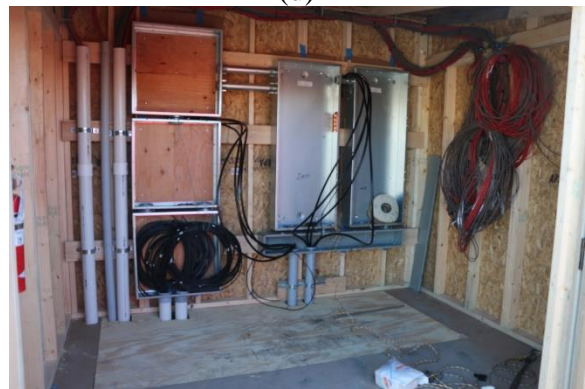
(f)

Figure 31. Electrode and sensor wiring and instrumentation: (a) anchor electrode to PCC layer, (b) wire electrodes, (c) install thermocouple sensor tree, (d) place thermocouple sensors, (e) install strain gauges, and (f) wire shed and sensors in shed

5.5.1. Installation of Electrodes

The location of each stainless-steel electrode was marked on each slab, and the electrodes were fixed using steel straps, as shown in Figure 31a. A drill was used to make the holes and secure the straps to the PCC layer. After anchoring the electrodes, all the electrodes were connected to electric wires using gauge-ring wire connectors for flat bars and hose clamps for circular bars (see Figure 31b).

5.5.2. Sensors Instrumentation

Sensors and a surveillance camera were installed to monitor the ECON HPS operation performance. The sensor types for this purpose include temperature sensors (i.e., wired thermocouples and wireless temperature sensors manufactured by Monnit), strain gauges, current sensors, and voltage sensors. Temperature sensors (i.e., wired thermocouples and wireless temperature sensors) can be utilized to continuously monitor ECON HPS temperature responses for activating and deactivating the ECON HPS operations. Strain gauges can be installed as well to capture the strain behavior of the ECON slabs under diurnal and seasonal environmental loads, the electric heating process, as well as passing vehicles. Furthermore, current sensors and voltage sensors (e.g., wireless electricity monitoring sensors manufactured by Monnit) can also be employed to monitor electric properties for estimating power consumption and operation cost.

Sensor instrumentation locations were chosen based on the critical response locations within a slab with regard to the temperature and strain variations. The temperature trees were mounted on a 0.25 in. (0.6 cm) fiberglass bar in order to eliminate temperature and electricity gradients in different layers. A hole was first drilled in the PCC layer at the center of each slab (see Figure 31c), and the temperature trees were installed inside and secured with cement grout (see Figure 31d). Each temperature tree consisted of six thermocouples in the following locations: top and bottom of the ECON layer, the middle and bottom of the PCC layer, the middle of the base layer, and one sensor in the subgrade layer. The detailed instrumentation processes of the temperature sensors are given in the following steps:

- Step 1: Mark sensor location after base PCC layer hardens
- Step 2: Drill holes at these predetermined locations at desired depth
- Step 3: Pull sensor cables through PVC conduits
- Step 4: Make sensor trees by mounting sensors at a predetermined height on the rods
- Step 5: Insert sensor trees into these holes
- Step 6: Check depth of sensors
- Step 7: Organize sensor cables
- Step 8: Connect sensors to data acquisition system and check sensor survivability

Strain gauges were mounted on the PCC layer using two plastic chairs and steel straps (see Figure 31e). The steel straps were screwed to the PCC layer to secure them. In the case where two strain gauges needed to be placed at different depths, two 0.25 in. (0.6 cm) fiberglass bars were used to place and secure the strain gauges. The chosen locations of strain gauges were the

46

center, edge, corner in the wheel path direction, and corner in a diagonal direction. The strain gauges were installed both in the ECON layer and PCC layer. The strain gauge configuration was chosen to measure the strain in both layers to monitor the effect of heating in the ECON layer. The detailed instrumentation processes of strain gauges are given in the following steps:

- Step 1: Mark sensor location after base PCC layer hardens
- Step 2: Pull sensor cables through PVC conduits
- Step 3: Set up strain gauges by using plastic chairs
- Step 4: Check strain gauges height
- Step 5: Use the concrete anchor to fix the location of strain gauges
- Step 6: Organize sensor cables
- Step 7: Connect sensors to data acquisition system and check sensor survivability

Sensors wires were guided to a separate PVC pipe to the shed (see Figure 31f). The PVC pipe for electrical wiring was not chosen to host the sensors wires to prevent possible interferences in the sensor signals and for safety purposes.

5.5.3. Integration of Power Supply and Control System

There was no existing power supply source close to the construction site; therefore, a new 45-1 pole with 3-100kVA XFMRS was placed at the southwest corner of the site. A meter was installed on the pole to measure electrical power usage, and a power line trench was excavated from the pole to the shed. This enabled powering the ECON HPS test area using either a three-phase 208 VAC or a single phase 120 VAC, both with a maximum of 600 A source.

Two three-phase double pole power panels were installed in the shed with two circuit breakers. Each circuit breaker can feed five slabs with 120/208 VAC. The three-phase 208 VAC was achieved by using two lines, one for each phase, while the 120 VAC was carried in each single line. The 120 VAC was achieved using one line and the neutral. The different electrode configuration design caused each slab to draw a different amount of current compared to the other slabs. Thus, the research team with the assistance of the Iowa DOT and/contractor conducted a series of tests and simulations and grouped the slabs in a way to distribute the power load evenly within each phase and to eliminate overloading on one phase.

Another added feature of using a PLC as a control system is the electrode-based control. The electrode-based control feature gave the research team an extra degree of control to create different electrode configurations (spacing) within one slab by being able to turn on/off individual electrodes. Therefore, the research team added more relays for the test slabs with 10 electrodes (4 slabs) to incorporate this feature. The electrode wiring diagram for the 10 electrode slabs is shown in Figure 32a.
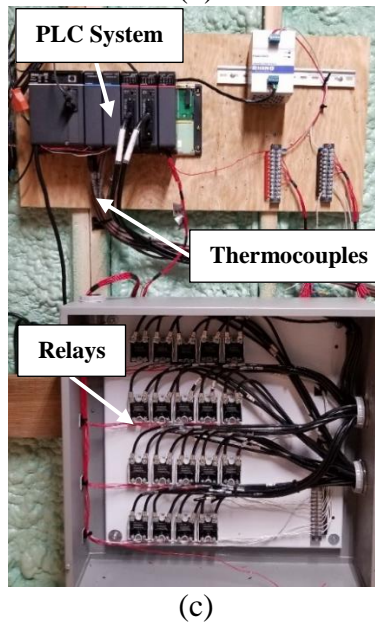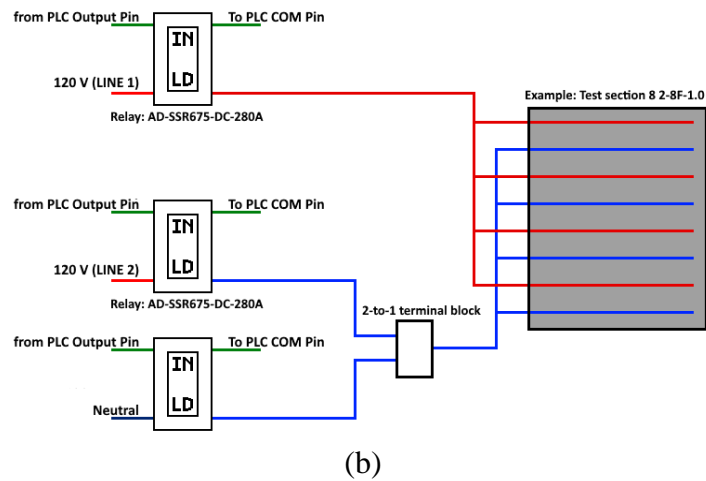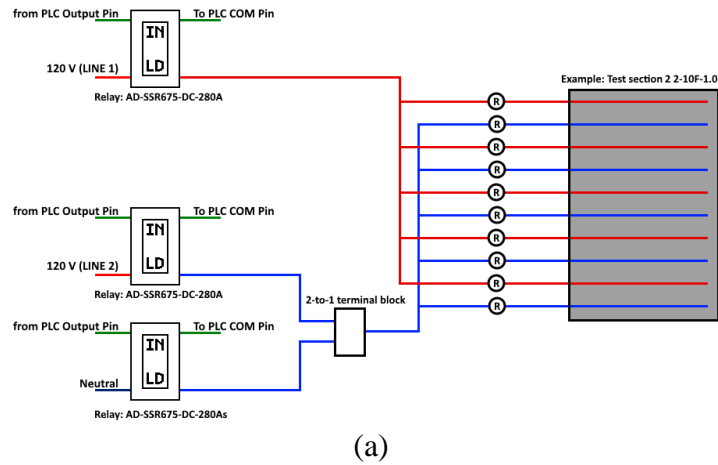
(a)

(b)

(c)

Figure 32. PLC control configurations: (a) electrode-based control, (b) slab-based control, and (c) system and relay wiring

The other six slabs were designed using slab-based control, which only turned on and off all of the electrodes in each slab at once (Figure 32b). The PLC system and its wiring are shown in Figure 32c.

The electrical work mainly conducted by the ISU research team was as follows:

- Prepare the design and programming of the PLC system
- Develop the PLC system hardware
- Test the developed PLC system in the laboratory to ensure the system worked as intended two weeks before installation
- Run initial tests to ensure the system was working properly

The Iowa DOT and/or contractor involved efforts on the electrical work were as follows:

- Confirm power source availability for the ECON HPS construction at least one month prior to construction (Iowa DOT)
- Provide the specification and location of the electric power supply panel at least one month prior to construction (Iowa DOT)
- Provide power outlets near the decided location to power the PLC system and connected laptop (Iowa DOT)
- Decide on the appropriate wire type (American wire gauge [AWG], strand, insulation, etc.) for a source to the electrode connections (Iowa DOT or contractor)
- Connect electrodes to ground conduit and wires to the PLC system (Iowa DOT or contractor)
- Install the PLC hardware into the electrical power supply panel based on the guidelines (Iowa DOT or contractor)
- Connect signal wires from the PLC output module to relays (Iowa DOT or contractor)
- Connect wires from source and wires from electrodes to relays (Iowa DOT or contractor)
- Check the connections of the PLC system to be safe and meet safety protocols (Iowa DOT or contractor)

5.5.4. Managing the Heat Dissipation by Relays

The solid-state relays generate heat, and this heat should be dissipated carefully to protect the relays for ensuring safe ECON HPS operation. To improve the heat transfer for dissipating the generated heat by the relays, the following steps (see Figure 33) were taken:

- Install relays on steel plates to allow for a higher rate of heat transfer through the backside of the relays
- Install cooling fans on the box covers to constantly blow on the relays

Figure 33. Cooling fans installed on the relays

Laboratory tests showed that the maximum measured temperature reached by the relays is about 131°F (55°C), while the allowable working temperature for these relays is 194°F (90°C). The detailed approval procedures for operating the ECON HPS are presented in Appendix B.

5.6. Construction Procedure

Construction started on October 11, 2018 and lasted for four weeks due to the weather conditions. The existing pavement was a 40-year-old PCC pavement with numerous cracks at the joints and midspan. The pavement had also been rehabilitated at several spots because of extensive damages. This parking lot section experiences a high amount of heavily loaded traffic, including 18-wheeler tractors and trailers, given that it's near the entrance of the Iowa DOT receiving station. The full-scale demonstration project was a reconstruction project, and the first task was to remove the existing 6 in. (15.2 cm) concrete pavement. The existing pavement did not have a base layer, and it lacked any drainage system; therefore, a geofabric system was utilized on top of the subgrade, and a 9 in. (22.9 cm) special backfill layer was compacted for the base layer.

The ECON HPS was designed with two layers: 7 in. (17.8 cm) standard PCC layer (bottom layer) and 3 in. (7.6 cm) ECON layer (top layer). The construction steps in sequence are shown in Figure 34.

(a)

(b)

(c)

(d)

(e)

(f)

(g)

(h)

Figure 34. ECON HPS construction steps: (a) place C-3WR-C20 PCC placement, (b) screed PCC layer, (c) install electrodes, (d) place PVC conduit, (e) clean surface, (f) inspect ECON layer, (g) place and compact ECON layer with vibrating screed, and (h) spray curing compound on surface

51

Dowel bars (0.75 in. [1.9 cm] in diameter) were used for proper load transfer between the adjacent slabs at sawn joints. A joint spacing of 15 ft (4.57 m) was designed, and the joints were matched with the surrounding concrete slabs. A vibrating screed was used to compact the PCC layer (Figure 34a). A broom was used perpendicular to the traffic flow after finishing the PCC layer to roughen the surface and increase the bond between the bottom PCC layer and the top ECON layer (Figure 34b). A curing compound was not suggested for curing the PCC layer due to its potential adverse impact on the bond between the two layers; therefore, wet curing using curing blankets was chosen for the bottom PCC layer.

The research team started mounting the electrodes on top of the PCC layer (Figure 34c). The electrodes were first washed and then dried in order to remove any debris or possible oil on their surface. This was an essential step to ensure a good bond between each electrode and the ECON layer. The perimeter of the ECON test sections, where it meets the standard concrete sections, were isolated using expansion joints to minimize any interaction and potential strain build-up with other unheated standard concrete slabs. The strain gauge and thermocouple trees were installed, and their wires were guided to their designated PVC conduits (Figure 34d). The surface of the PCC layer got cleaned using an air blower and damped to ensure a good bond between the two lifts (Figure 34e). A white flag was installed at each sensor location so that the sensors did not get stepped on during the ECON placing (Figure 34f).

The ECON layer was placed on October 25, 2018, and a vibrating screed was used to compact this layer (Figure 34g). After the ECON layer was placed, a curing compound was sprayed on top of the test section (Figure 34h) to prevent moisture loss. The shed was placed in the southwest corner of the test section, and the wires were installed to connect the electrodes to the power supply source. Meanwhile, the joints were cut full depth through the ECON layer to match those in the bottom PCC layer. The last step in the construction phase was to fill the trenches that hold the electrical and sensor PVC conduits with 6 in. (15.2 cm) hot-mix asphalt.

6. IOWA DOT ECON HPS PERFORMANCE EVALUATION

6.1. State of Practice

The current winter maintenance operation conducted by the Iowa DOT ground crew for their parking lot uses eight crews with eight units of snow-removal equipment. It takes the ground crew an average of five hours to remove snow from the entire Iowa DOT parking lot in a typical 2 in. (5 cm) snow event. The ground crew used 10 tons (9 metric tons) of deicing chemicals and sand between January 1, 2019, and February 20, 2019. The ground crew process is to first plow and gather the snow in several designated areas in the parking lot and then apply deicing chemicals and sand to the snow remaining on the pavement. Then, the crew hauls the gathered snow from the designated locations and transfers it to the Iowa DOT south parking lot to ultimately be melted by the sun. The Iowa DOT staff sends several emails to its employees before each snow event asking them to move both personal and Iowa DOT-owned vehicles from the south parking lot to facilitate the winter snow-removal operation.

Throughout the winter season, deicing chemicals usually get transferred to grassy areas, resulting in the surrounding vegetation being killed, and the sand accumulates. Thus, these processes require the ground crew each spring and summer to plant new grasses, especially near the parking lot, and gather the sand that was spread.

This current state of practice for removing ice and snow is time-consuming, labor-intensive, and environmentally unfriendly due to the usage of deicing chemicals.

6.2. First Seasonal Evaluation (2019)

Figure 35 depicts the ECON HPS system performance during February and March 2019.

The resistive heating performance of the ECON HPS was capable of maintaining a snow- and ice-free surface, while the remaining parking lot area was covered with about 2 in. (5 cm) of snow. The depicted snow event in Figure 35 began at 8 p.m. on February 11, 2019, and lasted until 2 a.m. the next day (6 hours), and the average air temperature and relative humidity in this period were 17°F (-8.4°C) and 86%, respectively. The system began operating at 8 p.m. and was capable of melting all the snow by 11 p.m. (3 hours) and maintaining a snow-free surface until the snow event ended. Appendix C was developed to show the step-by-step procedure of how to use the PLC program to operate the ECON HPS system.

The power density (P) is the amount of energy consumed by each slab per unit area, and it was calculated using the average current usage (I) and the voltage applied to the slabs during a snow event. The applied voltage for the operation was chosen to be 120 VAC for the ECON HPS performance evaluation. The power density range for all the slabs was between 10.2 W/ft^2 (109.8 W/m^2) and 45.6 W/ft^2 (491.5 W/m^2), with an average of 24.6 W/ft^2 (265.1 W/m^2).

(a)   (b)

(c)   (d)
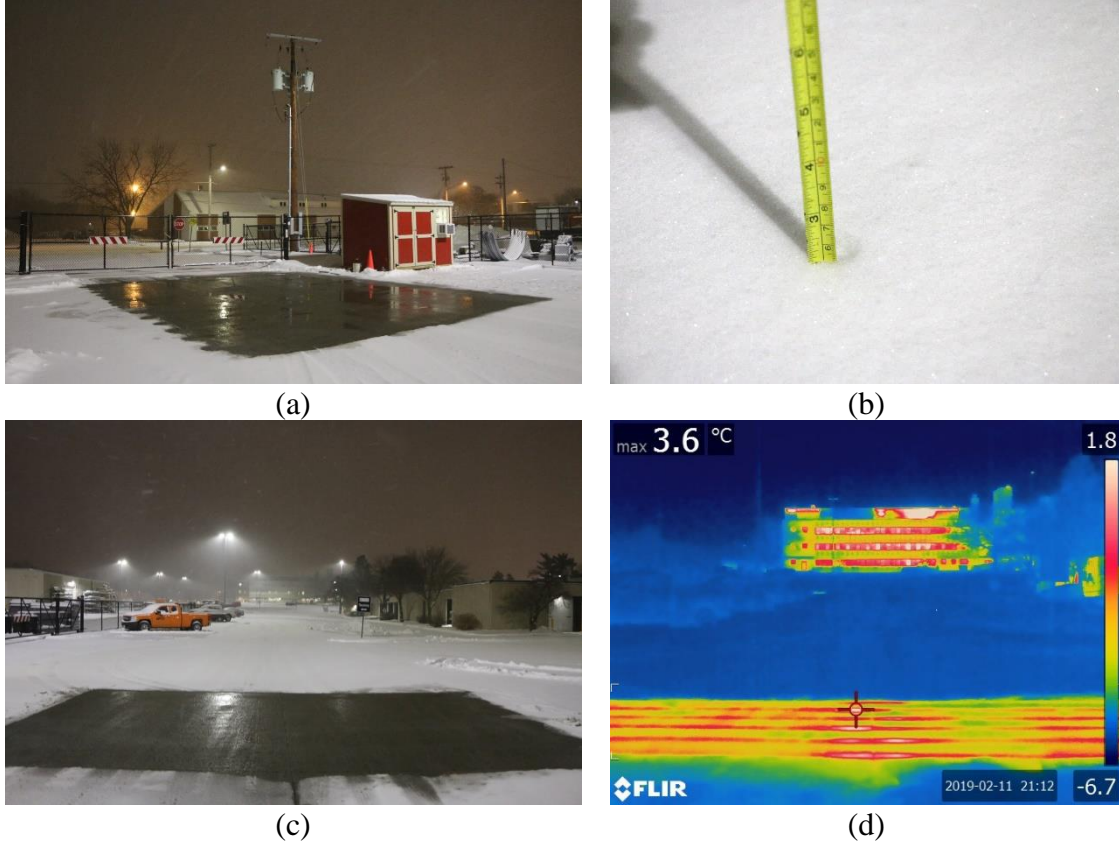
Figure 35. ECON HPS heating performance: (a) southside slabs performance, (b) 2 in. (5 cm) of snow accumulation on surrounding slabs, (c) northside slab performance, and (d) infrared thermography (°F = [°C × 1.8] + 32)

Given resistivity variation due to carbon fiber dispersion within each test section was observed among the slabs, to compare the power demand for each electrode configuration independent of slab electrical resistivity, the power density was normalized by the resistivity measurement for each slab. This normalization was necessary given the effect of resistivity is the linear inverse of that of power density, meaning that a slab with higher resistivity has a lower power density and vice versa. This normalization was essential to determine only the effect of electrode configuration and eliminate the effect of ECON resistivity on the analysis. The normalized power density for each test section and slab surface temperatures while in operation are shown in Figure 36 and Figure 37, respectively.
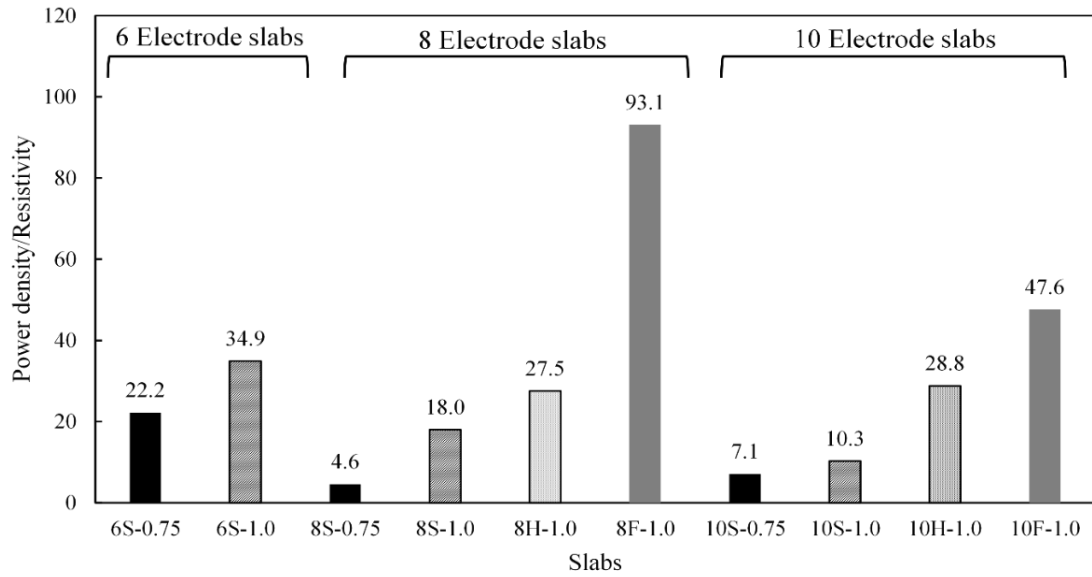
Figure 36. Power density per square feet per resistivity of each slab
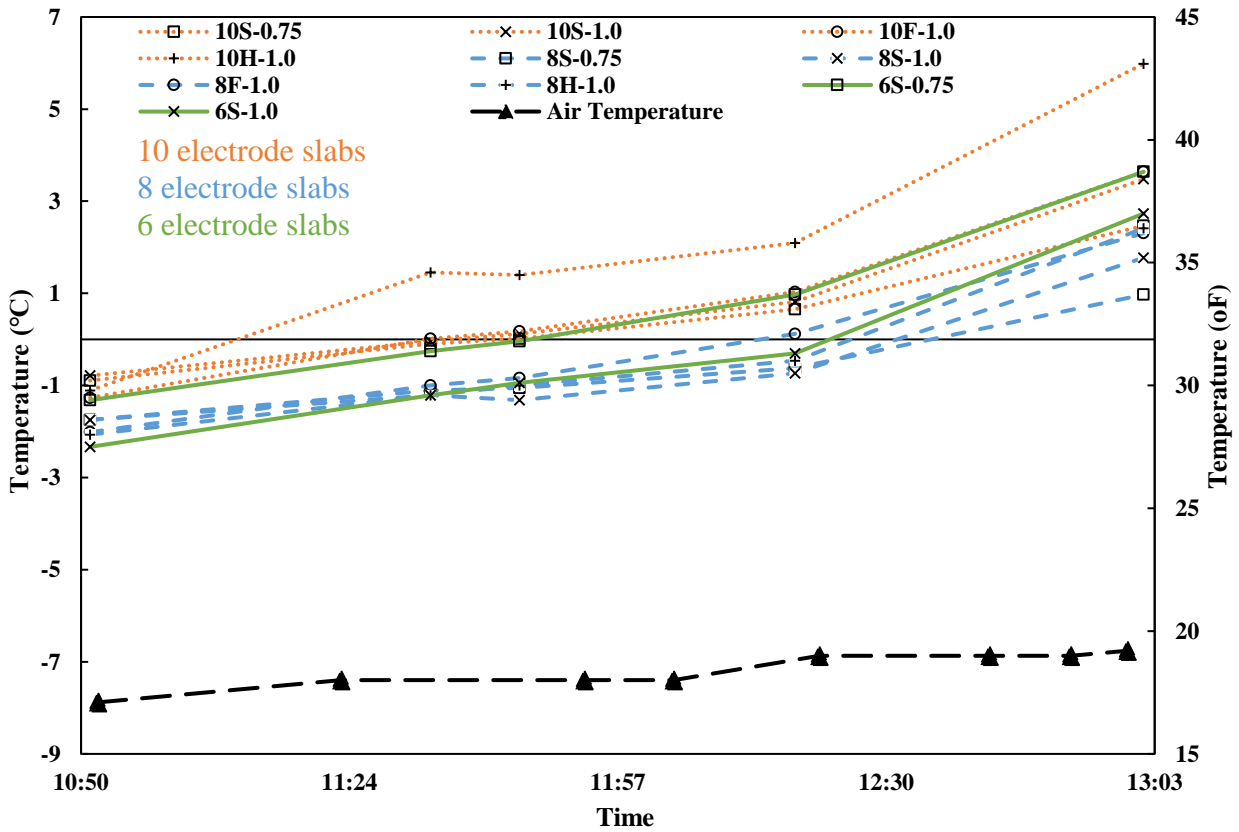
Figure 37. Slab surface temperature and air temperature vs. time

As shown in Figure 37, the electrode configuration directly affects the power density. In all cases, a flat bar, a 1.0 in. (2.5 cm) hollow bar, a 1.0 in. (2.5 cm) solid bar, and a 0.75 in. (1.9 cm) solid bar have the same trend that power density decreases when the number of electrodes increases. However, the flat bar has the highest and the 0.75 in. (1.9 cm) solid bar the lowest power density. It was also found that by increasing the electrode diameter in circular solid bars from 0.75 in. (1.9 cm) to 1.0 in. (2.5 cm), the power density increased in all different spacing options, due to the increase in the contact area between the electrode and the ECON layer. The power density was also decreased for the flat bar and the 1.0 in. (2.5 cm) circular solid bar by decreasing the spacing (increasing the number of electrodes within a slab).

Figure 37 shows the thermal performance of each slab and air temperature versus time. These data were gathered from thermocouples placed 0.5 in. (1.3 cm) below the pavement surface. The temperature in each slab increased after the slab was energized, but after some time, the slab temperature stayed constant due to melting snow on the surface (phase change). The 10H-1.0 slab exhibited the highest temperature increase (13.3°F [7.4°C] in two hours), while the 8S-0.75 slab exhibited the lowest. The average temperature rise for all the slabs was 9°F (5°C) in two hours. The slabs with 8 electrodes exhibited inferior heating performance compared to those with 10 electrodes.

6.3. Second Seasonal Evaluation (2020)

The ECON HPS slabs' thermal performance was evaluated during the 2019–2020 winter season, and the results are depicted in Figure 38.
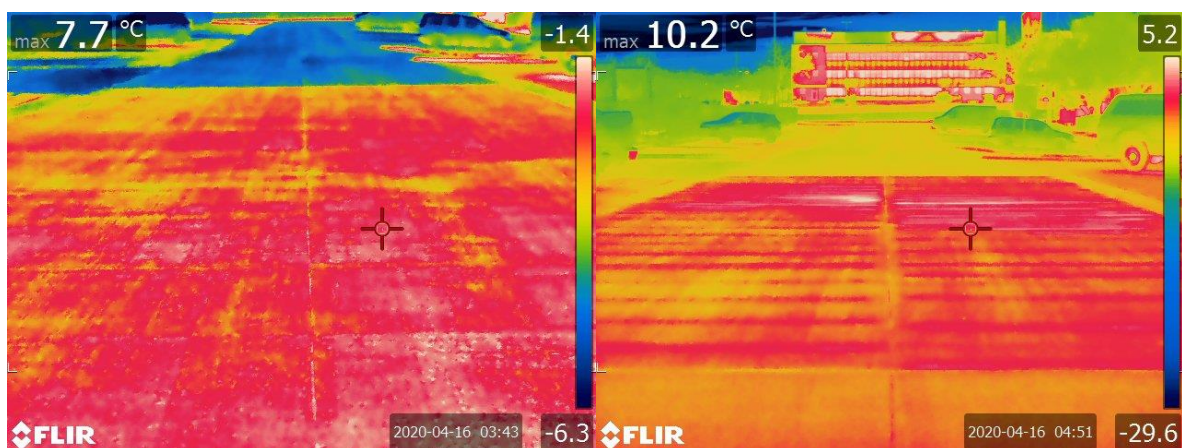
Figure 38. Thermal performance of ECON HPS slabs in the second seasonal evaluation
(°F = [°C × 1.8] + 32)

Figure 39 depicts current measurements drawn from each slab during the second seasonal evaluation.
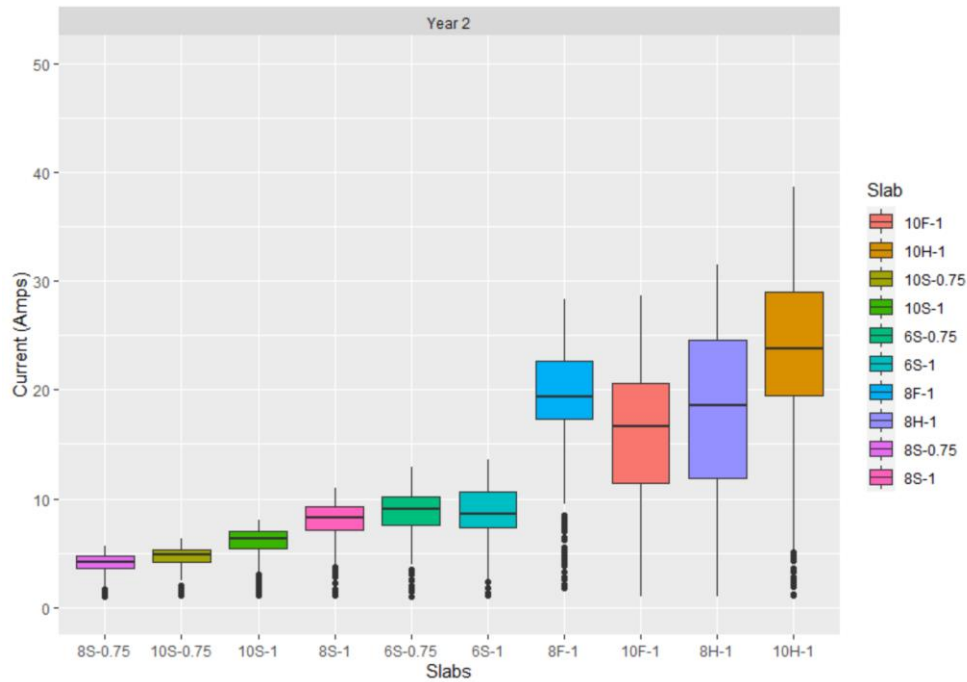
Figure 39. Second year current measurements of each slab

These data were used to calculate the power density for each slab shown in Figure 40, with higher power density translating to higher thermal performance.
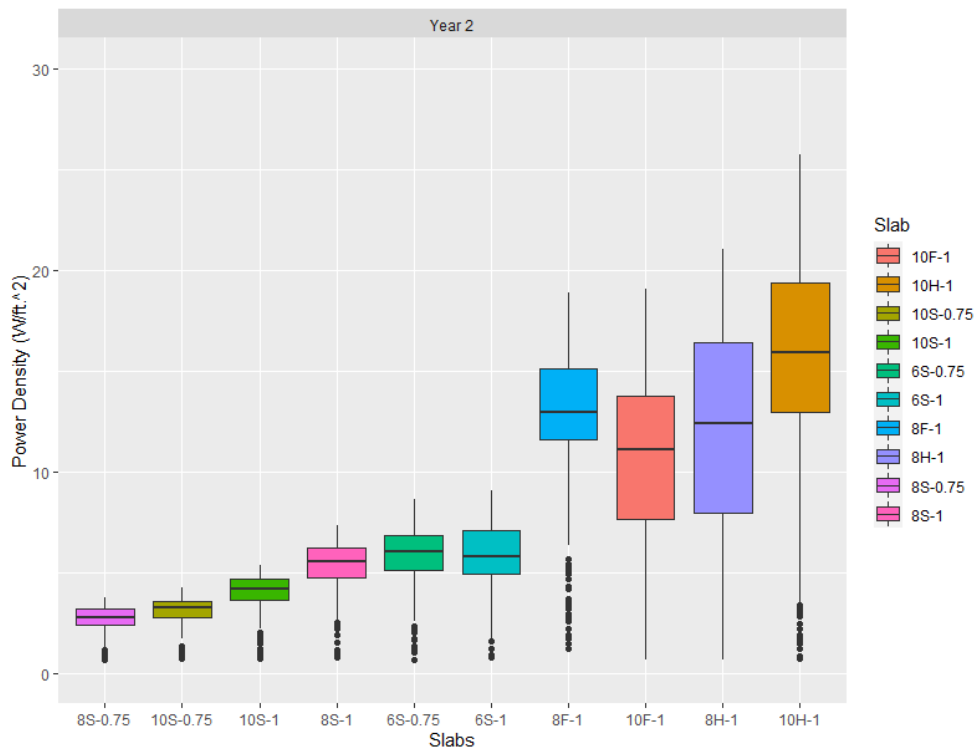
Figure 40. Second year power density measurements of each slab

57

Slab 10H-1 exhibited the highest and best thermal performance, while slab 8S-0.75 exhibited the poorest thermal performance among the 10 different design configurations. Figure 41 shows the measured resistivity of the 10 slabs during this seasonal evaluation.
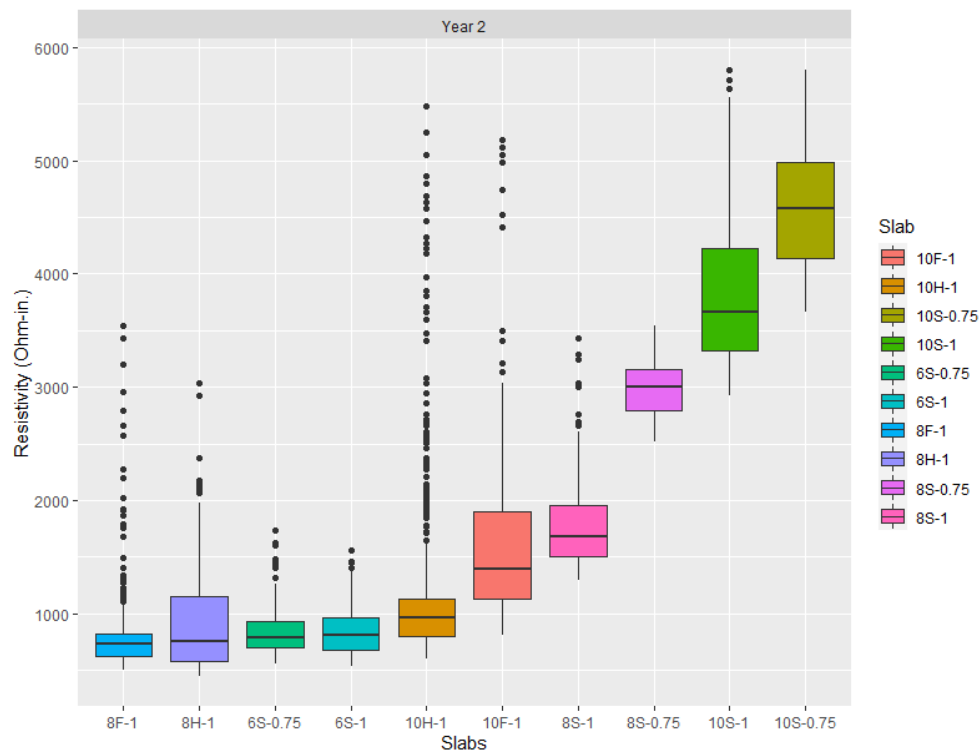
Figure 41. Second year slab resistivity measurements

Comparing the resistivity and power density data shows a clear relationship between resistivity and power density. Slabs with higher resistivity generated less power density and lower thermal performance, and vice versa.

6.4. Third Seasonal Evaluation (2021)

The ECON HPS slabs' thermal performance, also evaluated during the 2020–2021 winter season, are depicted in Figure 42.
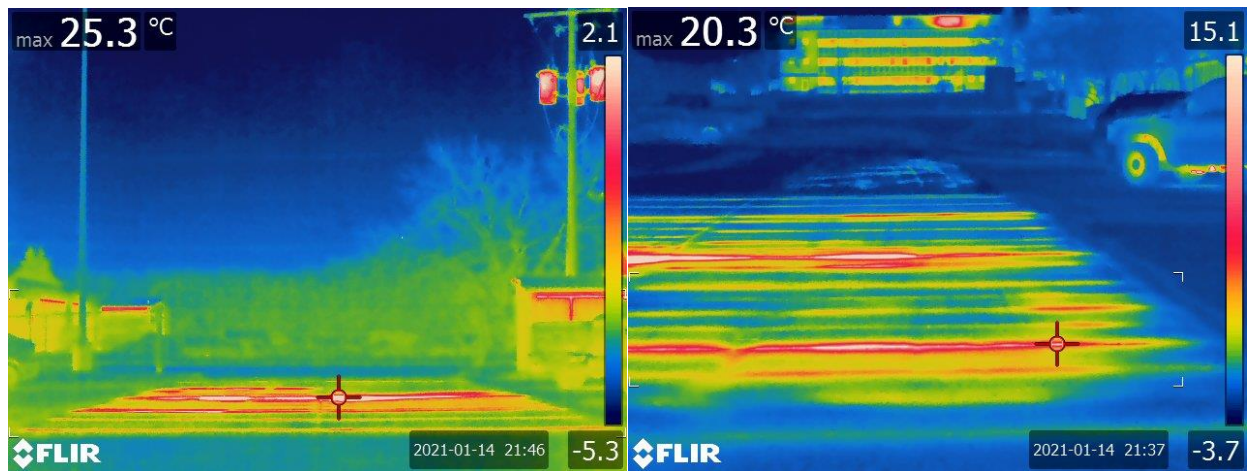
Figure 42. Thermal performance of ECON HPS slabs in the third seasonal evaluation (°F = [°C × 1.8] + 32)

Figure 43 depicts current measurements drawn from each slab during the third seasonal evaluation.
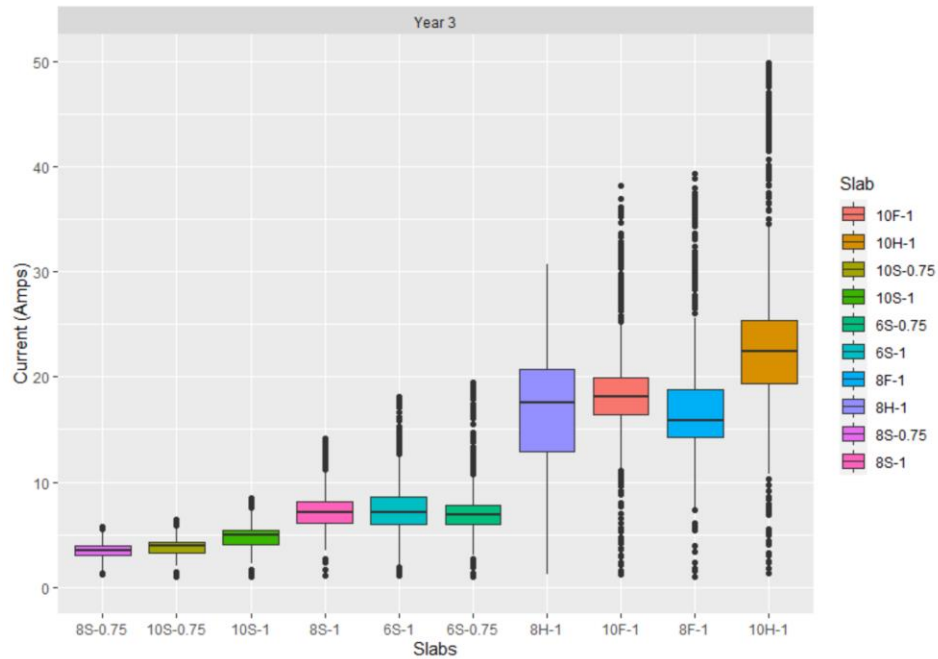
Figure 43. Third year current measurements of each slab

These data were used to calculate the power density shown in Figure 44 for each slab, with higher power density translating to higher thermal performance.
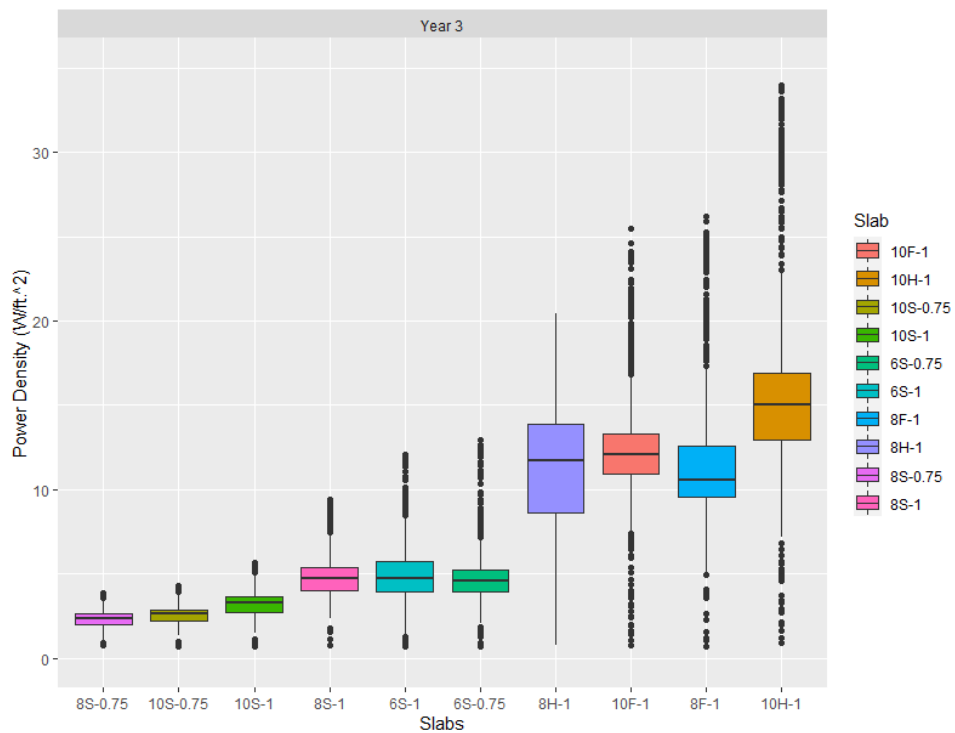
Figure 44. Third year power density measurements of each slab

Similar to observations from the second seasonal evaluation, slab 10H-1 exhibited the highest and best thermal performance while slab 8S-0.75 exhibited the poorest thermal performance slab among the 10 different design configurations. Figure 45 shows the measured resistivity of the 10 slabs in the third seasonal evaluation.
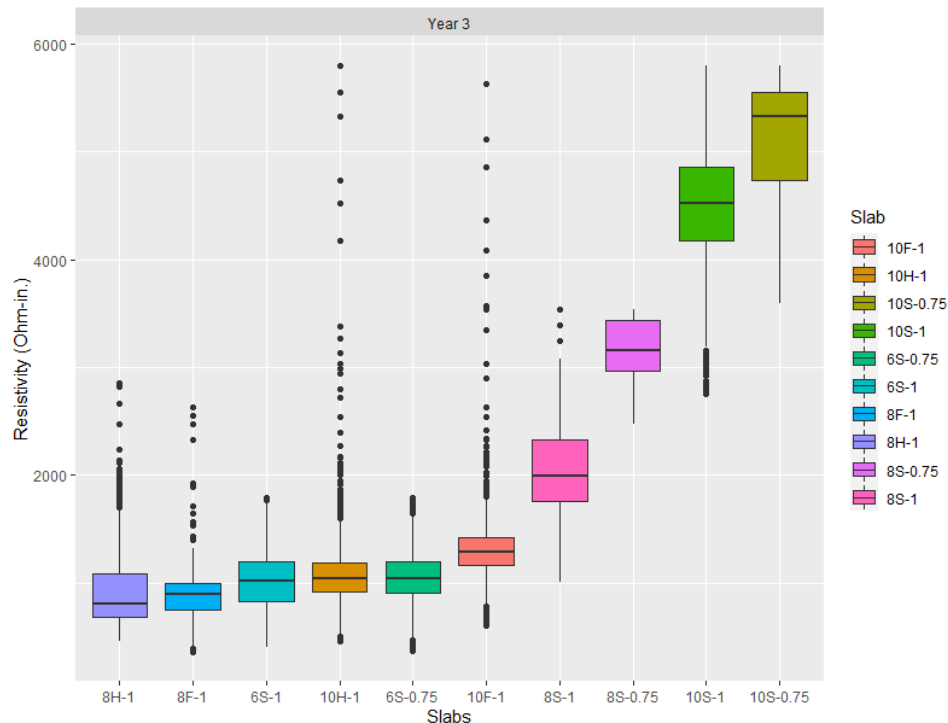
Figure 45. Third year resistivity measurements of each slab

Comparing the resistivity and power density data shows a clear relationship between resistivity and power density. Slabs with higher resistivity generated less power density and lower thermal performance, and vice versa.

6.5. Structural Evaluation

A structural evaluation of both the control and heated sections at the Iowa DOT test site was performed on September 30, 2019, using falling weight deflectometer (FWD) testing. An Iowa DOT FWD vehicle was used to perform the FWD testing with assistance from the Iowa DOT's special investigations section, as shown in Figure 46.

Figure 46. Iowa DOT FWD vehicle

The FWD load levels were 9 kips (40 kN), 12 kips (53.4 kN), and 15 kips (66.7 kN), with the loads applied both at the slab centers and at joints. The average FWD deflection plot for both the control and heated slabs is shown in Figure 47.

	D-12	D0	D8	D12	D18	D24	D36	D48	D60
Normal	3.93	4.17	4.02	3.90	3.71	3.50	2.99	2.34	1.88
Heated	3.51	3.75	3.61	3.50	3.36	3.14	2.63	2.20	1.77
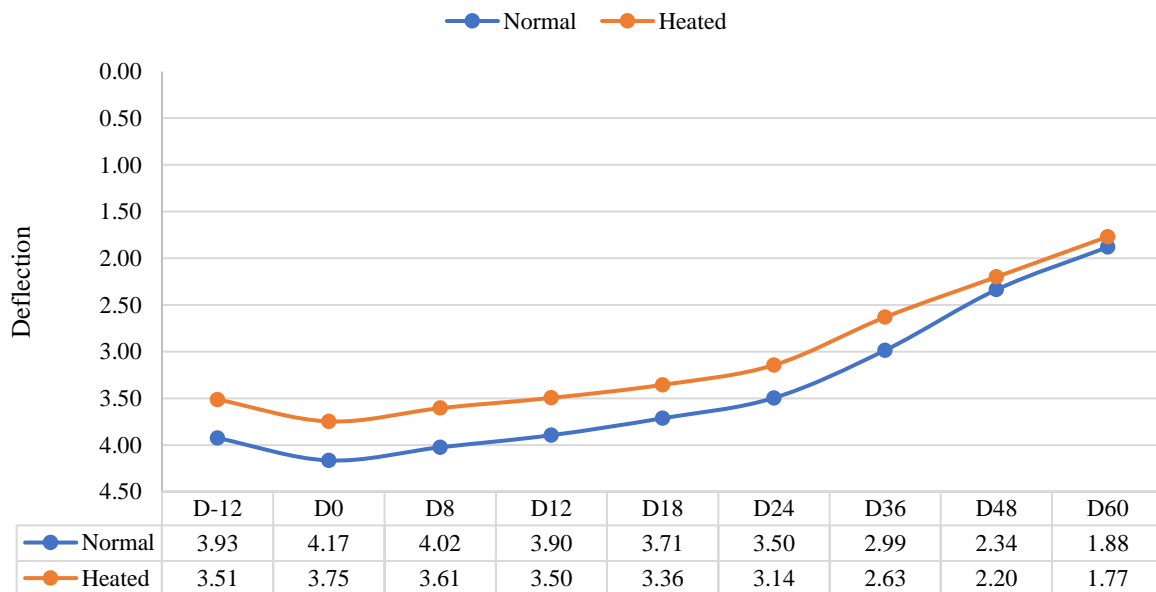
Figure 47. Average FWD deflection plot for both the control and heated slabs

The average heated-slab deflection is about 10% lower than for the control slabs, indicating that the heated slabs are stiffer with a higher modulus. BAKFAA 3.3.0 software (FAA 2020) was used for back-calculation, and the average back-calculated modulus values for the heated and control slabs were 5.5 million psi (38,000 million Pa) and 4.1 million psi (28,000 million Pa), respectively.

The average load transfer efficiency (LTE) was about 90% for both the heated and control slabs. It is worth mentioning that while the control slabs had 1.5 in. (3.81 cm) diameter dowel bars and the heated slabs had ¾ in. (1.9 cm) diameter dowel bars, this difference in dowel bar thickness did not result in any significant changes in the slab LTE value. In addition, no cracking was observed in the ECON HPS slabs after 3 years of monitoring. However, a crack was generated on a standard concrete pavement on the south side of the ECON HPS slabs after 1 year of construction. The ECON HPS slabs were located in a heavy loading area due to close proximity to the distribution center receiving line at the Iowa DOT.

7. SUMMARY, CONCLUSIONS, AND RECOMMENDATIONS

7.1. Conclusions

The objective of this study was to demonstrate the design, full-scale demonstration, and performance monitoring of the largest operational ECON HPS. Ten ECON HPS test slabs were designed and constructed at the south parking lot of the Iowa DOT headquarters in Ames, Iowa, during October 2018. A PLC system and slab instrumentation using temperature sensors were designed and implemented for remote-control operation and system performance monitoring. Deicing and anti-icing ECON HPS performance was evaluated during the 2018–2021 winter seasons.

The summarized findings of this study are as follows:

- Ten ECON HPS test slabs with various electrode configurations were constructed in the south parking lot of the Iowa DOT headquarters as the largest ECON HPS implementation project. All the test slabs showed promising snow- and ice-free capabilities during various winter weather events.

- Each ECON HPS test slab had a different electrode configuration in terms of electrode shape, size, and spacing. The flat bar, the 1.0 in. (2.5 cm) hollow bar, the 1.0 in. (2.5 cm) solid bar, and the 0.75 in. (1.9 cm) solid bar have the same trend that power density decreases when the number of electrodes increases. However, the flat bar has the highest and the 0.75 in. (1.9 cm) solid bar has the lowest power density among all the different spacing options.

- The power density range for all the slabs was between 10.2 W/ft^2 (109.8 W/m^2) and 45.6 W/ft^2 (491.5 W/m^2), with an average of 24.6 W/ft^2 (265.1 W/m^2). The power density normalized to the resistivity of each ECON HPS slab ranged between 0.42 W/ft^2 (4.6 W/m^2) (slab 8S-0.75) and 8.6 W/ft^2 (93.1 W/m^2) (slab 8F-1).

- Increasing the electrode diameter in circular solid bars resulted in an increase in power density in all electrode spacing.

- The power density was decreased in the flat bar and 1.0 in. (2.5 cm) circular solid bar slabs by decreasing the electrode spacing (increasing the number of the electrodes used in each slab).

- Based on the theory, the laboratory studies, and the FE models, the temperature increase rate of an electrode is influenced by its surface contact area (perimeter).

- A theoretical formulation was developed to describe the ECON HPS thermal behavior.

- An increase in electrode size resulted in an increase in energy conversion efficiency.

- FWD testing showed that the average heated pavement deflections were about 10% lower than those of regular concrete pavement slabs, indicating that the heated slabs were stiffer with a higher modulus.

- The slope of the temperature increase rate versus the perimeter curve for different electrodes was found to be identical in both water and ECON prototype slab tests.

- Flat-bar orientation (vertical versus horizontal) did not significantly change the heating performance of the electrodes according to water tests.

- The PLC exhibited better control flexibility than Arduino board microcontrollers in terms of autonomous control, expandability, and control capability.

7.2. Recommendations for Implementation and Future Research Directions

The findings of this study facilitate the design of an ECON HPS and provide detailed information on the construction steps. The following recommendations have been drawn from this study to facilitate the design and construction of future ECON HPS implementations:

- A designed, programmed, and implemented PLC system was found to be a promising and robust remote-control system to be used in ECON HPS technology.

- Testing electrodes in water for monitoring the temperature increase rate is a faster, repeatable, nondestructive, and cost-effective method for identifying favorable electrode sizes and comparing electrode performance for an ECON HPS.

- Considering initial costs of the electrodes, flat-bar and smaller-diameter electrodes were found to be more cost-effective than the larger electrodes due to the lower cost of smaller-sized electrodes relative to the temperature increase rates associated with them.

- Use of 20% fly ash Class C replacement and removal of methylcellulose and DCI admixtures helped improve the slump to 3.9 in. (10 cm) during the Iowa DOT project ECON placement.

- If sensors are to be incorporated into the ECON HPS design, their tips and cables must be electrically insulated and thermally operational.

- Using multiple voltages with the PLC control device gave ECON HPS users control over snow- and ice-melting speed.

- Premature cracking due to the use of an angle-shaped electrode can be eliminated by incorporating circular or flat-bar electrode shapes.

- The paths followed by water produced as the result of melting ice and snow from the heated slabs to the drainage outlet must be heated to eliminate ice formation near the heated slabs.

- The best operational practice of heated pavements is to turn the system on before the snow event starts so that snow accumulation will not occur and operation time and consequent operation cost will decrease.

Other applications and the rationale for prioritization among critical areas of Iowa transportation infrastructure systems for ECON HPS implementations, identified as being of interest to the Iowa DOT and Iowa county and city engineers, are discussed as follows:

- **Bridge decks**
  - Bridges are the first locations in a highway system to freeze during the winter season. Thin layers of black ice and frost form on top of the bridge deck, potentially resulting in vehicles sliding off the bridge and causing fatal crashes. Many highway agencies dedicate portions of their winter maintenance budget to deicing these locations (so-called frost-run operations) that help mitigate this hazard. Entrance and exit ramps on the highway system are also potential winter hazards due to higher vehicle speeds and the potential to slide off the ramp.

  - Given these frost-run operations are typically on bridges located over a body of water, resulting in a direct chloride load into the water system, heated-bridge technology can mitigate direct chloride load into nearby water bodies.

  - During this study, several highway agencies, such as those in Iowa and Wisconsin, have expressed strong interest in implementation of heated-bridge technology.

- **Rest areas**
  - Rest areas, specifically on interstate highway systems, experience high foot traffic throughout the year, and they are typically located in areas that would not be easily accessible to winter maintenance crews to clear the snow and ice in a timely manner.

  - ECON HPS technology is in full compliance with the Americans with Disabilities Act (ADA) mission to ease the commute of individuals with disabilities, especially during the winter season. Based on data from the U.S. Bureau of Labor Statistics, about 25% of ice- and snow-related falls occur in parking lots. Snow and ice can cause significant hardship for individuals with disabilities, and implementing heated pavement on parking lots and ramps could be a way to mitigate this hardship. In addition, the Iowa DOT has received dedicated funding for ADA-compliance projects that can be used to further implement ECON HPS, facilitating the contribution of people with disabilities to our society.

The versatility of the ECON HPS technology demonstrated for roadway application in this study is such that it can be custom-designed and optimized for each specific transportation infrastructure application depending on need and interest. This versatility stems from the fact that

the ECON HPS technology can be implemented as either a conductive concrete surface for a new construction project or a conductive concrete overlay on top of an existing structure for a rehabilitation project. However, the ECON HPS design requirements and considerations are somewhat different for each specific application, warranting detailed research investigations before being fully implemented in each situation. Therefore, pursuit of future research directions from this study is recommended to develop and implement custom-designed and optimized ECON HPS technology for each prioritized application area identified (i.e., bridge decks and rest areas).

REFERENCES

Abdualla, H. 2018. *Design, Construction, and Performance of Heated Concrete Pavements System*. PhD dissertation. Iowa State University, Ames, IA. https://lib.dr.iastate.edu/cgi/viewcontent.cgi?article=7275&context=etd.

Abdualla, H., H. Ceylan, S. Kim, K. Gopalakrishnan, P. C. Taylor, and Y. Turkan. 2016. System Requirements for Electrically Conductive Concrete Heated Pavements. *Transportation Research Record: Journal of the Transportation Research Board*, No. 2569, pp. 70–79.

Abdualla, H., H. Ceylan, S. Kim, M. Mina, K. S. Cetin, P. C. Taylor, K. Gopalakrishnan, B. Cetin, S. Yang, and A. Vidyadharan. 2018. Design and Construction of the World's First Full-Scale Electrically Conductive Concrete Heated Airport Pavement System at a U.S. Airport. *Transportation Research Record: Journal of the Transportation Research Board*, Vol. 2672, No. 23, pp. 82–94.

Abdualla, H., H. Ceylan, S. Kim, M. Mina, K. Gopalakrishnan, A. Sassani, P. C. Taylor, and K. S. Cetin. 2017. Configuration of Electrodes for Electrically Conductive Concrete Heated Pavement Systems. *Airfield and Highway Pavements 2017*, International Conference on Highway Pavements and Airfield Technology 2017, August 27–30, Philadelphia, PA, pp. 1–9.

Alimohammadi, H. and B. Izadi Babokani. 2019. Finite Element Analysis of a Piezoelectric Layered Plate with Different Materials. *International Journal of Engineering and Applied Sciences (IJEAS)*, Vol. 6, No. 8, pp. 18–21.

ANSYS, Inc. 2018. Ansys software.

Arabzadeh, A., H. Ceylan, S. Kim, K. Gopalakrishnan, A. Sassani, S. Sundararajan, P. C. Taylor, and A. Abdullah, A. 2017a. Influence of Deicing Salts on the Water-Repellency of Portland Cement Concrete Coated with Polytetrafluoroethylene and Polyetheretherketone. *Airfield and Highway Pavements 2017*, International Conference on Highway Pavements and Airfield Technology 2017, August 27–30, Philadelphia, PA, pp. 217–227.

Arabzadeh, A., H. Ceylan, S. Kim, K. Gopalakrishnan, A. Sassani, S. Sundararajan, and P. C. Taylor. 2017b. Superhydrophobic Coatings on Portland Cement Concrete Surfaces. *Construction and Building Materials*, Vol. 141, pp. 393–401.

Arabzadeh, A., H. Ceylan, S. Kim, A. Sassani, and K. Gopalakrishnan. 2018. Investigating the Heat Generation Efficiency of Electrically-Conductive Asphalt Mastic Using Infrared Thermal Imaging. *International Conference on Transportation and Development 2018*, July 15–18, Pittsburgh, PA, pp. 206–214.

Arabzadeh, A., M. A. Notani, A. Kazemiyan Zadeh, A. Nahvi, A. Sassani, and H. Ceylan. 2019. Electrically Conductive Asphalt Concrete: An Alternative for Automating the Winter Maintenance Operations of Transportation Infrastructure. *Composites Part B: Engineering*, Vol. 173, Article no. 106985, pp. 1–13.

ASHRAE. 2009. Snow Melting and Freeze Protection. *ASHRAE Handbook: Fundamentals*. American Society of Heating, Refrigerating, and Air-Conditioning Engineers, Atlanta, GA.

ASTM A240/A240M. 2017. *Standard Specification for Chromium and Chromium-Nickel Stainless Steel Plate, Sheet, and Strip for Pressure Vessels and for General Applications*. ASTM International, West Conshohocken, PA.

ASTM A66-15. 2015. *Standard Specification for Annealed or Cold-Worked Austenitic Stainless Steel Sheet, Strip, Plate, and Flat Bar*. ASTM International, West Conshohocken, PA.

Baskas, H. 2011. Winter Survival Strategies from the USA's Snowiest Airports. *USA Today*.

Bolen, W. P. 2020. Salt. *U.S. Geological Survey Mineral Commodity Summaries*, pp. 138–139.

Ceylan, H., K. Gopalakrishnan, S. Kim, and W. Cord. 2014. *Heated Transportation Infrastructure Systems: Existing and Emerging Technologies*. 12th International Symposium on Concrete Roads, September 23–26, Prague, Czech Republic. https://lib.dr.iastate.edu/cgi/viewcontent.cgi?article=1018&context=ccee_conf.

Chen, W. and P. Gao. 2012. Performances of Electrically Conductive Concrete with Layered Stainless Steel Fibers. *Sustainable Construction Materials 2012*, Second International Conference on Sustainable Construction Materials: Design, Performance, and Application, October 18–22, Wuhan, China, pp. 164–172.

Farnam, Y., M. Krafcik, L. Liston, T. Washington, K. Erk, B. Tao, and J. Weiss. 2016. Evaluating the Use of Phase Change Materials in Concrete Pavement to Melt Ice and Snow. *Journal of Materials in Civil Engineering*, Vol. 28, No. 4, Article no. 04015161.

FAA. 2020. Airport Safety Detail. BAKFAA 3.3.0. Federal Aviation Administration. https://www.airporttech.tc.faa.gov/Products/Airport-Safety-Papers-Publications/Airport-Safety-Detail/ArtMID/3682/ArticleID/11/BAKFAA-version-2101.

FHWA. 2017. FHWA Road Weather Management, How Do Weather Events Impact Roads? Federal Highway Administration. https://ops.fhwa.dot.gov/weather/q1_roadimpact.htm.

Forintos, N. and T. Czigany. 2019. Multifunctional Application of Carbon Fiber Reinforced Polymer Composites: Electrical Properties of the Reinforcing Carbon Fibers – A Short Review. *Composites Part B: Engineering*, Vol. 162, pp. 331–343.

Gomis, J., O. Galao, V. Gomis, E. Zornoza, and P. Garcés. 2015. Self-Heating and Deicing Conductive Cement. Experimental Study and Modeling. *Construction and Building Materials*, Vol. 75, pp. 442–449.

Gong, T., S. P. Peng, R. Y. Bao, W. Yang, B. H. Xie, and M. B. Yang. 2016. Low Percolation Threshold and Balanced Electrical and Mechanical Performances in Polypropylene/Carbon Black Composites with a Continuous Segregated Structure. *Composites Part B: Engineering*, Vol. 99, pp. 348–357.

Gopalakrishnan, K., H. Ceylan, S. Kim, S. Yang, and H. Abdualla. 2015. Electrically Conductive Mortar Characterization for Self-Heating Airfield Concrete Pavement Mix Design. *International Journal of Pavement Research and Technology*, Vol. 8, No. 5, pp. 315–324.

Guo, S., R. Si, Q. Dai, Z. You, Y. Ma, and J. Wang. 2019. A Critical Review of Corrosion Development and Rust Removal Techniques on the Structural/Environmental Performance of Corroded Steel Bridges. *Journal of Cleaner Production*, Vol. 233, pp. 126–146.

Habibzadeh-Bigdarvish, O., X. Yu, G. Lei, T. Li, and A. J. Puppala. 2019. Life-Cycle Cost-Benefit Analysis of Bridge Deck De-Icing Using Geothermal Heat Pump System: A Case Study of North Texas. *Sustainable Cities and Society*, Vol. 47, Article no. 101492, pp. 1–13.

Heymsfield, E., A. B. Osweiler, R. P. Selvam, and M. Kuss. 2013. *Feasibility of Anti-Icing Airfield Pavements Using Conductive Concrete and Renewable Solar Energy*. Federal Aviation Administration, Washington, DC.

Ho, C. Y., and T. K. Chu. 1977. *Electrical Resistivity and Thermal Conductivity of Nine Selected AISI Stainless Steels*. Thermophysical and Electronic Properties Information Analysis Center, Center for Information and Numerical Data Analysis and Synthesis, Purdue University, West Lafeyette, IN.

Hou, Z., Z. Li, and J. Wang. 2007. Electrical Conductivity of the Carbon Fiber Conductive Concrete. *Journal of Wuhan University of Technology-Material Science Edition*, Vol. 22, No. 2, pp. 346–349.

Iowa DOT. n.d. *Iowa DOT Standard Specification with GS-15008 Revisions*. Iowa Department of Transportation, Ames, IA.

IEM. 2019. ASOS Network, ASOS-AWOS-METAR Data Download. Iowa Environmental Mesonet, Iowa State University, Ames, IA. https://mesonet.agron.iastate.edu/request/download.phtml?network=TX_ASOS.

Jamil, A., S. Riaz, M. Ashraf, and M. R. Foolad. 2011. Gene Expression Profiling of Plants Under Salt Stress. *Critical Reviews in Plant Sciences*, Vol. 30, No. 5, pp. 435–458.

Kim, M., D. H. Sung, K. Kong, N. Kim, B.-J. Kim, H. W. Park, Y.-B. Park, M. Jung, S. H. Lee, and S. G. Kim. 2016. Characterization of Resistive Heating and Thermoelectric Behavior of Discontinuous Carbon Fiber-Epoxy Composites. *Composites Part B: Engineering*, Vol. 90, pp. 37–44.

De Langhe, K., E. Struyf, C. Sys, E. Van de Voorde, and T. Vanelslander. 2013. Economic Effects of a Temporary Shutdown of an Airport - Review and Case Study. *Proceedings of the WCTR 2013 Conference, the 13th World Conference on Transport Research*, Rio de Janeiro, Brazil, pp. 1–31.

Liang, J. Z. and Q. Q. Yang. 2017. Effects of Carbon Fiber Content and Size on Electric Conductive Properties of Reinforced High Density Polyethylene Composites. *Composites Part B: Engineering*, Vol. 114, pp. 457–466.

Liu, T. J.-C. 2017. Numerical Analysis of Joule Heating Behavior and Residual Compressive Stress around Crack Tip under High Electric Load. *Modelling and Simulation in Engineering*, Vol. 2017, pp. 1–9.

Malakooti, A. 2017. *Investigation of Concrete Electrical Resistivity As a Performance Based Test*. MS thesis. Utah State University, Logan, UT.

Malakooti, A., M. Maguire, and R. J. Thomas. 2018. *Evaluating Electrical Resistivity as a Performance Based Test for Utah Bridge Deck Concrete*. Center for Advanced Infrastructure and Transportation, Rutgers, The State University of New Jersey, Piscataway, NJ.

Malakooti, A., R. J. Thomas, and M. Maguire. 2019. *Investigation of Concrete Electrical Resistivity As a Performance Based Test*. Utah State University, Logan, UT.

Malakooti, A., W. S. Theh, S. Sadati, H. Ceylan, S. Kim, M. Mina, K. Cetin, and P. C. Taylor. 2020. Design and Full-Scale Implementation of the Largest Operational Electrically Conductive Concrete Heated Pavement System. *Construction and Building Materials*, Vol. 255, Article no. 119229, pp. 1–11.

Malakooti, A., H. Abdualla, S. Sadati, H. Ceylan, S. Kim, and K. Cetin. 2021. Experimental and Theoretical Characterization of Electrodes on Electrical and Thermal Performance of Electrically Conductive Concrete. *Composites Part B: Engineering,* Article no. 109003, pp. 1–12.

Melugiri-Shankaramurthy, B., Y. Sargam, X. Zhang, W. Sun, K. Wang, and H. Qin. 2019. Evaluation of Cement Paste Containing Recycled Stainless Steel Powder for Sustainable Additive Manufacturing. *Construction and Building Materials*, Vol. 227, Article no. 116696, pp. 1–9.

Mosavi, H., R. Alrashidi, M. Almarshoud, M. H. Alyami, K. A. Riding, C. C. Ferraro, M. D. A. Thomas, and H. DeFord. 2020. Use of Electrical Test Method on Determination Aging Factor of Concrete Incorporating Supplementary Cementitious Materials. *Proceedings of the International Conference of Sustainable Production and Use of Cement and Concrete*, pp. 299–306.

Nahvi, A., S. Sadati, K. Cetin, H. Ceylan, A. Sassani, and S. Kim. 2018. Towards Resilient Infrastructure Systems for Winter Weather Events: Integrated Stochastic Economic Evaluation of Electrically Conductive Heated Airfield Pavements. *Sustainable Cities and Society*, Vol. 41, pp. 195–204.

Nguyen, D.-L., M. Ngoc-Tra Lam, D.-J. Kim, and J. Song. 2020. Direct Tensile Self-Sensing and Fracture Energy of Steel-Fiber-Reinforced Concretes. *Composites Part B: Engineering*, Vol. 183, Article no. 107714, pp. 1–19.

Notani, M. A., A. Arabzadeh, H. Ceylan, S. Kim, and K. Gopalakrishnan. 2019. Effect of Carbon-Fiber Properties on Volumetrics and Ohmic Heating of Electrically Conductive Asphalt Concrete. *Journal of Materials in Civil Engineering*, Vol. 31, No. 9.

O'Donnell, M. J. 2008. *Airport Winter Safety and Operations.* Advisory Circular AC 150/5200-30C. Federal Aviation Administration, Washington, DC.

Rao, R., J. Fu, Y. Chan, C. Y. Tuan, and C. Liu. 2018. Steel Fiber Confined Graphite Concrete for Pavement Deicing. *Composites Part B: Engineering*, Vol. 155, pp. 187–196.

Rao, R., H. Wang, H. Wang, C. Y. Tuan, and M. Ye. 2019. Models for Estimating the Thermal Properties of Electric Heating Concrete Containing Steel Fiber and Graphite. *Composites Part B: Engineering*, Vol. 164, pp. 116–120.

Ravindren, R., S. Mondal, K. Nath, and N. C. Das. 2019. Prediction of Electrical Conductivity, Double Percolation Limit and Electromagnetic Interference Shielding Effectiveness of Copper Nanowire Filled Flexible Polymer Blend Nanocomposites. *Composites Part B: Engineering*, Vol. 164, pp. 559–569.

Sadati, S., K. Cetin, and H. Ceylan. 2017. Numerical Modeling of Electrically Conductive Pavement Systems. *Congress on Technical Advancement 2017*, 17th International Conference on Cold Regions Engineering, September 10–13, Duluth, MN, pp. 111–120.

Sadati, S., K. Cetin, H. Ceylan, A. Sassani, and S. Kim. 2018. Energy and Thermal Performance Evaluation of an Automated Snow and Ice Removal System at Airports Using Numerical Modeling and Field Measurements. *Sustainable Cities and Society*, Vol. 43, pp. 238–250.

Sadati, S., K. S. Cetin, H. Ceylan, and S. Kim. 2019. *A Methodology for Investigating Different Electrode Design Configurations of Electrically Conductive Concrete Heated Pavement Systems*. 98th Transportation Research Board Annual Meeting, January 13–17, Washington, DC.

Sadati, S., K. S. Cetin, H. Ceylan, and S. Kim. 2020a. Energy-Efficient Design of a Carbon Fiber-Based Self-Heating Concrete Pavement System through Finite Element Analysis. *Clean Technologies and Environmental Policy*, Vol. 22, pp. 1145–1155.

Sadati, S., A. Malakooti, K. S. Cetin, H. Ceylan, and S. Kim. 2020b. Proposed Improvements to the Construction of Electrically Conductive Concrete Pavement System Based on Lessons Learned. *Construction Research Congress 2020: Project Management and Controls, Materials, and Contracts*, March 8–10, Tempe, AZ, pp. 1049–1056.

Sassani, A., H. Ceylan, S. Kim, K. Gopalakrishnan, A. Arabzadeh, and P. C. Taylor. 2017. Influence of Mix Design Variables on Engineering Properties of Carbon Fiber-Modified Electrically Conductive Concrete. *Construction and Building Materials*, Vol. 152, pp. 168–181.

Sassani, A., A. Arabzadeh, H. Ceylan, S. Kim, S. Sadati, K. Gopalakrishnan, P. C. Taylor, and H. Abdualla. 2018a. Carbon Fiber-Based Electrically Conductive Concrete for Salt-Free Deicing of Pavements. *Journal of Cleaner Production*, Vol. 203, pp. 799–809.

Sassani, A., H. Ceylan, S. Kim, A. Arabzadeh, P. C. Taylor, and K. Gopalakrishnan. 2018b. Development of Carbon Fiber-Modified Electrically Conductive Concrete for Implementation in Des Moines International Airport. *Case Studies in Construction Materials*, Vol. 8, pp. 277–291.

Thurston, R. E., G. Culver, and J. W. Lund. 1995. Pavement Snow Melting in Klamath Falls - Rehabilitation of the ODOT Well. *Geo-Heat Center Quarterly Bulletin*, Vol. 16, No. 2.

Tian, X. and H. Hu. 2012. Test and Study on Electrical Property of Conductive Concrete. *Procedia Earth and Planetary Science*, Vol. 5, pp. 83–87.

Tian, Z., Y. Li, J. Zheng, and S. Wang. 2019. A State-of-the-Art on Self-Sensing Concrete: Materials, Fabrication and Properties. *Composites Part B: Engineering*, Vol. 177, Article no. 107437, pp. 1–17.

Whittington, H. W., J. McCarter, and M. C. Forde. 1981. The Conduction of Electricity Through Concrete. *Magazine of Concrete Research*, Vol. 33, No. 114, pp. 48–60.

Wu, J., J. Liu, and F. Yang. 2014. *Study on Three-Phase Composite Conductive Concrete for Pavement Deicing*. Transportation Research Board 93rd Annual Meeting, January 12–16, Washington, DC.

Xi, Y. and P. J. Olsgard. 2000. Effects of De-Icing Agents (Magnesium Chloride and Sodium Chloride) on Corrosion of Truck Components. Colorado Department of Transportation Research Branch, Denver, CO.

Xie, P. and J. J. Beaudoin. 1995. Electrically Conductive Concrete and Its Application in Deicing. *Proceedings of the Second Canadian Centre for Mineral and Energy Technology (CANMET)/American Concrete Institute (ACI) International Symposium*, Vol. 154, pp. 399–418.

Zhang, W., Q. Zheng, A. Ashour, and B. Han. 2020. Self-Healing Cement Concrete Composites for Resilient Infrastructures: A Review. *Composites Part B: Engineering*, Vol. 189, Article no. 107892, pp. 1–28.

APPENDIX A. DRAFT STANDARD SPECIFICATION FOR ECON HPS CONSTRUCTION AT THE IOWA DOT SOUTH PARKING LOT

A.1. Description

An electrically conductive concrete (ECON) heated pavement system (HPS) functions by applying an electric current through electrodes embedded in a top-layer ECON layer (Figure A-1).
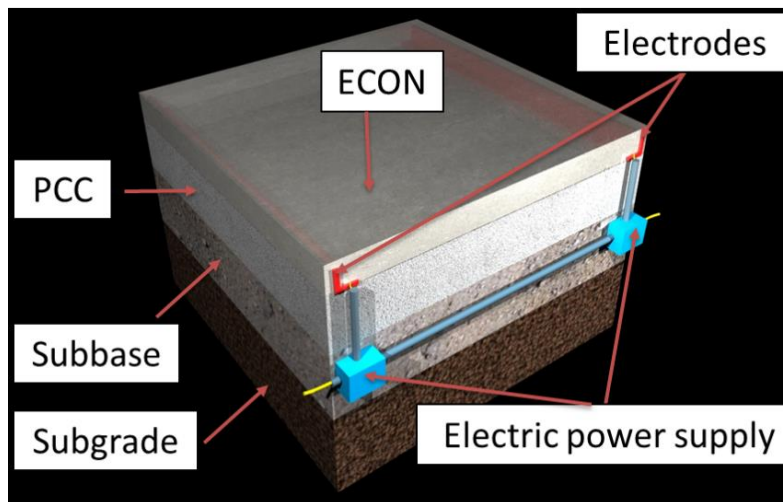
Figure A-1. Conceptual design of ECON HPS

Because it has lower electrical resistivity than normal concrete, ECON behaves like a conductor of electricity. The main components of the ECON HPS include conductive materials (heating elements) for ECON, electrodes, a power supply, and temperature sensors.

The proposed ECON HPS structure for the Iowa Department of Transportation (DOT) headquarters south parking lot construction project consists of four layers: 3.0 in. (7.6 cm) layer of ECON containing embedded electrodes on top of a 7.0 in. (17.8 cm) layer of portland cement concrete (PCC), comprising a 10.0 in. (25.4 cm) thick combined PCC layer, an aggregate base course, and the subgrade. Type and class of each pavement layer in an ECON HPS is specified in the contract. Additional details on each element are given as follows:

A. **PCC: Standard Concrete Pavement**
   Standard concrete pavement, reinforced or non-reinforced, can be utilized as the bottom layer in ECON HPS. Use the class of concrete specified in the contract documents. Reinforce as shown in the contract documents. Place within fixed forms, consolidate, and finish by equipment operating on forms.

B. **PCC: Slip-Form Concrete Pavement**
   Slip-form concrete pavement can be utilized as a bottom layer in an ECON HPS. It may be

reinforced or non-reinforced concrete of the class specified in the contract documents. Reinforce as shown in the contract documents. Place, consolidate, and finish without the use of fixed forms.

C. **ECON**

ECON is a cementitious mixture containing a certain amount of electrically conductive components in standard concrete, which is designed for pavement to serve as the heat source when electrical energy is applied. The general constituents of ECON are cement, aggregates, water, electrically conductive additives (ECAs), and possibly admixtures. ECON can be utilized as a top layer in an ECON HPS. An ECON layer requires the installation of electrodes to provide electric power to the ECON HPS for generating heat. In addition to electrodes, it may be reinforced or non-reinforced using fiberglass reinforcing steel bars or alternatives. Place, consolidate, and finish with the use of fixed forms or slip form. Reinforcement and paving type (i.e., fixed form or slip form) as are applied shown in the contract documents. Additional details on the pavement materials are given as follows:

A.2. Pavement Materials

A. **PCC Layer (Bottom Layer)**

Meet the requirements for the respective items in "Division 41. Construction Materials" and "Section 2301. Portland Cement Concrete Pavement" in the Iowa DOT Standard Specifications.

B. **ECON Layer (Top Surface Layer)**

1. **General**

   ECON should meet the general requirements of "Section 2301. Portland Cement Concrete Pavement" in the Iowa DOT Standard Specifications unless items are specified by the engineer. Given the consistency and workability of carbon fiber-reinforced concrete is different from an equivalent standard concrete, adjustments to aggregate gradations and cement paste to aggregate ratio are required to obtain desirable fresh and hardened properties.

2. **Electrically Conductive Additives (ECAs)**

   Carbon fiber with a nominal length of 0.25 in. (6 mm) and a diameter of 7 µm in dosages less than 1.25% by total volume of concrete can be used as an ECA.

3. **Combined Fine and Coarse Aggregate**

   Fine and coarse aggregate proportions are determined to obtain required concrete workability to meet consistency requirements of "Section 2301. Portland Cement Concrete Pavement" and gradation requirements for individual aggregates in "Section 4109. Aggregate Gradations" in the Iowa DOT Standard Specifications.

4. **Water, Consistency, and Batch Yield**
Water/cementitious materials ratio, consistency, and batch yield should conform to "Section 2301. Portland Cement Concrete Pavement" in the Iowa DOT Standard Specifications.

5. **Entrained-Air Content**
Conformance with the entrained-air content requirement in "Section 2301. Portland Cement Concrete Pavement" in the Iowa DOT Standard Specifications.

6. **Admixtures**
Air entraining, water-reducing admixture, and set-retarding admixtures were used in accordance to "Section 4103. Liquid Admixtures for Portland Cement Concrete" in "Division 41. Construction Materials" of the Iowa DOT Standard Specifications. Corrosion inhibitor admixture (e.g., DCI admixture manufactured by GCP Applied Technologies) can only be used as a conductivity-enhancing agent based on its compatibility with other admixtures.

7. **Use of Supplementary Cementitious Materials**
Class F fly ash that meets the requirements of "Section 4108. Supplementary Cementitious Materials" in "Division 41. Construction Materials" of the Iowa DOT Standard Specifications.

8. **Proportioning and Mixing of Concrete Materials**

   a. **Storage and Handling of Aggregates**
   Should be practiced according to "Section 2301. Portland Cement Concrete Pavement" in the Iowa DOT Standard Specifications.

   b. **Storage and Handling of Cement and Fly Ash**
   Should be practiced according to "Section 2301. Portland Cement Concrete Pavement" in the Iowa DOT Standard Specifications.

   c. **Measurement of Materials**
   Should conform to "Section 2301 Portland Cement Concrete Pavement" practice in the Iowa DOT Standard Specifications. In addition, the engineer independently tested the materials and verified the results given by the contractor two weeks prior to concrete placement.

   d. **Mixing of Materials**
   Carbon fiber should be fed into the concrete mixer along with fine and coarse aggregate and dry-mixed for 30 seconds before addition of water and cement. A portion of the water (10–20 gallons) should be added at the job site and mixed for an adequate length of time. To prevent excessive fiber wear by aggregates, the entire mixing procedure (the sum of the mixing time in the concrete plant and truck mixer)

should not take longer than 15 minutes. Preconstruction training and pretrial quality control tests of an ECON trial batch produced from the concrete plant is recommended at least 14 days before paving at the job site.

A.3. Construction

When the contract allows for either standard or slip-form pavement, the method used is the contractor's option. When the contract allows only one type, use the type specified. When slip-form is specified, small or irregular areas may be constructed with fixed forms. Irregularly shaped areas of either type of pavement may be formed and finished by hand methods. The construction steps are given as follows:

A. **General: Construction Procedures**
   Part of the construction procedure of the ECON slabs is shown in Figure A-2.

Figure A-2. ECON construction procedure

The construction sequence of the ECON HPS involves the following major steps:

- Step 1: Prepare the subgrade and base layer
- Step 2: Install dowel baskets and tie bars
- Step 3: Place polyvinyl chloride (PVC) conduits to house wires for sensors and power lines for electrodes
- Step 3: Place PCC layer as the bottom layer
- Step 4: Place electrode and sensor systems
- Step 5: Connect electrical wires for electrodes to an alternating current (AC) power supply and connect sensor wires to data acquisition systems
- Step 6: Place fiberglass on top of the electrodes
- Step 5: Clean the surface of the PCC layer and the electrodes
- Step 6: Place ECON layer as the top surface layer

B. **Base and Subgrade Preparation**
   Meet the requirements for the respective items in "Division 21. Earthwork, Subgrades, and Subbases;" "Division 22. Base Course;" and "Section 2301. Portland Cement Concrete Pavement" in the Iowa DOT Standard Specifications.

C. **Install Dowel Baskets and Tie Bars**
   Meet the requirements for these items in "Section 2301. Portland Cement Concrete Pavement" in Iowa DOT Standard Specifications. The dowel baskets and tie bars should also be covered by a PCC layer (bottom layer) so that electrodes can be easily installed on top of the surface of the PCC layer.

D. **PVC Conduit Installation**
   Installation should be practiced according to "Section 2523. Highway Lighting" in the Iowa DOT Standard Specifications. PVC conduits should be used to protect and house the wires for electrodes and sensors. To prevent interference between sensor signals, the electrical wires of the electrodes should be placed into separate conduits. PVC conduits and junction boxes should be installed to support placing wires through the conduits.

E. **PCC Layer (Bottom Layer)**
   Meet the requirements for the PCC layer in "Section 2301. Portland Cement Concrete Pavement" in the Iowa DOT Standard Specifications. In addition, the surface of the PCC layer should be screeded or roughened using brooms to create a rough surface or grooved to enhance the bond between the hardened PCC layer (bottom layer) and the later-placed ECON layer (top layer) (Figure A-3).
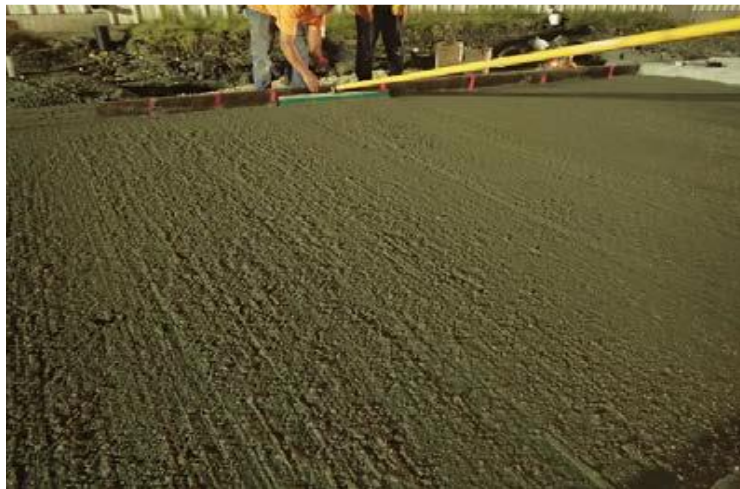

Figure A-3. Broom or screed PCC surface

F. **ECON Layer (Top Surface Layer)**
   Meet the requirements for the ECON layer in "Section 2301. Portland Cement Concrete Pavement" in the Iowa DOT Standard Specifications. These items include electrode installation, sensor installation, electrical connections for electrodes, fiberglass installation (if

needed), cleaning the surface of the PCC layer (bottom layer), and placing the ECON layer (top surface layer). Preconstruction training and pretrial quality control tests of ECON trial batch produced from the concrete plant are recommended at least 14 days before the paving at the job site. The final product and all the ingredients should meet the Iowa DOT Standard Specifications.

1. **Electrode Installation**
   Stainless steel 316L smooth electrodes (Figure A-4) are recommended as the electrode material. Given it is highly resistant to corrosion and given it can allow ECON to contract and expand with less resistance, it would not present any cracking potential.
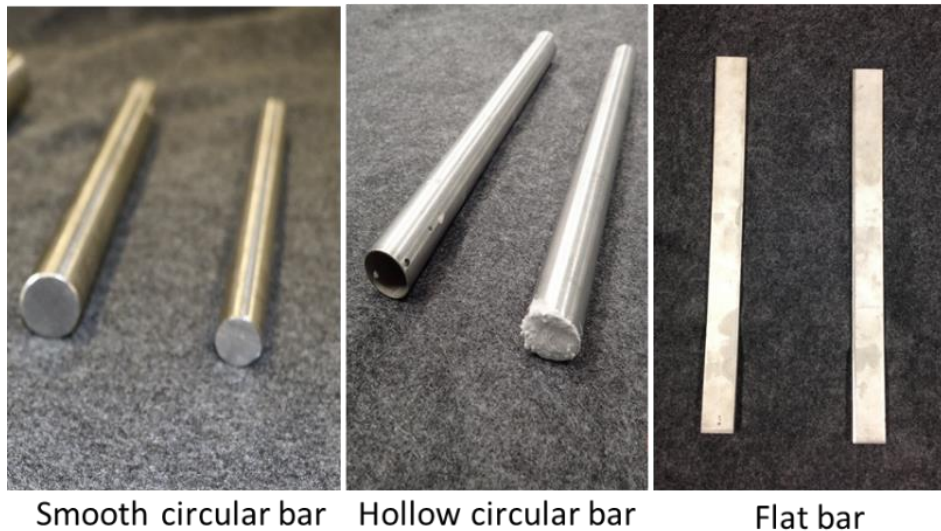

Smooth circular bar   Hollow circular bar   Flat bar

Figure A-4. Stainless steel 316L smooth electrodes

Nylon materials could be used to anchor and fix the electrodes to prevent movement during ECON layer placement because of its resistance to corrosion and its insulating properties that prevent current leakage into the ground. Given the electrodes should be anchored to the PCC layer, an electric drill should be used to drill holes in the PCC layer. Anchors should be placed in the holes to fix the electrodes, after which electrical wires to provide power to the system should be connected to the electrodes using gauge-ring wire connectors. Spacers can be used to bring electrodes closer to the surface and increase the efficiency of heat generation.

2. **Sensor System Installation**
   Temperature sensors can be used for measuring temperature and for activating the ECON HPS power manually or automatically. Current and voltage sensors (e.g., wireless electricity-monitoring sensors manufactured by Monnit) can also be employed to monitor the electrical properties for estimating power consumption and operation cost.

3. **Electrical Connections for Electrodes**
   Should conform in practice to "Section 2523. Highway Lighting" in the Iowa DOT

Standard Specifications. Electrodes should be connected to the AC power source. The ECON electric power supply system should be tested to check the wiring connections to the electrodes before placing the ECON layer. The electrical works required are described in more detail in "4 Electrical Works for Power Supply Management and Operation Control Systems" of this specification.

4. **Clean the Surface of the PCC Layer**
   The contractor should thoroughly clean the surface of the bottom PCC layer and the electrodes, using an air blower, brooms, and a pressure washer to provide sufficient bonding between the electrodes and the ECON layer.

5. **Placing ECON Layer**
   Meet the requirements for the ECON layer in "Section 2301. Portland Cement Concrete Pavement" in the Iowa DOT Standard Specifications. In addition, caution should be taken during the placement of the ECON layer to prevent damage to the electrode and sensor systems.

A.4. Electrical Works for Power Supply Management and Operation Control Systems

The following steps describe the required power supply and operation control management:

A. **Design of Power Supply Management and Operation Control Systems**
   An electrical power source should be identified for designing power supply management and operation control systems. Assuming construction and operation of 10 ECON slabs, three-phase 208 volt alternating current (VAC) would be appropriate. The 10 ECON slabs are grouped into three separate zones, each tied to a single phase of the source to better distribute the power going through the slabs. An industrial-standard programmable logic controller (PLC) system can be used as the control system. The PLC central processing unit (CPU) (Automation Direct D4-440) requires a conveniently available 120–240 VAC source (a common household power outlet has a rating of 110 V), because it has low power consumption, allowing the CPU to tap power from the source intended primarily for the ECON slabs as an option if necessary. The cost of this model is another advantage; the alternative CPU requires a volt direct current (VDC) source and is more expensive.

   In addition to the CPU, other peripherals and parts required for the system to be functional are as follows:

   - Electrically erasable programmable read-only memory (EEPROM) cartridge to store ladder logic (programming codes)
   - Output module to send on/off signals to relays
   - Relays (one for each slab) to control connections between sources and wires to electrodes based on signals from the output module
   - Input/Output (I/O) base to hook onto the modules

- Communication module to connect the PLC system to the internet for remote-access purposes

In addition to the parts mentioned previously, several other accessories are also needed including the following:

- Programming cable
- Serial adapter
- Pin connectors

The PLC system functions by sending signals to the relays. There are two sides of each relay: INPUT and LOAD. The INPUT pins are connected to the output module and common of the same module. The INPUT side detects the type of signal sent, either high (1) or low (0), and controls the connector built into the LOAD side. The LOAD pins are connected to the sources and the wires to the electrodes embedded into the ECON slabs. When INPUT detects a high signal, the LOAD is connected and current can flow from the source to the electrodes, then through the conductive ECON slabs into the grounded alternate electrodes (connected to neutral line of the source) to form a complete circuit.

B. **Electrical Works Procedures**

Step 1*: Connect alternate electrodes into a ground conduit to be connected to the neutral line of the power source

Step 2*: Connect remaining electrodes to wires pulled to the designated PLC system setup location

Step 3:   Install PLC hardware into panel with clear and consistent labeling for relays

Step 4:   Connect PLC hardware together based on user manual from the manufacturer

Step 5:   Connect output module and common pins from PLC to INPUT pins on relays

Step 6:   Connect source and wires to electrodes to LOAD pins on relays

Step 7:   Conduct safety check on PLC system

Step 8:   System startup and upload programming code

Step 9:   Run initial test

* These steps should be done before placing the ECON layer

APPENDIX B. ECON HPS APPROVAL PROCESS SUMMARY

The approval process for the electrically conductive concrete (ECON) heated pavement system (HPS) in this project consisted of two parts: (1) wiring from the utility line to circuit breakers that had been wired by the Iowa Department of Transportation (DOT) electricians and (2) control system and wire distribution to each slab performed by the Iowa State University (ISU) research team. The first part approval was granted to the project but only conditional operation was granted for the second part.

On February 02, 2019, the slabs were turned on in the presence of a state electrical inspector, electrical safety tests were performed on the slabs, and the slabs were found to be in a safe condition. Some of the slabs relays were experiencing overheating due to high conductivity of the slabs, and the state electrical inspector allowed the ISU team to turn on the slabs to fix any possible bugs in the system.

After the first visit by the state inspector, the ISU research team made the following list of modifications in the electrical system, and they were completed by November 2019:

- To address the unbalanced load on the circuit breakers, the 208 volt alternating current (VAC) source was changed to 120 VAC:
  - The system worked with 120 VAC, and the maximum current through each breaker was less than 40 Amps
- To provide better heat transfer and dissipate heat from the relays:
  - Relays were removed from wooden plates and installed on steel plates (The heated wooden plates smelled during inspector's first visit, so they were replaced by steel plates)
  - Cooling fans were installed on the box covers to constantly blow on the relays
  - The maximum temperature reached by the relays is currently about 131°F [55°C] (The allowable working temperature for these relays is 194°F [90°C])
  - Figure B-1 shows the modified boxes and the installed fans on the relays
- A surveillance camera was installed, which allowed monitoring the system continuously

Figure B-1. Modification to address the overheating of relays

On November 14, 2019, Dave Millard, a professional engineer (PE) in electrical engineering from the Millard Engineering firm, visited the heated pavement site at the Iowa DOT headquarters and provided a letter regarding the wiring of the second part of the project, performed by the ISU research team (Figure B-2), stating that the system was constructed "in accordance with the National Electrical Code."

MILLARD ENGINEERING

DAVID MILLARD, P.E.

1501 GLENDALE AVENUE   AMES, IOWA   50010   515-232-6597

November 25, 2019

Mr. Halil Ceylan, Professor, CCEE
410 Town Engineering Bldg.
Iowa State University
813 Bissell Road
Ames, IA 50011-1066

RE: IDOT Heated Concrete Project

Dear Mr. Ceylan:

On November 14, 2019, I visited the site of the heated concrete research project at the Iowa Department of Transportation parking lot to inspect the electrical installation in the control building. I reviewed the system drawings and observed the construction of the control system. It was my observation that the system was constructed in accordance with commonly accepted control panel construction practices and in accordance with the National Electrical Code. It is acceptable for automatic/remote control operation.

Please contact me if you have any questions or comments.

Sincerely,

MILLARD ENGINEERING

David Millard

David Millard, PE
Iowa License Number 9181

electrical and process control engineering, illumination engineering, water supply and wastewater treatment engineering

Figure B-2. Letter from a PE in electrical engineering regarding the wiring at Iowa DOT ECON HPS

APPENDIX C. DRAFT USER MANUAL FOR IOWA DOT ECON HPS

This is a step-by-step set of instructions for running the electrically conductive concrete (ECON) heated pavement system (HPS) system at the Iowa Department of Transportation (DOT). The seven steps are as follows:

Step 1: Place the status mode on the programmable logic controller (PLC) device itself to TERM and connect the USB cable to the computer.
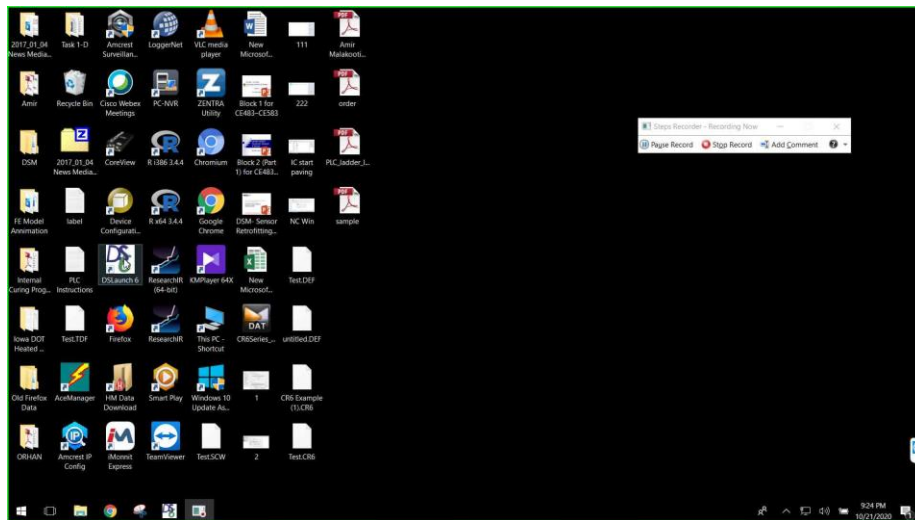
Step 2: Left double click on DSLaunch 6 software.

Figure C-1. Step 2 screenshot

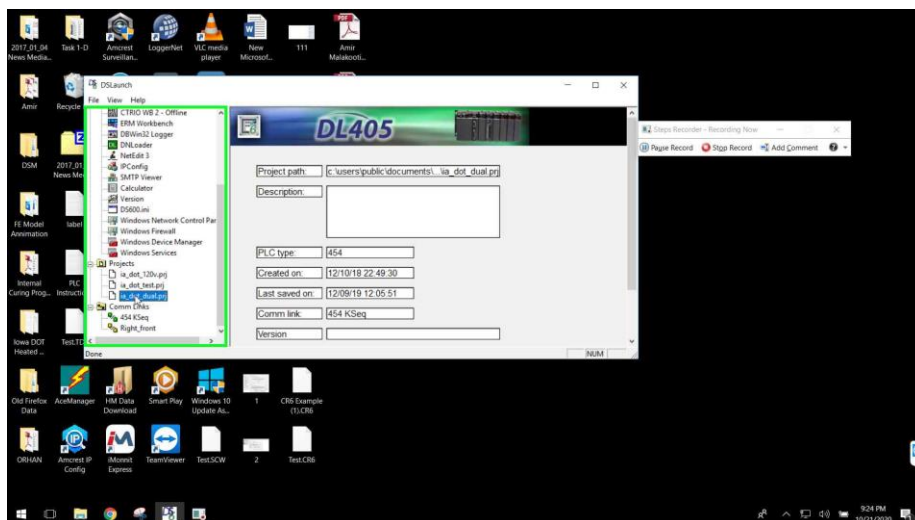**Step 3:** Left double click on ia_dot_dual.prj in DSLaunch.

Figure C-2. Step 3 screenshot

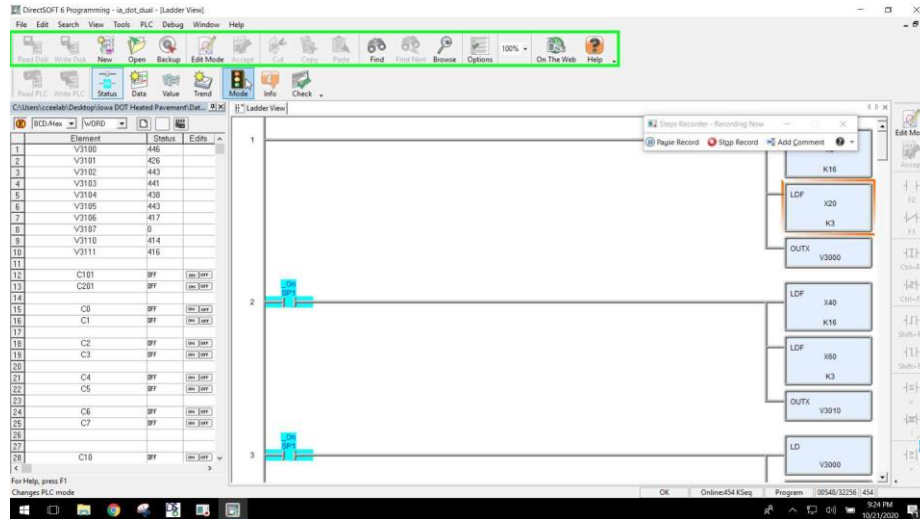**Step 4:** Left click on Mode in DirectSOFT 6 Programming - ia_dot_dual.

Figure C-3. Step 4 screenshot
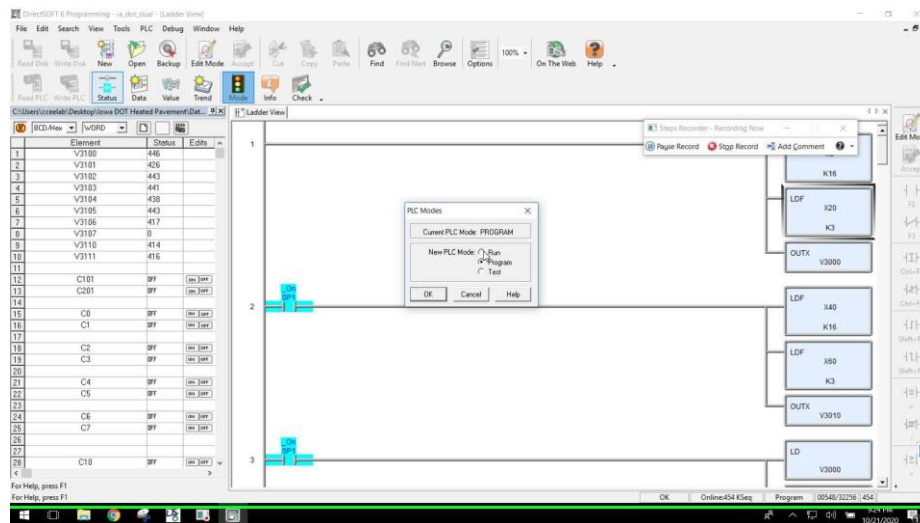
Step 5: The PLC Modes windows will appear.

Figure C-4. Step 5 screenshot

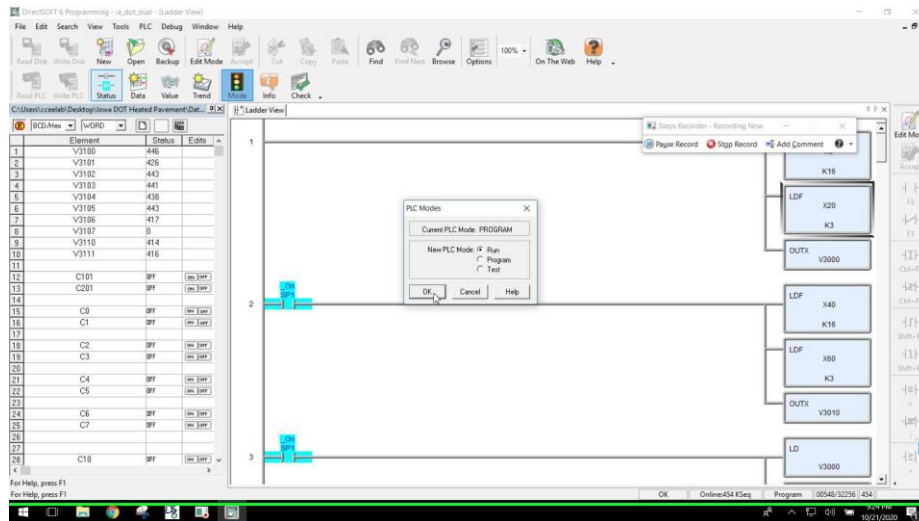**Step 6:** Choose Run mode, and click the OK button.

Figure C-5. Step 6 screenshot

Step 7: Left double click the ON button for the C101. This initiates automatic operation of the system. In order to end the operation, click the on/off button.
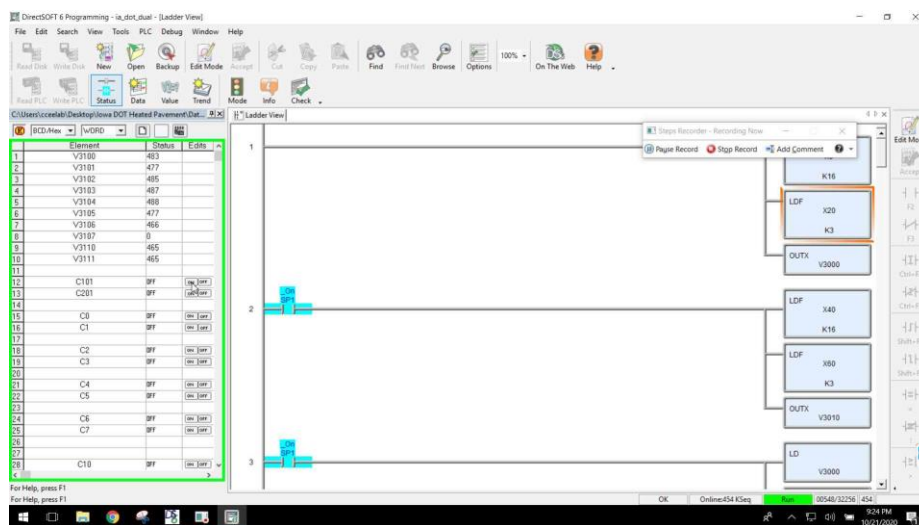

Figure C-6. Step 7 screenshot

THE INSTITUTE FOR TRANSPORTATION IS THE FOCAL POINT FOR TRANSPORTATION AT IOWA STATE UNIVERSITY.

InTrans centers and programs perform transportation research and provide technology transfer services for government agencies and private companies;

InTrans contributes to Iowa State University and the College of Engineering's educational programs for transportation students and provides K–12 outreach; and

InTrans conducts local, regional, and national transportation services and continuing education programs.

IOWA STATE UNIVERSITY

INSTITUTE FOR TRANSPORTATION

Visit **InTrans.iastate.edu** for color pdfs of this and other research reports.